Variations on a theme of nuclear matter*

V. R. Pandharipande and R. B. Wiringa†

Department of Physics, University of Illinois at Urbana-Champaign, Urbana, Illinois 61801

The authors review new techniques developed to apply the variational method to the nuclear matter problem. The variational wave function is taken to be $(S\Pi_{i<j}F_{ij})\,\Phi$; the correlation operators F_{ij} can in principle induce central, backflow, spin isospin, tensor, etc. correlations, and Φ is the ideal Fermi gas wave function. The application of diagrammatic cluster expansion and chain summation techniques to calculate expectation values with such wave functions is discussed in detail. The authors also give a brief overview of various other approaches to the calculation of the binding energies of quantum fluids, and a comparison of results for simple systems such ad helium liquids. Results obtained by various methods for simplified models of nuclear matter, which include central, spin, isospin, and tensor forces, have converged significantly in recent months. Results obtained with more realistic models which include the spin–orbit potentials are also discussed. The potential models considered so far either give too little binding or too high equilibrium density.

CONTENTS

GLOSSARY OF SYMBOLS IN VARIATIONAL CALCULATIONS WITH CORRELATION OPERATORS

A^p	Matrix defined by Eq. (5.1).
$[\overline{Aa}]$, $[\overline{A}][a]$	Notation for separable diagrams.
D_{pq}	Matrix defined by Eq. (5.22).
F_{ij}, $F_{ij}^{H(N)}$	The correlation operator for pair ij; superscripts H and N denote the specific forms used in liquid helium [Eq. (2.20)] and nuclear matter [Eq. (2.24)] calculations.
F_{ij}^p	Functions used to expand (ΠF_{ij}^2) [Eq. (4.2)]; the superscript p denotes the associated operator.
f_J, f_{JO}	Jastrow and optimized Jastrow correlation functions.
f_{ij}^p	Correlation function associated with operator O_{ij}^p.
$f_{T,S}$, $f_{t,T}$ and $f_{b,T}$	Correlations in two-body channels having isospin T and spin S.
$G_{xy,ij}^p$	Chain function associated with operator O_{ij}^p. The subscripts x and y denote the nature of vertices i and j at the ends of the chains.
g_{ij}	Two-particle distribution function.
H_{ij}^p	Part of the Hamiltonian associated with O_{ij}^p.
$J^p(x_y, x_z, x_q)$	Single operator ring integrals [Eqs. (6.29)–(6.33)].
K^{pqr}	Matrix defined by Eq. (5.2).
L^{pqr}	Matrix defined by Eq. (5.15).
$L(r)$	Generalized Slater function.
$M(t_p, x_t, x_y)$ or M_x^p	Vertex correction factors [Eq. (6.28)].
$m(x_t, x_y, x_z, z_q)$	Probability factors (Sec. V.C).
O_{ij}^p	Operator labeled by superscript p.
T_F	Fermi gas kinetic energy [Eq. (7.1)].
U, U_F	Parts of "three-body" kinetic energy [Eq. (7.1)].

*Supported by NSF PHYS 76-22147

†Current address: Los Alamos Scientific Laboratory, Los Alamos, New Mexico 87545.

v_{ij}^p	Part of the two-body potential associated with O_{ij}^p.
$v_{T,S}$, $v_{t,T}$ and $v_{b,T}$	Potentials in two-body channels with isospin T and spin S.
W, W_0, W_c, W_s, W_{cs} and W_F	Parts of "two-body" interaction energy.
$X_{xy,ij}^p$	Link functions associated with O_{ij}^p; x and y denote the type of vertices i and j.
α(A, B)	Generalizations of the tensor operator [Eq. (9.1)].
β(A)	Generalizations of the L·S operator [Eq. (9.2)].
Δ^p	Matrix whose $p=1-4$ elements equal unity and the rest are zero.
η_{ij}	Backflow correlation function [Eq. (2.20)].
θ_{ijk}^{pqr}	Integral operator in the chain equations.
ξ_{ijk}^{pqr}	Angle functions in the coupling of O_{ij}^p and O_{jk}^q [Eq. (5.5)].
Φ	Uncorrelated wave function.
Ψ_{IP}, Ψ_J and Ψ_{SP}	Variational wave functions of the independent pair [Eq. (2.26)], Jastrow [Eq. (2.6)], and symmetrized product [Eq. (2.19)] form.

I. INTRODUCTION

Nuclear matter is a hypothetical system of nucleons interacting without Coulomb forces. It is translationally invariant with a fixed ratio of protons and neutrons, and can be thought of as an idealization of matter inside a large nucleus. The goal of nuclear matter theory is to obtain empirically known bulk properties, such as the binding energy, equilibrium density, symmetry energy, incompressibility, etc., starting from the underlying two-body interactions.

A good many-body theory for nuclear matter may be used to study the details of nucleon–nucleon interactions. The observed phase shifts from scattering experiments plus the properties of the only bound two-nucleon system, the deuteron, are insufficient to pick out a unique nucleon–nucleon potential. Nuclear matter studies can help us understand better exactly how the different elements of a potential affect the matter properties, and what sorts of features are required to produce the observed saturation. It is also conceivable that a potential model for nuclear forces is simply not workable; nuclear matter studies may indicate whether or not this is true.

A solution of the infinite matter problem would also be useful as the starting point for a microscopic theory of finite nuclei. It is the first step in obtaining the equation of state for dense matter, which is essential in the study of neutron stars. Finally it is simply a very interesting many-body problem in its own right. Methods developed for it should be useful in other dense quantum fluids such as liquid helium.

A. Properties of nuclear matter

Symmetric nuclear matter is characterized by its binding energy and equilibrium density ρ_0. The binding energy is given by the volume term α in the semi-empirical mass formula for nuclei:

$$M(A,Z)=NM_n+ZM_H-\frac{1}{c^2}\left[\alpha A-\frac{\beta(N-Z)^2}{A}-\gamma A^{2/3}-\frac{3e^2Z^2}{5r_0A^{1/3}}+\text{pairing term}+\text{shell corrections}+\cdots\right]. \quad (1.1)$$

The original mass formula is due to von Weizsäcker (1935) and Bethe and Bacher (1936). Today there are many competing versions which add higher-order terms in the symmetry, surface, and Coulomb effects, and use different methods for calculating the shell corrections. Values for α, the symmetry term β, the surface term γ, the unit radius r_0 defined by

$$\tfrac{4}{3}\pi r_0^3\rho=1, \quad (1.2)$$

and other parameters are obtained by fitting over one thousand experimentally known nuclear masses, and the fission barriers for several dozen heavy nuclei. A collection of contemporary mass formulas by many different authors can be found in At. Data and Nucl. Data Tables 17 5–6, (1976). Typical values for α are 15 to 16 MeV; r_0 varies from 1.16 to 1.22 fm, corresponding to densities of 0.15 to 0.13 nucleons/fm^3 or a k_F between 1.31 and 1.25 fm^{-1}. The values for β and γ are in the ranges 30–40 MeV and 20–21 MeV, respectively.

Also of interest is the incompressibility of nuclear matter, K,

$$K=k_F^2\frac{\partial(E/A)}{\partial k_F^2}, \quad (1.3)$$

which appears as a parameter in some of the more sophisticated mass formulas, but is not well determined by them; the values given range from 240 to 300 MeV, with large error bars. Recent experimental observations of an isoscalar breathing mode in nuclei by Youngblood *et al.* (1977, 1978) provide a better estimate of K than ever before. They have measured an E_{0^+} resonance in ^{208}Pb at 13.7 MeV, in ^{144}Sm at 15.1 MeV, and in ^{90}Zr at 17 MeV. This energy is related to the incompressibility of a finite nucleus k_A in the liquid drop model by

$$E_{0^+}=(\pi/3r_0A^{1/3})\sqrt{(\hbar^2/m)k_A}. \quad (1.4)$$

If we insert the simple semiempirical mass formula (1.1) into Eq. (1.3), we get an expansion for k_A,

$$k_A=K+K_\beta\left(\frac{N-Z}{A}\right)^2+K_\gamma A^{-1/3}+\frac{6e^2Z^2}{5r_0A^{4/3}}, \quad (1.5)$$

where K_β and K_γ are symmetry and surface incompressibilities, respectively. A simple calculation indicates $K\simeq 260$ MeV, $K_\beta\simeq 3$ MeV, and $K_\gamma\simeq -405$ MeV. There is a question as to how valid the liquid drop model expression (1.4) is for extracting k_A from E_{0^+}. An RPA calculation by Blaizot *et al.* (1976) suggests that $K\simeq 210$ MeV will reproduce the observed data.

A good theory should be able to calculate the ground-state $E(\rho)$ curve for any given potential. The occur-

rence of a minimum will indicate both the equilibrium density ρ_0 and binding energy $E(\rho_0)$. The curvature of $E(\rho)$ at ρ_0 will give us K. To calculate β, we can allow the number of neutrons and protons to differ slightly and measure the curvature of $E(N,Z)$ at the point $N=Z$. A somewhat more difficult problem is the calculation of γ, which would obviously require the introduction of a surface of some kind. Additional quantities of interest that might be obtained by functional differentiation of $E(\rho)$ include the effective mass and Landau parameters. In principle we may deduce their values by analyzing the spectra of near closed-shell nuclei with the Landau–Migdal theory of finite Fermi systems (Speth *et al.*, 1977; Brown, 1971; Bäckman *et al.*, 1979).

B. Nucleon-nucleon potentials

The starting point for any nuclear matter calculation is a two-body potential that models the nucleon–nucleon interaction. A more fundamental viewpoint would be a meson theory of nuclear forces (Brown and Jackson, 1976), or even a quark model for the strong interaction. The former has not been quantitatively successful, however, while the latter is still in its infancy. At present it is necessary to resort to phenomenological potentials that fit the experimental data, and incorporate elements that are consistent with our fundamental knowledge of strong interactions. The potentials used are generally nonrelativistic, and of course cannot take into account many-body forces, about which very little is known.

"Realistic" potentials are those that give good fits to the low-energy ($\lesssim 300$ MeV) two-body scattering data, and get the binding energy and quadrupole moment of the deuteron correct. The phase-shift data varies greatly from channel to channel, indicating a very complicated potential. To fit the phase shifts in channels with $J \lesssim 2$ a potential requires at least ten operator components:

$$\begin{aligned} v_{ij} = {} & v^c + v^\sigma(\sigma_i\cdot\sigma_j) + v^\tau(\tau_i\cdot\tau_j) + v^{\sigma\tau}(\sigma_i\cdot\sigma_j)(\tau_i\cdot\tau_j) \\ & + v^t S_{ij} + v^{t\tau} S_{ij}(\tau_i\cdot\tau_j) + v^b(\mathbf{L}\cdot\mathbf{S})_{ij} + v^{b\tau}(\mathbf{L}\cdot\mathbf{S})_{ij}(\tau_i\cdot\tau_j) \\ & + v^q L_{ij} + v^{q\tau} L_{ij}(\tau_i\cdot\tau_j), \end{aligned} \tag{1.6}$$

where $S_{ij} = 3(\sigma_i\cdot\hat{r})(\sigma_j\cdot\hat{r}) - \sigma_i\cdot\sigma_j$ is the tensor operator, $(\mathbf{L}\cdot\mathbf{S})_{ij}$ is the spin–orbit operator, and $L_{ij} = (\sigma_i\cdot\sigma_j)\mathbf{L}^2 - \frac{1}{2}[(\sigma_i\cdot\mathbf{L})(\sigma_j\cdot\mathbf{L}) + (\sigma_j\cdot\mathbf{L})(\sigma_i\cdot\mathbf{L})]$ is the quadratic spin–orbit operator. The v^i are then simple functions of the radial distance $|\mathbf{r}_i - \mathbf{r}_j|$. Even greater operator dependence might be called for in (1.6) if the lesser studied phase shifts in $J>2$ channels were to be fitted.

All realistic nucleon-nucleon potentials exhibit some common features. These include a very strong repulsion at short distances, an intermediate-range attraction, and a long-range behavior that is well described by the one-pion exchange potential (OPEP):

$$v_\pi = \frac{1}{3}\frac{f^2}{\hbar c} m_\pi c^2 (\tau_i\cdot\tau_j)\left[(\sigma_i\cdot\sigma_j) + S_{ij}\left(1 + \frac{3}{\mu r} + \frac{3}{(\mu r)^2}\right)\right]\frac{e^{-\mu r}}{\mu r}. \tag{1.7}$$

Here $\mu = m_\pi c/\hbar = .7$ fm^{-1} is the inverse Compton wavelength of the pion, and $f^2/\hbar c = 0.08$ is the coupling strength in πN interactions. All NN potentials contain the OPEP but the treatment of the intermediate-range attraction, which is probably due to multiple π exchange, and the short-range repulsion, which comes from ω- and ρ-meson exchange, is highly varied. One choice is a superposition of Yukawa forces:

$$(v - v_\pi)^i = \sum_n y_n^i \frac{e^{-n\mu r}}{\mu r}. \tag{1.8}$$

Here n may take on a series of integer values, as in the potential of Reid (1968) ($n = 2, 3, 4, 6, 7$), or it may have noninteger values to represent the actual ω–ρ range ($n = 5.5$), as in some of the models of Bethe and Johnson (1974). These soft-core potentials may be contrasted to the earlier hard-core potentials such as those of Hamada and Johnston (1962), which use Yukawa forces as in Eq. (1.8) at intermediate distances, but an infinite hard core at short distances, i.e., $v = +\infty$ for $r < r_c$, $r_c \simeq 0.5$ fm. The hard core was originally used because of its simplicity, although it is not physically reasonable.

The v^p obtained from the Reid potentials in the singlet states $^1S_0$ and $^1P_1$, and the triplet states $^3S_1$–$^3D_1$ and $^3P_2$–$^3F_2$, are shown in Fig. 1. The strong operator dependence is quite evident, particularly the $\mathbf{L}\cdot\mathbf{S}$ force at short distances and the pion part ($\sigma\tau$ and $t\tau$) at large distances. There are many other types of potentials that can be used to adequately explain the low-energy (<300 MeV) scattering data and deuteron properties, as reviewed by Bethe (1971). The onset of inelastic processes at higher energies makes it difficult to predict the correct potential behavior inside $\simeq 0.5$ fm.

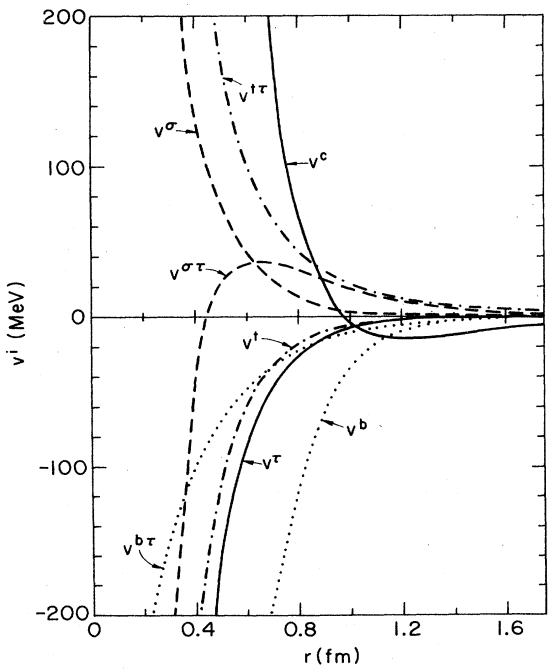

FIG. 1. The $v^i(r)$ in models v_6 and v_8 based on the Reid potentials.

C. Nuclear matter problem

The problem to be solved may be summarized as follows. A large box of volume Ω contains A nucleons which interact via a two-body potential v_{ij},

$$H=\sum_i\left(\frac{-\hbar^2}{2m}\nabla_i^2\right)+\sum_{i<j}v_{ij}. \tag{1.9}$$

We wish to calculate the ground-state energy $AE(\rho)$ of this system in the limit $A,\Omega\to\infty$, while the density $\rho=A/\Omega$ is kept constant. The minimum in the curve $E(\rho)$ will give both the binding energy and equilibrium density for the given potential.

At present it is very difficult to do a good many-body calculation for the full operator-dependent potential (1.6). Bethe (1977) has suggested that the many-body theory could be developed in a series of steps by considering homework potentials that successively incorporate more and more sophistication. Starting from any full potential, one may define a sequence of homework potentials which have successively more of the operator dependences given in Eq. (1.6). At present it appears that the so-called v_6 problem, which includes central, spin, isospin, and tensor forces, can be treated with reasonable accuracy. Some preliminary work on the v_8 problem which incorporates spin–orbit forces is also available. It may not be profitable to calculate anything beyond the $E(\rho)$ curve until many-body calculations can be done for a full realistic potential.

II. OVERVIEW OF THEORETICAL METHODS

A. History of the many-body problem

Just two years after the semiempirical mass formula was first suggested, the first nuclear matter calculations were performed by Euler (1937). Very little was known about the interaction of nucleons at that time, however, and only a nonsingular potential was studied. The modern studies began after the need for a strong repulsive core in the potential was realized. The specialized perturbation methods required were pioneered by Brueckner [Brueckner (1954), Brueckner and Levinson (1955)], Bethe (1956), and Goldstone (1957); this approach is called the BBG expansion. It is a low-density expansion, whose convergence properties are still not fully understood. It may be useful at nuclear matter density, but its application to denser quantum fluids like liquid helium or neutron star matter is thought to be very difficult.

At the same time the perturbation theory of Brueckner was first being formulated, Jastrow (1955) suggested an alternate variational approach for treating the strong repulsive core. Jastrow recommended the use of a trial wave function where the unperturbed wave function is modified by a product of two-body correlation functions. However, it was thought that the spin, isospin, tensor, etc., correlations would be difficult to handle in this way. The discovery of pulsars and their identification as neutron stars in 1968 revived the interest in the variational approach, because the method does not have the density limitations of the BBG expansion. The study of astronomical objects whose central densities could be several times that of nuclear matter would clearly require the development of such an alternate approach.

Nuclear matter calculations in lowest-order versions of both the variational and BBG methods were in substantial agreement by 1972 (Pandharipande, 1972), but disturbingly no realistic potentials had been found that could explain the energy and density saturation; typical potentials either gave too little binding or too high a density (Day and Coester, 1976). More advanced variational studies by Bäckman *et al.* (1972) and Pandharipande *et al.* (1975) indicated a considerable discrepancy with the lowest-order results for some simple model potentials. It has since become clear that much more careful calculations are required, particularly for a weakly bound system like nuclear matter, where the kinetic and potential energies cancel to a large extent.

In the following pages we give a brief review of the approaches being actively pursued at present. Whether the previous failure to achieve the correct matter properties is attributable solely to the inadequacy of the many-body theory is not yet clear. In the future when the various theories are developed to a point where we have confidence in them, we must still examine the question of whether a satisfactory nucleon–nucleon potential can be found. At present we can only speculate on that subject.

B. Brueckner-Bethe-Goldstone expansion

The BBG theory has been reviewed by Day (1967, 1978a) and Bethe (1971). It is based on the Goldstone (1957) linked-cluster expansion for the ground state $E(\rho)$. The Hamiltonian is broken into two parts, H_0 and H_1:

$$H_0=\sum_i\left[\frac{-\hbar^2}{2m}\nabla_i^2+U(k_i)\right],$$

$$H_1=\sum_{i<j}v_{ij}-\sum_i U(k_i). \tag{2.1}$$

Here the single-particle potential U is introduced for ease of calculation; it is chosen so that the perturbation expansion for H_1 is rapidly convergent. The singular matrix elements of v are replaced by the reaction matrix G,

$$G=v-v(Q/e)G, \tag{2.2}$$

where Q is the Pauli operator and e is an energy denominator. The nonsingular G sums the interaction between two particles to all orders. It is obtained by calculating the perturbed wave function Ψ from the ideal gas wave function Φ,

$$\Psi=\Phi-(Q/e)v\Psi, \tag{2.3}$$

which implies

$$v\Psi=G\Phi. \tag{2.4}$$

A perturbation expansion in powers of G is not convergent, but the cluster diagrams can be grouped instead according to the number of independent hole lines. Formal arguments for the convergence of the hole-line expansion have been advanced by Brandow

(1966) which indicate an n-hole-line diagram should be proportional to κ^{n-1}, where κ measures the probability that there is an unoccupied state below the Fermi surface. If we neglect many-body clusters, κ is given by

$$\kappa \approx \rho \int |\phi - \psi|^2 d\tau , \tag{2.5}$$

where ψ and ϕ are two-body correlated and uncorrelated wave functions. This estimate of κ, however, depends critically on the choice of U, a topic of much discussion in the recent literature. The standard choice in the past has been to set U to zero for particle states, and to the self-consistent Hartree–Fock potential in hole states. For this choice and the Reid potential, $\kappa \simeq 0.15$ near the saturation density. However, the standard choice has an unphysical gap at the Fermi surface, and several recent calculations use what is called the "continuous choice" advocated by Jeukenne *et al.* (1975).

The hole-line expansion seems to be valid, i.e., obeys the κ^{n-1} prescription, for the short-range correlations induced by the strong repulsive core. A number of internal checks have been performed by Day (1978a) without any inconsistencies being found. However, Friman and Nyman (1978) point out that the pion exchange ring diagrams may need to be summed to all orders. Recent three-body cluster calculations of Day go up to twice nuclear matter density. Even at these densities, which are below those expected for neutron star interiors, the necessity of calculating through at least four-body clusters to get within 10% of the binding energy is indicated. This is a very difficult task, which has not yet been accomplished.

C. Jastrow theory

The variational wave function in Jastrow theory, Ψ_J, is taken as

$$\Psi_J = \prod_{i<j} f_J(r_{ij})\Phi . \tag{2.6}$$

Jastrow (1955) anticipated that the two-body correlation f_J could be an operator in general, but for our nomenclature we shall use it to designate the case of simple radial dependence, $r_{ij} = |\mathbf{r}_i - \mathbf{r}_j|$. The f_J is usually parametrized in some form, and the parameters are varied so as to minimize the variational energy E_J,

$$E_J = \frac{\langle \Psi_J | H | \Psi_J \rangle}{\langle \Psi_J | \Psi_J \rangle} , \tag{2.7}$$

which should give an upper bound for $E(\rho)$.

The E_J can be evaluated exactly with a Monte Carlo integration, or approximately by means of cluster expansions. The most popular expansion uses the method of hypernetted chains (HNC), which is based on the Mayer cluster expansion of statistical mechanics. This chain summation method was developed by van Leeuwen, Groeneveld, and de Boer (1959) for Bose systems, and extended to Fermi systems (FHNC) by Fantoni and Rosati (1975). There is a hierarchy of approximations in the method, the simplest being called (F)HNC, followed by (F)HNC/4, (F)HNC/5, etc. HNC calculations in a wide variety of simple Bose systems by Pandharipande and Schmidt (1977) and simple Fermi systems by Zabolitzky (1977) show excellent agreement with the exact Monte Carlo integrations.

Calculations designed to solve the variational problem $\partial E_J / \partial f_J = 0$ exactly are called optimized Jastrow calculations. The optimum correlation f_{JO} has a long-range tail, i.e., $[f_{JO}(r) - 1] \propto r^{-2}$ as $r \to \infty$, for which the energy calculation is very difficult (Smith *et al.*, 1978). Lantto and Siemens (1977, 1979) have devised a method of minimizing the (F)HNC energy to obtain f_{JO}, but the long tail f_{JO} does not seem to lower the energy significantly.

The basic shortcomings of the choice of Eq. (2.6) for Ψ_J are that it does not allow for momentum dependence appropriate to interacting systems, or the complicated operator dependence indicated by the nucleon–nucleon potential (1.6). Nor does it allow for three-body or higher correlations. The simple Jastrow studies have been useful, however, as a starting point for the more sophisticated methods we describe below.

D. Green's function Monte Carlo method

The GFMC method developed by Kalos *et al.* (Kalos, 1970; Kalos *et al.*, 1974) and reviewed by Ceperley and Kalos (1978) gives an exact solution for the energy of an A-body system in a box of volume Ω. It has not been extended to nuclear matter or even to Fermi systems at present, but it is useful as a standard of comparison in Bose systems, and requires a good solution for the Jastrow Ψ_J as input.

Let R denote a multidimensional vector representing the coordinates $\mathbf{r}_1, \mathbf{r}_2, \ldots, \mathbf{r}_A$ of the A particles. The Schrödinger equation for the ground-state energy E_0 is

$$H\Psi_0(\mathrm{R}) = E_0\Psi_0(\mathrm{R}) . \tag{2.8}$$

Let Ψ_n denote the nth eigenstate corresponding to E_n, and $G(\mathrm{R}, \mathrm{R}')$ be the Green's function

$$G(\mathrm{R}, \mathrm{R}') = \sum_n \frac{|\Psi_n(\mathrm{R})\rangle\langle\Psi_n(\mathrm{R}')|}{E_n} . \tag{2.9}$$

An initial guess for Ψ_0 is labeled $\Psi(0, \mathrm{R})$; the Ψ_J is used here. A series of successive improved guesses $\Psi(i, R)$ is calculated by iterating the equation

$$\Psi(i+1, \mathrm{R}) = E(i) \int G(\mathrm{R}, \mathrm{R}')\Psi(i, \mathrm{R}')d\mathrm{R}' , \tag{2.10}$$

where $E(i)$ is a normalization constant for $\Psi(i+1, \mathrm{R})$, and all the $\Psi(i, \mathrm{R})$ are assumed to be normalized. In the limit $i \to \infty$,

$$\Psi(i \to \infty, \mathrm{R}) = \Psi_0(\mathrm{R}) , \tag{2.11}$$

$$E(i \to \infty) = E_0 . \tag{2.12}$$

The $G(\mathrm{R}, \mathrm{R}')$ is actually not known, and it is not practical to solve Eq. (2.10) directly. However, one can again use the Ψ_J from the Jastrow problem to define a $\tilde{\Psi}$,

$$\Psi(i, \mathrm{R}) = \tilde{\Psi}(i, \mathrm{R})\Psi_J^{-1}(\mathrm{R}) , \tag{2.13}$$

and corresponding Green's function $\tilde{G}$,

$$\tilde{G}(\mathrm{R}, \mathrm{R}') = \Psi_J(\mathrm{R})G(\mathrm{R}, \mathrm{R}')\Psi_J^{-1}(\mathrm{R}') . \tag{2.14}$$

so that Eq. (2.10) becomes

$$\tilde{\Psi}(i+1, \mathrm{R}) = E(i) \int \tilde{G}(\mathrm{R}, \mathrm{R}')\tilde{\Psi}(i, \mathrm{R}')d^3\mathrm{R}' . \tag{2.15}$$

The $\tilde{G}(\mathbf{R},\mathbf{R}')$ is still not known, but it can be sampled in a Monte Carlo fashion, and very accurate energies are obtained after about forty iterations of Eq. (2.15). The practical necessity of using $\tilde{\Psi},\tilde{G}$ is where the limitation to Bose systems comes in. Whereas Ψ_J will always be positive definite in a Bose system, it can have nodes in a Fermi system causing Ψ_J^{-1} in Eqs. (2.13) and (2.14) to blow up. Whether or not this difficulty can be overcome in the future is not clear.

E. Correlated basis perturbation theory

A perturbation theory has been developed by Feenberg (1969) and collaborators [see the recent review by Clark (1978)] that gives a prescription for improving on the Jastrow E_J. If $\mathcal{G}$ is a suitable many-body correlation operator and $|\Phi_m\rangle$ is the complete set of ideal gas states, then the set $|\Psi_m\rangle$,

$$|\Psi_m\rangle = \mathcal{G}|\Phi_m\rangle\langle\Phi_m|\mathcal{G}^\dagger\mathcal{G}|\Phi_m\rangle^{-1/2}, \tag{2.16}$$

is a normalized, complete, but nonorthogonal set of "correlated basis functions." A formal perturbation expansion can be made for the exact ground-state energy E, which to second order is given by

$$E=\langle\Psi_0|H|\Psi_0\rangle-\sum_{m\neq 0}\frac{|\langle\Psi_m|H|\Psi_0\rangle-\langle\Psi_0|H|\Psi_0\rangle\langle\Psi_m|\Psi_0\rangle|^2}{\langle\Psi_m|H|\Psi_m\rangle-\langle\Psi_0|H|\Psi_0\rangle}. \tag{2.17}$$

Here the subtracted part in the numerator of the second term corrects for the nonorthogonality of $|\Psi_m\rangle$. If $\mathcal{G}$ is just the usual Jastrow choice (2.6) then $\langle\Psi_0|H|\Psi_0\rangle=E_J$. We also see that the second-order perturbation correction in Eq. (2.17) always lowers the energy below the variational result.

The disadvantage of this treatment is that its convergence is difficult to establish; no third-order perturbation terms have ever been calculated, and the second-order terms must be approximated at a small-cluster level. The most extensive calculations to date have been done on the Bose liquid ^{4}He by Chang and Campbell (1977) where the only Ψ_m used are

$$\Psi_0=\Psi(0)=N(0)\prod_{i<j}f_J(r_{ij}),$$

$$\Psi_2=\Psi(m,-m)=N(m,-m)\prod_{i<j}f_J(r_{ij})\times\sum_{i,j}\exp(i\mathbf{k}_m\cdot\mathbf{r}_i-i\mathbf{k}_m\cdot\mathbf{r}_j),$$

$$\Psi_3=\Psi[m,n,-(m+n)]=N[m,n,-(m+n)]\prod_{i<j}f_J(r_{ij})\times\sum_{i,j,k}\exp(i\mathbf{k}_m\cdot\mathbf{r}_i+i\mathbf{k}_n\cdot\mathbf{r}_j-i(\mathbf{k}_m+\mathbf{k}_n)\cdot\mathbf{r}_k). \tag{2.18}$$

The N functions are normalization constants, Ψ_2 is a "two-phonon" state with zero total momentum, and Ψ_3 is a "three-phonon" state. (The corresponding "one-phonon" state Ψ_1 is not used because it cannot conserve momentum.) When placed in Eq. (2.17) the perturbation correction due to Ψ_2 can be used to optimize the f_J; in fact its contribution is zero when f_{JO} is used. The three-phonon term Ψ_3 essentially introduces three-body correlations, which are of course absent in Ψ_J. In nuclear matter the perturbation correction in Eq. (2.17) to date has only been evaluated at the two-phonon level (Kürten *et al.*, 1978, 1979).

F. Correlation operator method

Let F_{ij} be a general operator that acts on the degrees of freedom of particles i and j. The variational wave function is then of a generalized Jastrow form,

$$\Psi_{SP}=\left\{S\prod_{i<j}F_{ij}\right\}\Phi, \tag{2.19}$$

where a symmetrized product is required because F_{ij} and F_{ik} may not commute. The F_{ij} includes the Jastrow $f_J(r_{ij})$ plus other terms that help to overcome the limitations of the simple Jastrow choice.

Pandharipande (1978) has found that a very good choice for F in liquid helium is

$$F_{ij}^H=f_J(r_{ij})+\eta(r_{ij})\mathbf{r}_{ij}\cdot\nabla_{ij}. \tag{2.20}$$

The ∇_{ij} in Eq. (2.20) can operate either on other F_{ik} or on Φ. This is a generalization of the wave function used by Pandharipande and Itoh (1973) to explain the effective mass of a ^{3}He impurity in liquid ^{4}He. For this case the conventional Jastrow choice would be

$$\Psi(k_j)=\prod_m f_J(r_{jm})\prod_{m<n}f_J(r_{mn})\exp[i\mathbf{k}_j\cdot\mathbf{r}_j], \tag{2.21}$$

where j specifies the ^{3}He impurity. The effective mass m^* of the impurity is defined by

$$\lim_{k_j\to 0}\frac{\partial}{\partial k_j}\frac{\langle\Psi(k_j)|H|\Psi(k_j)\rangle}{\langle\Psi(k_j)|\Psi(k_j)\rangle}=\frac{\hbar^2}{m^*}k_j, \tag{2.22}$$

and experimentally is found to be $m^*=2.34m_3$. The two terms involving k_j in the energy expectation value are $\nabla_j f_J(r_{jm})\cdot\nabla_j\exp[i\mathbf{k}_j\cdot\mathbf{r}_j]$ and $\nabla_j^2\exp[i\mathbf{k}_j\cdot\mathbf{r}_j]$; the first gives zero contribution because f_J is spherically symmetric, while the latter gives only $\hbar^2k_F^2/2m_3$, which obviously implies $m^*=m_3$. If instead we use the F^H of Eq. (2.20) and let the ∇_{ij} operate only on the $\exp[i\mathbf{k}_j\cdot\mathbf{r}_j]$, the variational wave function becomes

$$\Psi(k_j)=\prod_m[f_J(r_{jm})+i\mathbf{k}_j\cdot\mathbf{r}_{jm}\eta(r_{jm})]\prod_{m<n}f_J(r_{mn})\exp[i\mathbf{k}_j\cdot\mathbf{r}_j]. \tag{2.23}$$

This is essentially the backflow wave function of Feynman and Cohen (1956), which describes mathematically the physical flow of ^{4}He atoms around the ^{3}He impurity. The backflow term boosts m^* to near its correct value (2.1 to 2.25 m_3 according to the potential used) through the extra kinetic piece $\nabla_j[i\mathbf{k}_j\cdot\mathbf{r}_{jm}\eta(r_{jm})f_J(r_{jm})]\cdot\nabla_j\exp[i\mathbf{k}_j\cdot\mathbf{r}_j]$. The general behavior of m^* as the liquid ^{4}He density is changed is also explained.

In addition to the generation of backflow terms, the form (2.20) for F_{ij} also allows for many-body correlations by letting the ∇_{ij} operate on other F_{ik}. To date, only three-body correlations of the type $\eta(r_{ij})\mathbf{r}_{ij}\circ\nabla_{ij}f_J(r_{ik})$ have been used, but they provide

a significant improvement over the simple Jastrow choice in liquid helium.

It has long been recognized that the F_{ij} used to describe the correlations induced by the nucleon–nucleon potential (1.6) must contain several operators, for example,

$$F_{ij}^{N} = \sum_{p} f^{p}(r_{ij}) O_{ij}^{p}, \tag{2.24}$$

where $O_{ij}^{p} = 1, (\sigma_i \cdot \sigma_j), (\tau_i \cdot \tau_j)$, etc.

At small relative momenta the F^{H} reduces to a correlation that is different in $l=0$ and 1 partial waves. Interestingly this difference can also be simulated by the spin–isospin correlations f^{σ}, f^{τ}, and $f^{\sigma\tau}$ in F^{N}. Thus F^{N} provides an approximate method of including the backflow effects contained in F^{H} at low densities.

The symmetrization of the product of F_{ij} in the wave function (2.19) increases substantially the complexity of calculating energy expectation values. The two-body correlation operator (2.24) can as well be written in the form $f_{ij}^{c}(1+u_{ij})$, where

$$u_{ij} = \sum_{p>1} \frac{f_{ij}^{p}}{f_{ij}^{c}} O_{ij}^{p}. \tag{2.25}$$

An alternative approach is the independent-pair approximation suggested by Owen (1979a), where the many-body variational wave function is taken to be

$$\Psi_{\mathrm{IP}} = \prod_{i<j} f_{ij}^{c} \left[1 + \sum_{i<j} u_{ij} + \sum_{\substack{i<j,k \\ k<l}} u_{ij} u_{kl} + \cdots \right] \Phi, \tag{2.26}$$

so that no products of noncommuting operators are included. The wave functions (2.19) and (2.26) are identical in linear terms of u_{ij}, but the former contains higher-order terms, such as $\frac{1}{2}\sum_{i,j,k}\{u_{ij}, u_{jk}\}$, which are absent in (2.26).

The chief disadvantage of the correlation operators is in the difficulty of evaluating accurately the energy expectation value or other quantities. Much of the work on this problem has gone into the generalization of the chain summation techniques developed for the simple Jastrow f_J, so that expectation values with F^{N} can be calculated. While the convergence of (F)HNC methods has been checked against accurate Monte Carlo integrations in the Jastrow case, there are no such checks at present for operator-dependent correlations. The advantages of the method are its simplicity and wide range of applicability. The method is easily applied to both Bose and Fermi systems, and can be used over a wide range of densities. It has been used successfully in studying many systems in a relatively short period of development and still has much room for improvement. The computational facilities required are miniscule compared to present-day BBG or GFMC calculations.

G. Comparison of results for simple systems

Before beginning our detailed discussion of the theory for nuclear matter, it would be worthwhile to compare the results of the various methods in simpler systems. This will point out some of the relative merits and limitations of the different approaches. We shall look at liquid ^{4}He and ^{3}He and a simple model potential, v_2, which has been widely studied.

There has been very little success in applying the BBG theory to liquid helium because of the large value of $\kappa(>0.5$ in ^{3}He), which makes convergence practically impossible. The Bose liquid ^{4}He has been studied in simple Jastrow, GFMC, CBPT, and correlation operator approaches. The results are shown in Fig. 2 for the Lennard-Jones potential due to de Boer and Michaels (1938):

$$v_{LJ}(r) = 4\varepsilon[(\sigma/r)^{12} - (\sigma/r)^{6}], \tag{2.27}$$

where $\varepsilon = 10.22\,^{\circ}$K, $\sigma = 2.556$ Å. The experimental equilibrium density is $\rho_0 = 0.365\sigma^{-3}$ and the binding energy is $E(\rho_0) = -7.14\,^{\circ}$K. The GFMC curve of Kalos (1977) has a minimum at $\rho_0 = 0.375\sigma^{-3}$ with $E(\rho_0) = -6.85\,^{\circ}$K. The GFMC results may be considered exact for v_{LJ}, and the discrepancy with experiment can be attributed to the inaccuracy of the potential.

Many variational calculations in the simple Jastrow approximation have been made; the results of Pandharipande and Schmidt (1977) are typical, yielding $\rho_0 = 0.35\sigma^{-3}$ and $E(\rho_0) = -5.9\,^{\circ}$K. The exact choice of f_J does not seem to be too critical; with reasonable but different choices of f_J Kalos *et al.* (1974), Pandharipande and Schmidt (1977), and Smith *et al.* (1978) seem to get very similar $E(\rho)$. The f_J used by Smith *et al.* should be very close to the f_{JO}. The fact that the Jastrow results lie $\simeq 1\,^{\circ}$K above the exact GFMC value is attributable largely to the lack of three-body or higher correlations in Ψ_J.

Both the CBPT and correlation operator (CO) methods include three-body effects, and their results agree quite well with the GFMC curve. The CBPT calculation of Chang and Campbell (1977) gives $\rho_0 = 0.36\sigma^{-3}$ and $E(\rho_0) = -6.6\,^{\circ}$K, while the correlation operator calculation of Pandharipande (1978) gives $\rho_0 = 0.375\sigma^{-3}$ and $E(\rho_0) = -6.7\,^{\circ}$K. There are approximations in both

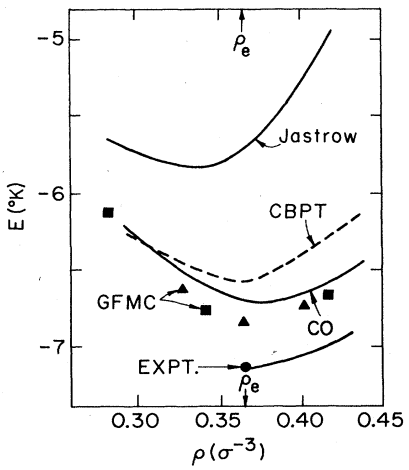

FIG. 2. The curves labeled Jastrow, CBPT, CO, GFMC, and EXPT, respectively, show the $E(\rho)$ of liquid ^{4}He obtained with Jastrow, correlated-basis perturbation theory, correlation operator, and Green's function Monte Carlo calculations with Lennard-Jones potential, and the experimental data.

of these advanced variational calculations, but the energies are probably correct to within $\simeq 0.2\,^\circ$K. It is clear that the simple inclusion of three-body correlations makes up for most of the deficiency of the simple Jastrow Ψ_J.

In liquid ^{3}He there are fewer calculations available. Jastrow and correlation operator results are shown in Fig. 3, along with the experimental $E(\rho)$ curve which has $\rho_0 = 0.277\sigma^{-3}$ and $E(\rho_0) = -2.52\,^\circ$K. The GFMC method cannot be used in Fermi systems, but since the potential for ^{3}He should be the same as in ^{4}He, we can estimate from the Bose results that v_{LJ} should underbind ^{3}He by $\simeq 0.3\,^\circ$ K, and get approximately the correct density.

The Jastrow calculation has been done with an FHNC/4 energy evaluation by Zabolitzky (1977) and by Monte Carlo integrations by Ceperley *et al.* (1977) with various kinds of parametrization for the f_J. Again the two methods agree closely, the exact choice for f_J is not critical, and the typical Jastrow results have too little binding with $E(\rho_0) = -1.2\,^\circ$K at a density $\rho_0 = 0.24\sigma^{-3}$ that is too low.

The correlation operator method has been applied recently by Schmidt and Pandharipande (1979a) with a wave function of the form

$$\Psi = \left\{ \sum_{i<j} \left(f_J(r_{ij}) + \eta(r_{ij}) \mathbf{r}_{ij} \cdot \nabla^R_{ij}\right) \sum_{i<j<k} f_3(r_{ij}, r_{jk}, r_{ki}) \right\} \Phi , \tag{2.28}$$

where the ∇^R_{ij} is only allowed to operate on Φ. The inclusion of backflow and three-body correlations lowers the $E(\rho)$ curve to near its expected value: $E(\rho_0) = -2.2\,^\circ$K, $\rho_0 = 0.29\sigma^{-3}$. However, it should be noted that the $E(\rho)$ obtained with the CO method is much too flat. This is a reflection of the difficulties associated with the calculation of the energy expectation value with the wave function (2.28). The CBPT calculations have not been done with comparable sophistication in ^{3}He.

From the liquid helium studies, it is clear that the correlation operator F^H of Eq. (2.20) is a significant improvement over the Jastrow f_J, and does a reasonable job of predicting the binding energy and density for simple systems. In the v_2 model of nuclear matter the potential is assumed to be the central part of the Reid $(^3S_1 - {}^3D_1)$ potential. It is thus similar to helium liquids, and was first studied by Pandharipande, Wiringa, and Day (1975) to compare lowest-order BBG and variational methods. It has since been studied more extensively by many authors utilizing different methods. In Fig. 4 we show Jastrow results for both Monte Carlo and FHNC energy evaluations, correlation operator results for F^H and F^N, and more recent BBG results.

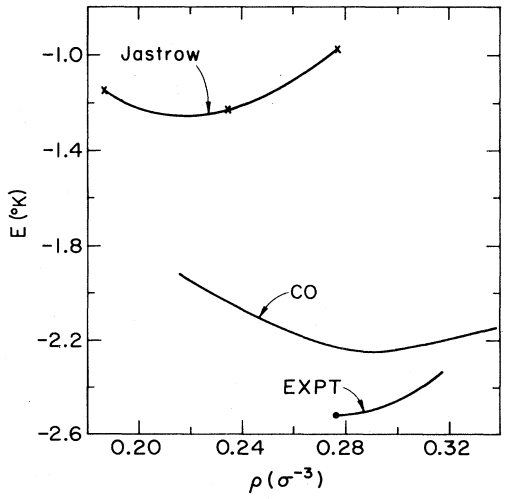

FIG. 3. The curves labeled Jastrow, CO, and EXPT, respectively, show the $E(\rho)$ of liquid ^{3}He obtained with Jastrow calculations, correlation operator calculations with Lennard-Jones potential, and the experimental data.

The Monte Carlo evaluation of Ceperley *et al.* (1977), labeled E_J(MC), was done with an f_J of the form:

$$f_J = A \exp[-Br](1 - \exp[-r/D])/r , \tag{2.29}$$

the parameters A, B, and D being varied to minimize the energy. Zabolitzky (1977) has carried out FHNC-FHNC/4 calculations with this f_J. He found the convergence to be very good up to more than twice nuclear matter density, the exact FHNC/4 energy being $\simeq 2$ MeV higher than FHNC at $\rho = 0.39$ fm^{-3}, and in agreement with the Monte Carlo evaluation. The Jastrow results, labeled J, and the F^H results are due to Schmidt and Pandharipande (1978), who use correlation functions parametrized by a healing distance. They use an approximate FHNC/4 calculation, whose error estimates are shown in Fig. 4. The F^H values are several MeV lower than the Jastrow ones throughout the density range, and indicate that v_2 is a bound system. This is a very subtle feature to pick out in view of the fact that the small energies shown in Fig. 4 are the result of a very large cancellation between kinetic and potential energy terms ($\simeq -98$ MeV potential and $+97$ MeV kinetic at $\rho = 0.39$ fm^{-3}). The lower F^H values are almost totally attributable to the $\eta \mathbf{r} \cdot \nabla$ terms rather than three-body effects.

The F^N of Eq. (2.24) has no three-body terms, but can simulate backflow at low momenta through the noncentral correlations. In this case F^N, as calculated in Sec. III, takes the simple form

$$F^N_{ij} = f^c_{ij} + f^\sigma_{ij}(\sigma_i \cdot \sigma_j) + f^\tau_{ij}(\tau_i \cdot \tau_j) + f^{\sigma\tau}_{ij}(\sigma_i \cdot \sigma_j)(\tau_i \cdot \tau_j) , \tag{2.30}$$

and $f^\sigma = f^\tau = f^{\sigma\tau}$. The F^N results lie between the Jastrow and F^H values, with roughly half the energy lowering due to the k-dependent backflow terms being picked up by F^N at nuclear matter densities. This fraction decreases as ρ increases, as would be expected. Nevertheless, the F^N is a sufficient improvement over f_J to pick out the bound feature of the v_2 model. The FHNC/SOC equations discussed in subsequent sections are used to calculate the energies with F^N, and the error in these could be comparable to that in the Jastrow calculation.

Finally there are recent calculations of Day (1978b) in which a complete three-body cluster BBG evaluation has been done. The points in Fig. 4 labeled BBG include the three-body cluster plus an estimate of the four-body cluster; the assigned error bar is ± the estimated magnitude of the four-body cluster. These results are in close agreement with the advanced vari-

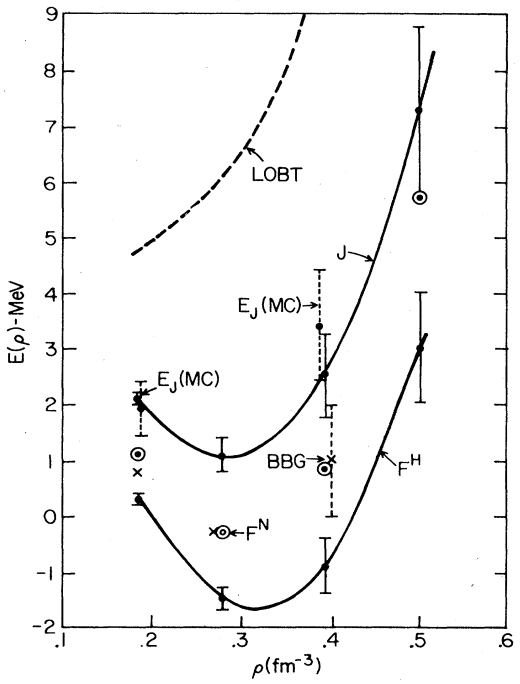

FIG. 4. The $E(\rho)$ of nuclear matter model v_2. Curves/points labeled J, F^N, and F^H show results of variational calculations with the Jastrow, F^N, and F^H correlation operators and FHNC, FHNC/4 integral equations. The E_J(MC) show exact Monte Carlo results with the Jastrow wave function. Results of lowest-order Brueckner calculations with standard spectrum are labeled LOBT, while BBG is the sum of two-, three-, and (approximate) four-hole line terms of the Brueckner–Bethe–Goldstone expansion.

ational results F^H and F^N. Also shown is the lowest-order BBG result (curve labeled LOBT), which includes only the two-body cluster contribution with the standard dispersion correction.

From the results in these simple systems, we draw the following conclusions. Variational calculations of the Jastrow type, with energy evaluated by means of chain summation techniques, give reliable upper bounds to the energy in simple Bose and Fermi systems. The use of correlation operators, which include backflow and/or three-body effects, gives lower energies than the simple Jastrow correlation, and good agreement with experiment in the liquid heliums. It has not been proved that the upper bound property is maintained when the more elaborate chain summation techniques needed for evaluation of operator-dependent correlations are used. The results in simpler systems are encouraging, however, and we believe the energy calculation can be made with reasonable accuracy.

III. CALCULATION OF F

The first step in the variational theory for nuclear matter is the selection of the correlation operator F. We discuss here a commonly used method for obtaining a reasonable correlation operator for the v_8 problem, in which v_{ij} is given by the first eight terms of Eq. (1.6). The F is assumed to be

$$F_{ij} = \sum_{p=1,8} f^p(r_{ij}) O^p_{ij}, \tag{3.1}$$

where the $f^p(r_{ij})$ are to be determined by minimizing the energy. This complicated variational problem is often simplified somewhat as follows. The two-body cluster contribution, C_2, is minimized subject to the constraint that the correlated wave function "heal" smoothly at some distance d. This constraint implies $f^c(r>d)=1$, and $f^{p>1}(r>d)=0$, and the variation gives a series of Schrödinger-type equations that include Lagrange multipliers λ^p chosen so that the $\partial f^p/\partial r$ are continuous at $r=d$. The solutions of these equations gives a set of $f^p(r_{ij},d)$ characterized by the healing distance d.

The general approach for obtaining correlation functions parametrized by the healing distance was originally developed by Pandharipande (1971, 1972) for a lowest-order constrained-variation method, and its physical assumptions have been studied by Pandharipande and Schmidt (1977). Briefly, this approach assumes that the long-range part of the potential, $v(r>d)$, only contributes to the average one-body potential, and should not be used in calculating F. It thus neglects the long-range r^{-2} component of optimal two-body correlations, which we believe is relatively unimportant in nuclear matter. The nature of F is primarily determined by $v(r<d)$, a smooth part of which must also contribute to the average field. The Lagrange multipliers λ^p essentially approximate this part by a constant. The λ^p and d are related by the requirement that Ψ be continuous.

The one-parameter family $f^p(d)$, obtained from the Schrödinger-type equations, can be generalized by multiplying each f^p by a constant factor β_p, to produce a variational F_{ij} with parameters d and β_p:

$$F_{ij}(d,\beta_p) = \sum_{p=1,8} \beta_p f^p(r_{ij},d) O^p_{ij}. \tag{3.2}$$

Normalization requires that $\beta_c=\beta_1=1$, but the $\beta_{p>1}$ may be arbitrary. The full energy $E(\rho,d,\beta_{p>1})$ is calculated and minimized with respect to variations in d and $\beta_{p>1}$ at each density.

It is convenient here to use the eight channel functions $f_{T,S}$, $f_{t,T}$, and $f_{b,T}$, where the subscripts T and S give the total isospin and spin of the pair, while t and b denote the tensor and spin–orbit parts. The potentials in the T,S channels are denoted by $v_{T,S}, v_{t,T}, v_{b,T}$. The channel functions are related to the f^p and v^p by the general equations

$$x_{T,S} = x^c + (4S-3)x^\sigma + (4T-3)x^\tau + (4S-3)(4T-3)x^{\sigma\tau}, \tag{3.3}$$

$$x_{t,T} = x^t + (4T-3)x^{t\tau}, \tag{3.4}$$

$$x_{b,T} = x^b + (4T-3)x^{b\tau}, \tag{3.5}$$

where x may be f or v. The two-body cluster energy C_2 in the van Kampen cluster expansion (1961) can also be broken into its T and S channels,

$$C_2 = \sum_{T,S} C_{2,T,S}, \tag{3.6}$$

with

$$C_{2,T,S}=\frac{(2S+1)(2T+1)}{2A\Omega^2}\sum_{k_m,k_n<k_F}\int d^3r_m d^3r_n\{\exp[-i(\mathbf{k}_m\cdot\mathbf{r}_m+\mathbf{k}_n\cdot\mathbf{r}_n)]-(-1)^{T+S}\exp[-i(\mathbf{k}_m\cdot\mathbf{r}_n+\mathbf{k}_n\cdot\mathbf{r}_m)]\}$$
$$\times[f_{T,S}+\delta_{S1}(f_{t,T}S_{mn}+f_{b,T}(\mathbf{L}\cdot\mathbf{S})_{mn})][(-\hbar^2/m)(\nabla^2_{mn}+k^2_{mn})+v_{T,S}+\delta_{S1}$$
$$\times(v_{t,T}S_{mn}+v_{b,T}(\mathbf{L}\cdot\mathbf{S})_{mn})]$$
$$\times[f_{T,S}+\delta_{S1}(f_{t,T}S_{mn}+f_{b,T}(\mathbf{L}\cdot\mathbf{S})_{mn})]\exp[i(\mathbf{k}_m\cdot\mathbf{r}_m+\mathbf{k}_n\cdot\mathbf{r}_n)]\,. \tag{3.7}$$

The ∇^2_{mn} operates only on the relative coordinate $\mathbf{r}_{mn}=(\mathbf{r}_m-\mathbf{r}_n)$, and $\mathbf{k}_{mn}$ is the relative momentum $\frac{1}{2}(\mathbf{k}_m-\mathbf{k}_n)$; k^2_{mn} is subtracted here to eliminate the one-body contribution from ∇^2_{mn} operating on the plane waves.

In the $S=0$ channels the tensor and spin–orbit potentials and correlations do not contribute. In this case we find, after doing the k summations and integrating over $\mathbf{R}_{mn}=\frac{1}{2}(\mathbf{r}_m+\mathbf{r}_n)$, that

$$C_{2,T,0}=\frac{(2T+1)}{32}\rho\int d^3r_{mn}\,\phi_{T,0}f_{T,0}$$
$$\times(-(\hbar^2/m)[\phi_{T,0}\nabla^2 f_{T,0}+2\nabla\phi_{T,0}\cdot\nabla f_{T,0}]$$
$$+v_{T,0}f_{T,0}\phi_{T,0}), \tag{3.8}$$

where

$$\phi_{T,S}=[1-(-1)^{T+S}l^2(k_Fr)]^{1/2}. \tag{3.9}$$

The $l(x)$ is the familiar Slater function,

$$l(x)=3[\sin(x)-x\cos(x)]/x^3. \tag{3.10}$$

Minimization of Eq. (3.8) with the healing constraint

$$f_{T,0}(r\geq d)=1, \tag{3.11}$$

gives the Euler–Lagrange equation

$$-(\hbar^2/m)[\phi_{T,0}\nabla^2 f_{T,0}+2\nabla\phi_{T,0}\cdot\nabla f_{T,0}]$$
$$+(v_{T,0}-\lambda_{T,0})f_{T,0}\phi_{T,0}=0 \tag{3.12}$$

where $\lambda_{T,0}$ is adjusted so that

$$\left.\frac{\partial f_{T,0}}{\partial r}\right|_{r=d}=0. \tag{3.13}$$

The $S=1$ channels are more complicated because of the tensor and spin–orbit potentials and correlations. A study of the possible operator products shows that the only terms with nonzero contributions in the integral (3.7) are accompanied by either the unit operator or $\mathbf{L}^2$. A procedure similar to that for $S=0$ states leads to three coupled equations for $f_{T,1}, f_{t,T}, f_{b,T}$:

$$\frac{-\hbar^2}{m}[\phi_{T,1}\nabla^2 f_{T,1}+2\nabla\phi_{T,1}\cdot\nabla f_{T,1}]+(v_{T,1}-\lambda_{T,1})f_{T,1}\phi_{T,1}$$
$$+8(v_{t,T}-\lambda_{t,T})f_{t,T}\phi_{t,T}+\frac{2}{3}(v_{b,T}-\lambda_{b,T})\frac{\phi_{b,T}}{\phi_{T,1}}f_{b,T}\phi_{b,T}=0, \tag{3.14}$$

$$\frac{-\hbar^2}{m}\left[\phi_{t,T}\nabla^2 f_{t,T}+2\nabla\phi_{t,T}\cdot\nabla f_{t,T}-\frac{6}{r^2}f_{t,T}\phi_{t,T}\right]$$
$$+[v_{T,1}-\lambda_{T,1}-2(v_{t,T}-\lambda_{t,T})-3(v_{b,T}-\lambda_{b,T})]f_{t,T}\phi_{t,T}$$
$$+(v_{t,T}-\lambda_{t,T})f_{T,1}\phi_{T,1}-\frac{1}{12}\frac{\phi_{b,T}}{\phi_{t,T}}(v_{b,T}-\lambda_{b,T})f_{b,T}\phi_{b,T}=0, \tag{3.15}$$

$$\frac{-\hbar^2}{m}[\phi_{b,T}\nabla^2 f_{b,T}+2\nabla\phi_{b,T}\cdot\nabla f_{b,T}]+[v_{T,1}-\lambda_{T,1}-(v_{t,T}-\lambda_{t,T})$$
$$-\frac{1}{2}(v_{b,T}-\lambda_{b,T})]f_{b,T}\phi_{b,T}+(v_{b,T}-\lambda_{b,T})(f_{T,1}-f_{t,T})\phi_{b,T}=0, \tag{3.16}$$

where

$$\varphi_{t,T}=\varphi_{T,S=1}, \tag{3.17}$$

$$\varphi_{b,T}=[(k_F^2r^2/5)+(-1)^T r l l']^{1/2}. \tag{3.18}$$

The $\lambda_{T,1}$, $\lambda_{t,T}$, and $\lambda_{b,T}$ are chosen so that $f_{T,1}$ heals smoothly to unity and $f_{t,T}$ and $f_{b,T}$ go smoothly to zero at $r=d$.

If, as in most of the work described below, the $v_{b,T}$ is set to zero, i.e., the v_6 problem, then there is no $f_{b,T}$ correlation. Similarly if $v_{t,T}=0$, then there is no $f_{t,T}$. However, if a pure central potential is taken, there is still a $(-1)^{T+S}$ dependence in Eq. (3.9) which will give different $f_{T,S}$ in different T,S channels. The projected F will then have f^σ, f^τ, and $f^{\sigma\tau}$ terms, even though the potential is purely central. These terms approximately simulate the backflow discussed in Secs. II.F and II.G. In the $k\to 0$ limit the correlation operator (2.20) just gives f in $l=0$ states to be f_J and that in $l=1$ states to be $(f_J+\eta)$. For a pure central potential, the $f^\sigma=f^\tau=f^{\sigma\tau}\equiv f^x$, so that f is f^c+3f^x in odd l and f^c-5f^x in even l states. Thus at small k the operator correlation f^x can be used to get backflow effects. However, at large k the correlation operator (2.20) implies an explicit k dependence and differences between correlations in $l=0,2,4$ states, etc., which the f^x cannot simulate (see Schmidt and Pandharipande, 1978).

The projected f^p in models v_6 and v_8 of the Reid potential are shown in Figs. 5 and 6. The inclusion of $\mathbf{L}\cdot\mathbf{S}$ forces changes all the f^p because of the couplings in Eqs. (3.14)–(3.16). We note that f^c is large and infinite ranged, but the $f^{p>1}$ tend to be small and of course are of range d only. It is dangerous to draw conclusions from the magnitudes of $f^{p>1}_{ij}$ without considering the contribution of accompanying O^p_{ij}.

The chain summation methods [(F)HNC, (F)HNC/4, etc.] commonly used to calculate E in simple systems have a better convergence when used with correlations obtained from a Schrödinger equation such as (3.12) (Zabolitzky, 1977). These methods are least accurate at short distances, but since the large bare interaction is mostly canceled by the $\nabla^2 f$ term in the Schrödinger equation, this deficiency in the chain summations becomes relatively unimportant. We expect that this will also be true for the more complicated correlations in nuclear matter.

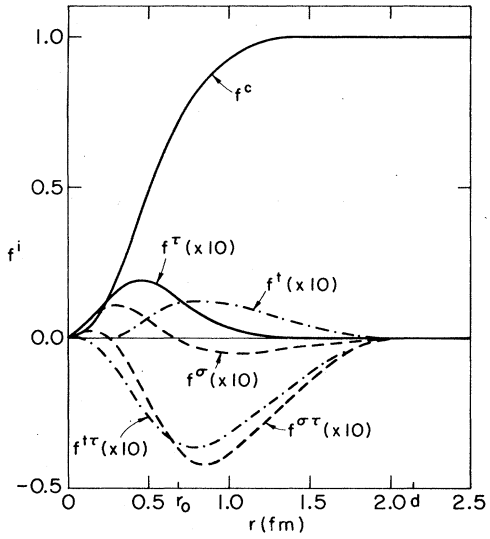

FIG. 5. The correlation functions $f^p(r,d)$ in the Reid v_6 model at $k_F=1.6$ fm^{-1} and $d=2.25r_0$.

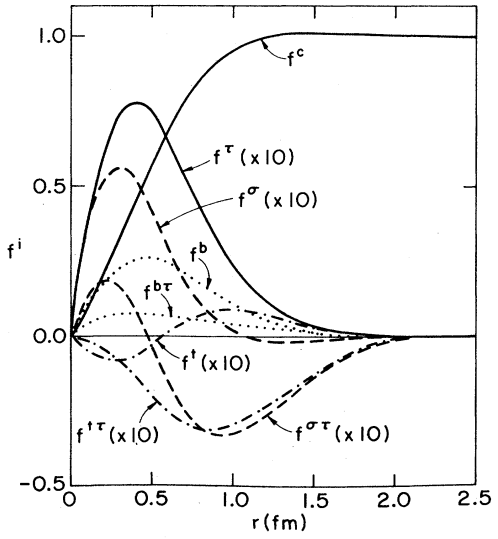

FIG. 6. The correlation functions $f^p(r,d)$ in the Reid v_8 model at $k_F=1.6$ fm^{-1} and $d=2.25r_0$.

A simpler but less sophisticated method for calculating E is by direct cluster expansion in the number of particles. Generally the expansion does not converge with the number of particles in the cluster, and so only a much more restricted class of F can be used with this method. Hoping to obtain F for which the cluster expansion is convergent, Kürten, Ristig, and Clark (1978) have introduced an additional Pauli constraint in the equations for F. Their equations are slightly more complicated than those given above.

IV. DIAGRAMMATIC CLUSTER EXPANSION

A. Expectation values and diagram rules

The many-body expectation value for any two-body operator X_{mn} is given by

$$\langle X\rangle = \sum_{m<n} \frac{\int A\left(\prod_a \phi_a^*\right) S\left(\prod_{a<b} F_{ab}^\dagger\right) X_{mn} S\left(\prod_{a<b} F_{ab}\right) \prod_a \phi_a d\tau}{\int A\left(\prod_a \phi_a^*\right) S\left(\prod_{a<b} F_{ab}^\dagger\right) S\left(\sum_{a<b} F_{ab}\right) \prod_a \phi_a d\tau}, \tag{4.1}$$

where for simplicity we antisymmetrize only the left-hand side Ψ^*. The ΠF_{ab} is of course symmetrized because the F_{ab} do not commute. It is impossible to evaluate Eq. (4.1) exactly for an infinite system, so the expression is approximated by expanding the ΠF^2 in the integrals for both numerator and denominator in powers of the short-ranged functions, $F_{ab}^c, F_{ab}^{p>1}, f_{ab}^{p>1}f_{ab}^{q>1}$, where

$$F_{ab}^c = F_{ab}^1 = f_{ab}^{c2} - 1, \quad F_{ab}^{p>1} = 2f_{ab}^c f_{ab}^{p>1}. \tag{4.2}$$

(From this point on we assume each $f_{ab}^{p>1}$ has an implicit factor of $\beta_{p>1}$ associated with it.) This expansion is conveniently represented by generalized Mayer diagrams, and a very general diagrammatic cluster expansion is given in Wiringa and Pandharipande (1978). The expansion is valid for noncommuting operators of the type used in nuclear matter or others such as those used in helium [Eq. (2.20)]. We first give the diagram rules, and then the derivation of the expansion.

A typical diagram representing one of the integrals in the expansion will have i points, each standing for the coordinates $\mathbf{r}_i$ of particle i. An integration over all $\mathbf{r}_i$ is implied. The points are connected by the various lines shown in Fig. 7, that represent the f^p, exchange effects due to the antisymmetrized Ψ^*, and the effects of the two-body operator X_{mn}. The operator of primary interest will of course be the Hamiltonian (1.9). Any F_{ab} not operated on by X_{mn} is called a passive correlation, and all passive f_{ab}^{c2} are replaced by $1+F_{ab}^c$. The f_{mn}^c is not treated this way because X_{mn} may be singular, as in the case of the potential. The F_{ab}^c are represented by dashed lines, the $F_{ab}^{p>1}$ by single wavy lines, and the $f_{ab}^{p>1}f_{ab}^{q>1}$ by doubly wavy lines. The single (double) wavy lines are labeled with the operator index $p(pq)$ associated with them. Thus every wavy line indicates the presence of an operator-dependent link.

The F that are operated on by X_{mn} are called interacting correlations. This generally includes F_{mn}, and perhaps F_{ma} or F_{na} as in the case of a ∇_m^2 or ∇_n^2 in the Hamiltonian. We separate out those terms where X_{mn} only operates on F_{mn}, and represent the quantity $F_{mn}X_{mn}F_{mn}$ by a thick solid line, called an interaction line, with indices i,j,k where j is associated with the operator dependence of X_{mn}, and i and k with the operator dependence of the $F_{mn}^\dagger$ and F_{mn}, respectively. Those terms where X_{mn} operates on quantities other than F_{mn} are treated separately. In particular, the ∇_m^2 term in the Hamiltonian can operate to give $\nabla_m F_{mn} \circ \nabla_m \phi_m$ or $\nabla_m F_{mn} \cdot \nabla_m F_{ma}$. In this case the $\nabla_m F$ are represented

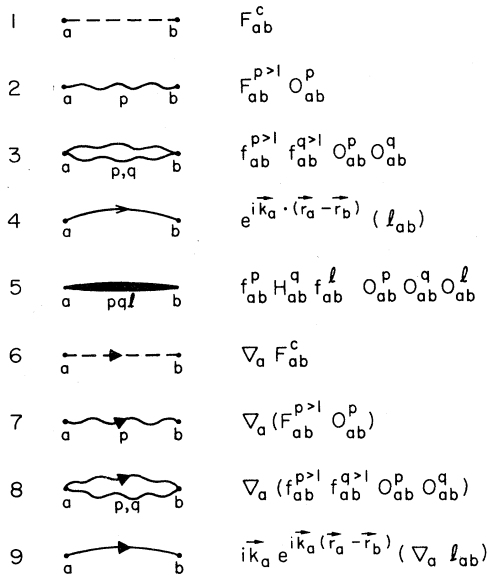

FIG. 7. The elements in the diagrams giving the energy expectation value. On summation over $\mathbf{k}_a$ the elements 4 and 9, respectively, give l_{ab} and $\nabla_a l_{ab}$.

by the appropriate dashed, single wavy, or double wavy lines, with a superposed solid directional arrow pointing away from point m, and we shall refer to them as derivative lines.

Since the Ψ^* is antisymmetrized, we need to keep track of the plane-wave states occupied by the particles in Ψ^*. For this we use solid lines with directions (open arrows) which are called exchange or state lines. By convention the particles $1, 2, \ldots, A$ occupy states $\mathbf{k}_1, \mathbf{k}_2, \ldots, \mathbf{k}_A$ in the Ψ. Those terms in the Slater determinant $A\Pi_a \exp[-i\mathbf{k}_a\cdot\mathbf{r}_a]$ of Ψ^* where the particles remain in the same states are called direct, and their diagrams contain no exchange lines. An exchange line going from a to b represents the contribution of a term in Ψ^* where particle b occupies state $\mathbf{k}_a$. Since each particle must end up in a definite state, all exchange lines must join to form closed loops, and only one exchange line may pass through any point. The total exchange pattern in any exchange diagram will consist of one or more nontouching exchange loops.

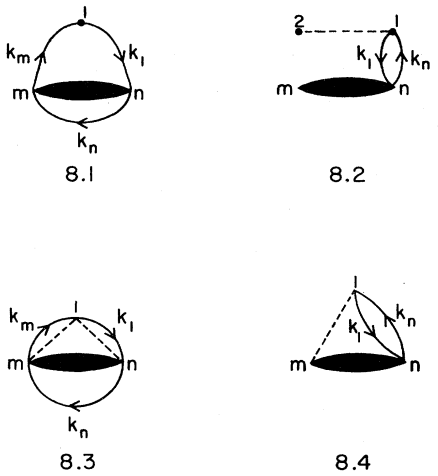

FIG. 8. Examples of proper (8.3,8.4) and improper (8.1,8.2) exchange diagrams.

The exchange of particles also involves operator-dependent terms. The exchange of particles a and b can be represented by an operator e_{ab}:

$$e_{ab} = -\tfrac{1}{4}\exp[i(\mathbf{k}_a - \mathbf{k}_b)\cdot\mathbf{r}_{ab}][1 + \sigma_a\cdot\sigma_b + \tau_a\cdot\tau_b + (\sigma_a\cdot\sigma_b)(\tau_a\cdot\tau_b)]\,. \tag{4.3}$$

An n-particle exchange loop is equivalent to a series of $(n-1)$ two-body exchanges. Thus every such loop has an associated factor of $(-1/4)^{n-1}$, and all but one of the exchange lines has an operator label n to represent $O^{n\le 4}_{ab}$. Every exchange line also has the $\exp[i\mathbf{k}_a\cdot\mathbf{r}_{ab}]$ factor.

Diagrams like 8.1, 8.2, etc. of Fig. 8, in which uncorrelated particles are exchanged, give zero contribution due to the orthogonality of plane waves. We shall refer to these as "improper" exchange diagrams. In "proper" exchange diagrams only correlated or interacting particles are exchanged; the correlations could be through other particles, as in diagram 8.4.

The summation over k's can be carried out independently for every exchange line in a "proper" exchange diagram. For example, the contribution of diagram 8.4 is given by:

$$\frac{1}{\Omega^3}\sum_{m\neq n\neq 1}\int e^{i\mathbf{k}_n\cdot\mathbf{r}_{n1}}e^{i\mathbf{k}_1\cdot\mathbf{r}_{1n}}F^c_{m1}f^i_{mn}H^j_{mn}f^k_{mn}\left\{-\frac{1}{4}\sum_{p=1,4}O^p_{n1}\right\}O^i_{mn}O^j_{mn}O^k_{mn}\,d^3r_m d^3r_n d^3r_1\,.$$

We may sum over m, n, and 1, ignoring the restriction $m\neq n\neq 1$ because the error is of order $1/\Omega$, and obtain

$$\rho^3\int l^2_{n1}F^c_{m1}f^i_{m1}H^j_{mn}f^k_{mn}\left\{-\frac{1}{4}\sum_{p=1,4}O^p_{n1}\right\}O^i_{mn}O^j_{mn}O^k_{mn}\,d^3\mathbf{r}_m d^3\mathbf{r}_n d^3\mathbf{r}_1\,,$$

for diagram 8.4. The exchange lines in "proper" diagrams simply become Slater functions on particle summation. Note that all "improper" exchange diagrams must be discarded before replacing exchange lines by Slater functions.

The $\nabla_m\phi_m\cdot\nabla_m F_{ma}$ terms in the energy expectation value give zero contribution, unless particle m is exchanged, provided F is independent of k. When the particle m is exchanged, the $\exp[i\mathbf{k}_m\cdot\mathbf{r}_{mb}]i\mathbf{k}_m\circ\nabla F_{ma}$ leads to $\nabla_m l(k_F r_{mb})\cdot\nabla_m F_{ma}$, and we mark the exchange line from m to b with a solid arrow to differentiate it from the regular exchange line. In this notation, derivative exchange and correlation lines appear in pairs, and there is an implied $\cos\theta$ dependence between the directions of the solid arrows.

The contribution of any diagram can be separated into

two factors. One is the spatial integral that contains all the functions F^c, $F^{p>1}$, X^p, $\exp[i\mathbf{k}\cdot\mathbf{r}]$, etc., represented in the diagram. The other is the operator-dependent part which we may write as $\sum_i w^i \Pi^i O^p_{ab}$ where w^i is a weight factor giving the probability that the operator product will appear in the specific order i, denoted by $\Pi^i O^p_{ab}$. The Pauli identity

$$(\sigma_1\cdot\mathbf{A})(\sigma_1\cdot\mathbf{B}) = \mathbf{A}\cdot\mathbf{B} + i\sigma_1\cdot(\mathbf{A}\times\mathbf{B}), \tag{4.4}$$

can be used to express the operator product as

$$\Pi^i\, O^p_{ab} = C^i + \text{rest}, \tag{4.5}$$

where C^i is a constant independent of spin or isospin operators, and the rest contains terms in which each σ_a or τ_a occurs at most once. Since the expectation value requires a sum over all spin–isospin states, the contribution of $\Pi^i O^p_{ab}$ is just given by C^i. In general C^i depends on the ordering of operators in $\Pi^i O^p_{ab}$, so that all possible orderings allowed by the $S\Pi F_{ab}$ must be considered in any given evaluation. We note also that any operator product due to the exchange of particles must be kept in the order indicated by the direction of the exchange. Some useful rules for calculating C parts will be given in the next section.

If there were no operator dependence in the problem then only irreducible numerator diagrams would need to be evaluated to obtain the expectation value (4.1). An irreducible diagram is a connected diagram that cannot be sliced into two disconnected pieces by cutting at a single point. It is found (see Pandharipande and Bethe, 1973) that reducible and disconnected diagrams from the numerator cancel with the denominator terms to within factors of order A^{-1}, which are negligible for infinite systems. When operators are present, however, this cancellation of diagrams which have one or more articulation points at which the diagram is separable into different pieces is not exact. The more general diagrammatic cluster expansion for use when operators are present is given below.

B. Cluster expansion

Let us divide all possible connected diagrams into two classes: interacting and noninteracting. Interacting diagrams can occur only in the numerator; they contain the interaction line X_{mn} (or two derivative lines), and an arbitrary number of correlation lines. Noninteracting diagrams can contain only correlation lines, and may appear either in the numerator or the denominator. Diagrams of both classes may have any number of "proper" exchange loops. There is a countably infinite number of diagrams in each class. Let $[I]$ denote the Ith connected diagram in the interacting class, and $[i]$ the ith connected diagram in the noninteracting class.

The expectation value is given by

$$\frac{N}{D} = \frac{[I] + [I][i] + \frac{1}{2}[I][i][j] + \cdots}{1 + [i] + \frac{1}{2}[i][j] + \cdots} = \frac{\sum_p N_p}{1 + \sum_p D_p} \equiv \sum_p E_p, \tag{4.6}$$

where we have assumed normalization $\Omega^{-1/2}$ for the plane-wave states, so that the first term of the denominator is unity, and ordered the N, $D-1$, and E in the series such that the pth term contains diagrams having p disconnected pieces. Thus N_3 contains diagrams represented by $[I][i][j]$; it is the sum of the products of diagrams I, i, and j, the summation over these being restricted so that I, i, and j do not have a common particle. Similar restrictions occur in the summation over $i_1, i_2, \ldots, i_p$ in D_p:

$$D_p = \frac{1}{p!}[i_1][i_2]\cdots[i_p] = \sum_{\substack{i_1,i_2,\ldots,i_p \\ \text{no common particles}}} \frac{1}{p!}\ \text{product of diagrams } i_1, i_2, \ldots, i_p; \tag{4.7}$$

the $1/p!$ takes care of the overcounting when $i_1\cdots i_p$ are independently summed.

In contrast a product N_pD_q, for example, is also a sum of diagrams having $p+q$ disconnected pieces, but the above restrictions do not occur. We represent such products by a multiplication symbol $\times$; for example,

$$N_1D_1 = [I]\times[i] = [I][i] + \overbrace{[I][i]} + \overbrace{[I][i]} + \cdots \tag{4.8}$$

where the number of overhead lines denotes the number of common particles,

$$\overbrace{[I][i]} = \sum_{\substack{I,i \\ \text{one common particle}}} \text{product of diagrams } I \text{ and } i. \tag{4.9}$$

In a general term shown as $[\overbrace{I][i}][\overbrace{j][k}]\cdots$ a summation over $I, i, j, k\cdots$ is implied, with the restriction that $I, i, j, k\ldots$ do not have any common particles other than those indicated by the overhead bars. The E_p are obtained by solving the set of equations

$$E_p = N_p - \sum_{q,r} D_qE_r\delta(p-r-q), \tag{4.10}$$

starting from $p=1$. This gives

$$\begin{aligned} E_1 &= [I], \\ E_2 &= [I][i] - [I]\times[i] = -\overbrace{[I][i]} - \overbrace{[I][i]} - \ldots, \\ E_3 &= \tfrac{1}{2}[I][i][j] - \tfrac{1}{2}[i][j]\times[I] + [i]\times(\overbrace{[I][j]} + \overbrace{[I][j]} + \cdots) \\ &= [\overbrace{I][i}][\overbrace{j}] + \tfrac{1}{2}[\overbrace{\overbrace{I][i}][j}] + [\overbrace{I][i}][\overbrace{j}] + [\overbrace{\overbrace{I][i}][j}] + \cdots. \end{aligned} \tag{4.11}$$

The first term in E_3 represents diagrams in which one common particle occurs in all the three pieces I, i, and j. The second term in E_3 is the sum of $-\frac{1}{2}[\overbrace{I][i}][\overbrace{j}]$ coming from D_2E_1 and $+[\overbrace{I][i}][\overbrace{j}]$ from D_1E_2. Giving a general expression for E_p is a combinatorial problem beyond the scope of this work. However, it is clear that E_p consists of terms of type

$$[\overbrace{I][i_1}][\overbrace{i_2}]\cdots[\overbrace{i_{p-1}}],$$

which are completely connected with overhead bars and have no gaps of the type shown between i_2 and i_3:

$$[\overbrace{I][i_1}][\overbrace{i_2}][\overbrace{i_3}]\cdots[\overbrace{i_{p-1}}].$$

A connected diagram having n particles has a con-

tribution proportional to Ω^{-m+1}. However, there exist $\simeq A^n$ such diagrams which have the same topology and differ only in particle labels. Thus all connected diagrams of a given topology have a contribution $\propto A\rho^{n-1}$. Disconnected diagrams of a given topology and p pieces have a contribution $\propto A^p$. An overhead line restricts the summation over one particle index, however, and reduces the contribution by a factor A^{-1}; we consider $\overbrace{\quad}$ indicating a common particle in three pieces as two overhead lines, etc. The contributions of E_p diagrams are proportional to A^{p-q} where q is the number of overhead lines. Since at least $p-1$ lines are needed to completely connect p pieces, E cannot have contributions $\propto A^{r>1}$, and in the limit $A\to\infty$ we need to consider only those terms in E_p that have $p-1$ overhead lines. This gives

$$E_{A\to\infty}=[I]-[\overbrace{I}\overbrace{i}]+\tfrac{1}{2}[\overbrace{I}\overbrace{i}\overbrace{j}]+[\overbrace{I}\overbrace{i}\overbrace{j}]+[\overbrace{I}\overbrace{i}\overbrace{j}]$$
$$+\text{four-piece terms}+\cdots . \tag{4.12}$$

Now there is a countably infinite set of inseparable diagrams containing no articulation points. The Ath (ath) inseparable interacting (noninteracting) diagram is denoted by $[A]$ ($[a]$). A connected diagram that is separable into s inseparable pieces $[I_s]$ or $[i_s]$ may be represented as

$$[I_s]=[\overbrace{A}\overbrace{a}_1\overbrace{a}_2\cdots\overbrace{a}_{s-1}], \tag{4.13}$$

where the overhead lines (which all appear inside a square bracket) now denote the articulation points at which the diagram $[I_s]$ is separable. For example, diagram 9.3 of Fig. 9 is represented by the expression $[\overbrace{Aa}]$, where the A and a denote the disconnected inseparable diagrams of 9.4. The overhead line specifies the connection of these two pieces, which yields the connected diagram. We obviously have

$$[I]=[A]+[\overbrace{Aa}]+[\overbrace{Aab}]+\tfrac{1}{2}[\overbrace{\overbrace{Aab}}]+\tfrac{1}{2}[\overbrace{Aab}]+\cdots , \tag{4.14}$$
$$[i]=[a]+\tfrac{1}{2}[\overbrace{ab}]+\cdots , \tag{4.15}$$

with which we may now order E according to the number of inseparable pieces it contains:

$$\begin{aligned}E=&[A]+\{[\overbrace{Aa}]-[\overbrace{A}][a]\}\\&+\{[\overbrace{Aab}]-[\overbrace{Aa}][\overbrace{b}]-[\overbrace{A}][\overbrace{ab}]+[\overbrace{A}][\overbrace{a}][\overbrace{b}]\}\\&+\{\tfrac{1}{2}[\overbrace{\overbrace{Aab}}]-[\overbrace{Aa}][\overbrace{b}]+\tfrac{1}{2}[\overbrace{\overbrace{A}}][\overbrace{a}][\overbrace{b}]\}\\&+\{\tfrac{1}{2}[\overbrace{Aab}]-[\overbrace{Aa}][\overbrace{b}]-\tfrac{1}{2}[\overbrace{A}][\overbrace{ab}]+[\overbrace{A}][\overbrace{a}][\overbrace{b}]\}\\&+\text{terms having}\geq 4\text{ inseparable pieces}.\end{aligned} \tag{4.16}$$

The first term in E is just $[A]$, which represents the sum of all connected inseparable interacting diagrams. The second term is the difference between the expectation value of all connected diagrams $[\overbrace{Aa}]$ that could be separated at one point into two inseparable pieces, and the product of expectation values of the two corresponding disconnected diagrams $[\overbrace{A}][\overbrace{a}]$.

The thrice-separable terms have been grouped into three categories where (i) a and b share one point in common, while A shares a different point with a; (ii) a and b have no points in common, but each shares one point with A; and (iii) a, b, and A all share one common point.

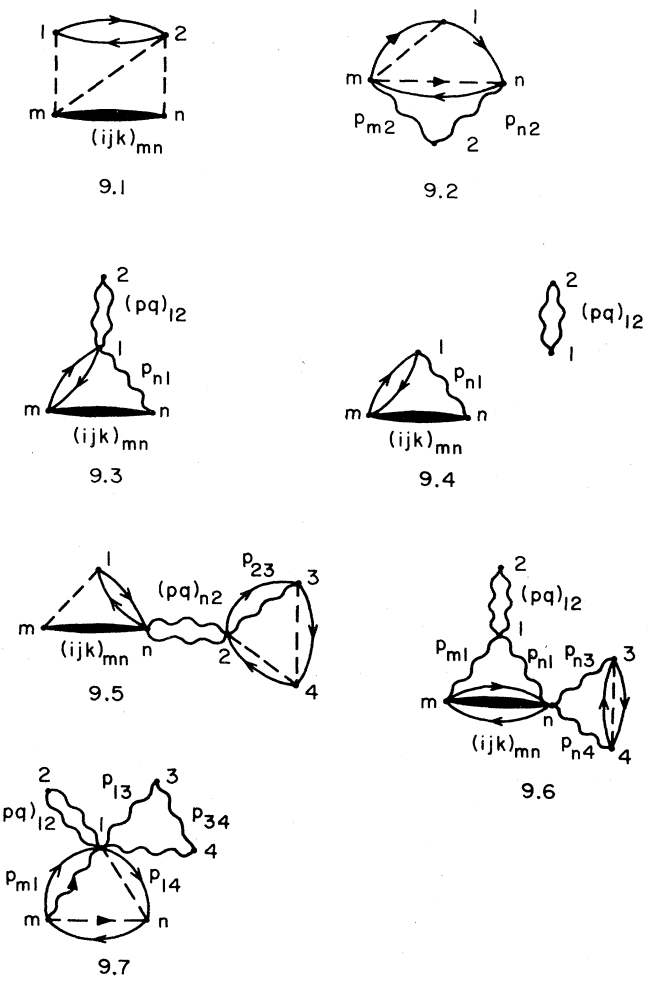

FIG. 9. Examples of diagrams in the cluster expansion of the energy expectation value.

The radial integrals of a separable diagram factorize, and thus are identical in both the separated and connected cases. When no operators are present then all terms in curly brackets are zero, and only the irreducible diagrams $[A]$ contribute to E. In this case the expansion reduces to the well-known irreducible cluster expansion. When operators are present, the additional terms may be nonzero due to the dependence of C parts on the ordering of operators in the products, which is in general different for the connected and separated cases.

C. Examples of diagrams

We discuss here some examples of different diagrams, as shown in Fig. 9, to illustrate the cluster expansion. Diagram 9.1 is a typical irreducible interacting diagram. The interaction between particles m and n is labeled with its operator dependence $(ijk)_{mn}$, while particles 1 and 2 are correlated to m and n by a number of central correlations, and exchanged with each other. Diagram 9.2 is also an irreducible interacting diagram representing a $\nabla_m F^c{}_{mn}\cdot i\mathbf{k}_m$ term. The operator correlations $F^{p>1}_{m2}$, $F^{p>1}_{n2}$ are also present and

labeled p_{m2}, p_{n2}, respectively. Both diagrams 9.1 and 9.2 are included in the class $[A]$ of Eq. (4.16).

Diagram 9.3 is a connected, separable diagram of the type $[\overbrace{Aa}]$. Point 1 is an articulation point at which the diagram could be broken into two parts, so it is reducible. The correlation $f_{12}^{p>1} f_{12}^{q>1}$ is labeled by $(pq)_{12}$, and the other operator-dependent correlations are labeled as usual; although the exchange carries operator dependence, often we do not lable it. Diagram 9.3 arises strictly from the numerator of Eq. (4.1). The separated counterpart of 9.3 is shown in diagram 9.4 and is of type $[\overbrace{A}][\overbrace{a}]$. The interacting portion containing particles $m, n, 1$ comes from the numerator of Eq. (4.1), but the separated portion with particles 1, 2 comes from the denominator. The C parts of the two separate pieces in diagram 9.4 are calculated independently, while the C part of 9.3 must be calculated all at once. In general these are different and thus the difference between $[\overbrace{Aa}]$ and $[\overbrace{A}][\overbrace{a}]$ is nonzero.

Some further examples of connected separable diagrams are shown in 9.5, 9.6, and 9.7. They are, respectively, of type $[\overbrace{Aab}]$, $[\overbrace{Aab}]$, and $[\overbrace{Aab}]$.

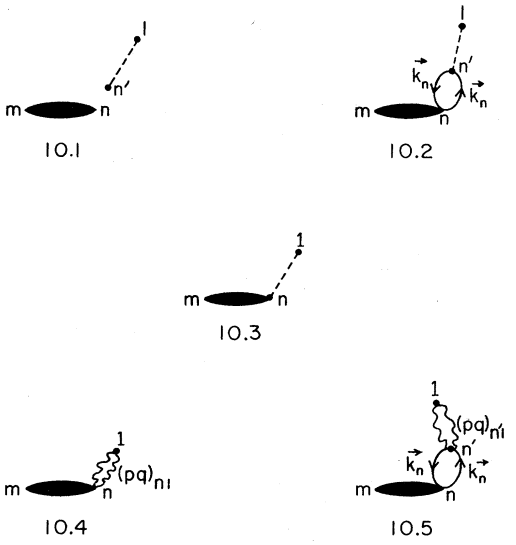

FIG. 10. Cancellation of diagrams violating the exclusion principle.

D. Other cluster expansions

There are a number of other methods for obtaining the cluster expansion with noncommuting operators. Some of these are the power-series (PS) method of Fantoni and Rosati (1978), Owen's (1979a) generalization of the method of Gaudin, Gillespie and Ripka (GGR) (1971), and factorized cluster expansions such as those of Iwamato and Yamada (1957) and van Kampen (1961). All these are presumably equivalent, as can be easily verified at the three-body cluster level.

The Iwamato and Yamada and van Kampen methods are not diagrammatic, and it is much more laborious to obtain many-body cluster contributions with them than with the other methods. The method presented above is applicable to Bose, Fermi, or Boltzmann systems, whereas the PS and the GGR methods are primarily developed for Fermi systems.

In Fermi systems we may consider diagrams having two or more particles in the same momentum state. On considering all exchanges these will add up to zero; for example, the two diagrams 10.1 and 10.2 of Fig. 10 having two particles n and n' in state $\mathbf{k}_n$, obviously cancel each other. The diagram 10.1 is essentially of type $[\overbrace{I}][\overbrace{i}]$, since n' is indistinguishable from n. When all diagrams of type 10.1 are added to the numerator, the term N_2 becomes $[I]\times[i]$. By adding terms having up to three particles in a given $\mathbf{k}$ state we can convert N_3 to $\frac{1}{2}[I]\times[i][j]$, etc. The denominator can then be canceled against all "disconnected" diagrams, as is done in the GGR and PS methods. The expectation value is given by the sum of all "connected" diagrams, but these now include reducible diagrams such as 10.3 and diagrams like 10.2 which superficially look like "improper" exchange diagrams but have nonzero contributions.

In the simple Jastrow theory the reducible diagrams are canceled by the nonzero "improper" exchange diagrams, and the resulting expansion is irreducible. However, in the presence of operator correlations, diagrams 10.4 and 10.5 do not cancel because the O_{n1} in 10.4 does not commute with O_{mn} as the $O_{n'1}$ in 10.5 does. The C parts of 10.4 and 10.5 are different, and their sum is simply a term in the $[\overbrace{Aa}]-[\overbrace{A}][\overbrace{a}]$ of Eq. (4.16).

V. CALCULATION OF C PARTS

A. Operator diagrams

In this section we review some useful rules for calculating the C^i of $\Pi^i O_{ab}^p$. We give the rules for $p=1, 6$, but they are extendible to $\mathbf{L}\cdot\mathbf{S}$ or other operators. The rules can be expressed most easily in terms of operator diagrams (OD) in which every particle a, b involved in the $\Pi^i O_{ab}^p$ is represented by a point. Every operator O_{ab}^p is represented by a line ab labeled p. The OD corresponding to any regular diagram may be obtained simply by deleting all central correlations and putting in the appropriate number of lines for every operator-dependent leg, e.g., three lines for the interaction line $f_{mn}^i X_{mn}^j f_{mn}^k$ labeled i, j, and k. The OD do not specify the order of operators in $\Pi^i O_{ab}^p$; these must be considered explicitly if necessary.

A sample of the kinds of operator diagrams that we shall evaluate in this work is shown in Fig. 11. Diagram 11.1 is just the operator diagram for the direct two-body interaction, either by itself or with various central dressings added. It is the operator diagram appropriate to the full diagram 9.1. Similarly the OD 11.2 corresponds to diagram 9.2.

For an OD to have a nonzero C part, at least two operator lines must meet at each point. This is because single operators $O_{ab}^{p>1}$ are linear in σ_a and/or τ_a. If a point is connected to only one operator line, the sum over the spin and isospin coordinates at that point will vanish identically and the OD will give no contribution. If only two operator lines meet at a given point, they must be of the same "type" to give a nonzero C part. For the operators 2–6 there are only three types,

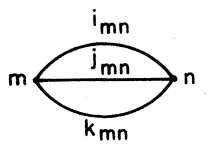

11.1

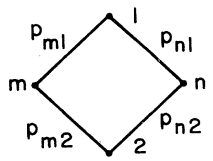

11.2

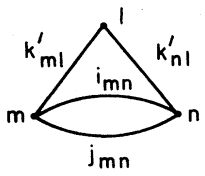

11.3

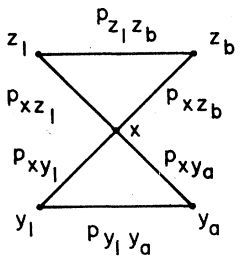

11.4

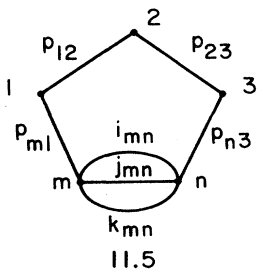

11.5

FIG. 11. Examples of operator diagrams.

which we denote as σ, τ, and ν. They are linear in the σ_a, τ_a, and $\sigma_a\tau_a$, respectively. Obviously O^σ and O^t are σ-type, O^τ is τ-type, and $O^{\sigma\tau}$ and $O^{t\tau}$ are ν-type.

Consider an operator diagram in which two points are joined by a pair of operator lines p_{12}, q_{12} and no other operator lines are present. This would be the OD corresponding to the separated, noninteracting piece of diagram 9.4. The C part of the product of these two operators is a simple constant A^p,

$$C(O^p_{12}O^q_{12}) = A^p\delta_{pq}, \tag{5.1}$$

where $A^p = 1, 3, 3, 9, 6, 18$ for $p = 1, 6$.

If three or more operator lines meet at a point, as in the OD 11.1, the C part may be easily evaluated with the K^{pqr} matrix defined as follows:

$$O^p_{ab}O^q_{ab} = \sum_r K^{pqr}O^r_{ab}. \tag{5.2}$$

Comparing Eqs. (5.1) and (5.2) we find that $K^{pq1} = A^p\delta_{pq}$. The C part of the OD 11.1 is then easily evaluated:

$$C(O^i_{mn}O^j_{mn}O^k_{mn}) = C\left(\sum_l K^{ijl}O^l_{mn}O^k_{mn}\right) = K^{ijk}A^k. \tag{5.3}$$

The K^{ijk} is particularly simple for the $O^{p=1,6}$ because they form a closed set. If $i, j \leq 6$, then for $k > 6$, $K^{ijk} = 0$. The order of operators in Eq. (5.3) does not matter, and we find trivially that $K^{ijk}A^k = K^{jik}A^k = K^{jki}A^i$, etc. This is simply because operators $O^{p=1,6}$ between the same two points commute with each other. The values of K^{ijk} for $i, j, k \leq 6$ are given in Table I.

B. Single-operator rings

The order of operators in the $\Pi^i O^p_{ab}$ is also unimportant for determining the C part if the operators form a single-operator ring (SOR) as in diagram 11.2 of Fig. 11. This case was first discussed by Pandharipande and Wiringa (1976). The ring may be arbitrarily large, but of course to get a nonzero C part all the operators must be of the same type. That the order is unimportant can be proved simply by noting that

$$C\{O(^p12)O(^p23)\cdots[O(^pab), O(^pbc)]\cdots O[^p(n-1)n]O(^pn1)\} = 0. \tag{5.4}$$

Here we denote O^{pab}_{ab} as $O(^pab)$ for convenience. The commutator in Eq. (5.4) will be linear in either σ_b or τ_b, thus making the C part zero. Of course operators with completely different indices commute anyway, i.e., $[O^p_{ab}, O^q_{cd}] = 0$. Thus in practice, if only two operators connect at a point b, they effectively commute for the purpose of calculating the C part.

Further, we can use the Pauli identity (4.4) to eliminate completely the operator dependence on point b. Let O^p_{ab} and O^q_{bc} be the only two operators meeting at b. Summing over spin and isospin states for particle b, and integrating over the azimuthal angle ϕ of $\mathbf{r}_{ab}$, the product of operators $O^p_{ab}O^q_{bc}$ reduces to a sum over operators O^r_{ac}:

$$\sum_{\sigma_b,\tau_b}\int d\phi_b O^p_{ab}O^q_{bc} = \sum_r \int d\phi_b \xi^{pqr}_{abc}O^r_{ac}. \tag{5.5}$$

The coefficients ξ^{pqr}_{abc} are functions of the inside angles of the triangle abc, and are zero unless the operators are of the same type:

$$\xi^{\sigma\sigma r}_{abc} = \delta_{\sigma r}, \tag{5.6}$$

$$\xi^{\sigma t r}_{abc} = \delta_{tr}\tfrac{1}{2}(3\cos^2\theta_c - 1), \tag{5.7}$$

$$\xi^{t\sigma r}_{abc} = \delta_{tr}\tfrac{1}{2}(3\cos^2\theta_a - 1), \tag{5.8}$$

$$\xi^{ttr}_{abc} = \delta_{\sigma r}(3\cos^2\theta_b - 1) + \delta_{tr}\tfrac{1}{2}[-9\cos\theta_a\cos\theta_b\cos\theta_c - 3(\cos^2\theta_a + \cos^2\theta_b + \cos^2\theta_c) + 2], \tag{5.9}$$

$$\xi^{\tau\tau r}_{abc} = \delta_{\tau r}. \tag{5.10}$$

The ξ^{pqr}_{abc} for p and q of type ν are given by

$$\xi^{(p\tau)(q\tau)(r\tau)}_{abc} = \xi^{pqr}_{abc}; \quad p, q, r = \sigma, t. \tag{5.11}$$

The ability to thus reduce a product of two operators with a common point to just one operator and some simple radial dependence makes it very easy to calculate the C part for any SOR. Because the order of operators does not matter, we may simply arrange them in a continuous fashion, e.g., $O(^pab)O(^pbc)O(^pcd)\ldots$, and then successively contract pairs of operators over their common points. Every contraction will give a ξ function, and eventually we reach the final two operators which must have both points in common. These give a final factor of A^p.

TABLE I. The matrix K^{ijk} for $O^{p=1,6}$.

	i \ j	1	2	3	4	5	6
$k=1$	1	1					
	2		3				
	3			3			
	4				9		
	5					6	
	6						18
$k=2$	1		1				
	2	1	−2				
	3				3		
	4			3	−6		
	5					2	
	6						6
$k=3$	1			1			
	2				3		
	3	1		−2			
	4		3		−6		
	5						6
	6					6	−12
$k=4$	1					1	
	2				1	−2	
	3		1			−2	
	4	1	−2	−2	4		
	5						2
	6					2	−4
$k=5$	1					1	
	2					1	
	3						3
	4						3
	5	1	1			−2	
	6			3	3		−6
$k=6$	1						1
	2						1
	3					1	−2
	4					1	−2
	5				1	1	−2
	6	1	1	−2	−2	−2	4

The total C part will just be A^p times the product of ξ functions. For example, Eq. (5.10) indicates that a τ-type SOR always has a C part of 3, regardless of how many operator links are present.

C. Multiple-operator diagrams

In diagrams 11.3 and 11.4 the order of operators does matter in determining the C part of $\Pi^i O^p_{ab}$. For any given order, however, it is relatively simple to calculate the C part, and one must then simply multiply in the appropriate weights w^i for the different orderings possible to get the total C part. Operator diagrams of type 11.3 and 11.4, and generalizations of these, are important in nuclear matter, so we discuss them in detail.

First we prove a very useful theorem: the C part of a product of operators of type $p=1, 6$ is unchanged by cyclic permutations of the operators. That is,

$$C\left[O(^pab)\prod O(^pij)\right]=C\left[\prod O(^pij)O(^pab)\right], \tag{5.12}$$

where $\Pi O(^pij)$ is any series of operators. This can be seen quickly in the case that $O(^pab)=\tau_a\cdot\tau_b$. The most general form for the $\Pi O(^pij)$ is

$$\prod O(^pij)=\text{terms independent of } \tau_a \text{ and } \tau_b$$
$$+\text{terms linear in } \tau_a \text{ and/or } \tau_b, \text{ and other } \tau_i$$
$$+\text{terms linear in } \tau_a\cdot\tau_b. \tag{5.13}$$

Clearly $O(^pab)$ commutes with the last portion of Eq. (5.13), while the product with the other terms will not have any C part. The argument can be easily extended to σ- and ν-type operators.

As a consequence of this theorem, there will be only two different orders for the operators in the OD 11.3. There is a "successive" order in which the $O(^imn)$ and $O(^jmn)$ can be placed adjacent to each other, and an "alternate" order in which they are separated by $O(^{k'}m1)$ or $O(^{k''}n1)$. In the first case we may replace the two mn operators with a $\sum_k K^{ijk}O(^kmn)$, reducing the product to an SOR with three operators. The C part is then given by

$$\int d\phi_1 C(O^i_{mn}O^j_{mn}O^{k'}_{m1}O^{k''}_{n1})=\sum_k K^{ijk}A^k\int d\phi_1\xi^{k'k''k}_{m1n}. \tag{5.14}$$

The C part in the alternate order is defined as

$$\int d\phi_1 C(O^i_{mn}O^{k'}_{m1}O^j_{mn}O^{k''}_{n1})=\sum_k L^{ijk}\int d\phi_1\xi^{k'k''k}_{m1n}. \tag{5.15}$$

The L^{ijk} is trivially related to the product $K^{ijk}A^k$:

$$L^{ijk}=\pm A^kK^{ijk}. \tag{5.16}$$

The + sign applies if

$$C(O^i_{mn}[O^j_{mn},O^{k'}_{m1}]O^{k''}_{n1})=0, \tag{5.17}$$

and the − sign if

$$C(O^i_{mn}\{O^j_{mn},O^{k'}_{m1}\}O^{k''}_{n1})=0. \tag{5.18}$$

TABLE II. The matrix L^{ijk} for $O^{p=1,6}$.

	i	j	1	2	3	4	5	6
$k=1$	1		1					
	2			3				
	3				3			
	4					9		
	5						6	
	6							18
$k=2$	1				3			
	2		3		6			
	3						9	
	4					9	18	
	5							−6
	6							−18
$k=3$	1				3			
	2					9		
	3		3		6			
	4			9		18		
	5							18
	6						18	36
$k=4$	1						9	
	2					9	18	
	3				9		18	
	4		9	18	18	36		
	5							−18
	6						−18	−36
$k=5$	1						6	
	2						−6	
	3							18
	4							−18
	5		6	−6			12	
	6				18	−18		36
$k=6$	1							18
	2							−18
	3						18	36
	4						−18	−36
	5					18	−18	36
	6		18	−18	36	−36	36	72

It can be verified that either Eq. (5.17) or Eq. (5.18) is always true, and if both are true, the L^{ijk} and K^{ijk} are both zero. The values of L^{ijk} are given in Table II. Any diagram having a number of operator lines between two points, plus a single-operator chain (SOC) connecting the same two points, as in diagram 11.5, can have its C part expressed in terms of the matrices A, K, L, and ξ.

Diagram 11.4 is of interest because of the diagrammatic expansion (4.16). There we found that terms like $[\overbrace{Aa}] - [\overbrace{A}][\overbrace{a}]$ must be calculated, and the OD 11.4 is representative of any separable diagram which has two SOR touching at the separable point. One ring will contain the interacting particles, one of which could be the common point, and the other will be noninteracting. We label these rings Y and Z, respectively, and the common point is x. The SOR Y in diagram 11.4 just contains x, y_1, and y_a, but in general there could be many particles y_2, y_3, etc., forming a single-operator chain between y_1 and y_a, or alternatively y_1 and y_a could be the same point. Similarly, a general SOR for Z would contain $x, z_1, \ldots, z_b$.

Although the spatial integrals of Y and Z are the same in both the connected ($[\overbrace{Aa}]$) and the separated ($[\overbrace{A}][\overbrace{a}]$) diagrams, the C parts can be different. For convenience we define the C part of a separable diagram to be the difference between the C parts of the connected and separated diagrams.

Let C_y and C_z denote the C parts of Y and Z when they are separated:

$$C_y = C\left\{O(^pxy_1)\left[\prod_{j=1,a-1} O(^py_j\,y_{j+1})\right]O(^py_ax)\right\}, \tag{5.19}$$

$$C_z = C\left\{O(^pxz_1)\left[\prod_{j=1,b-1} O(^pz_jz_{j+1})\right]O(^pz_bx)\right\}. \tag{5.20}$$

The C part of the separated diagram is C_yC_z. That of the unseparated diagram depends upon the order of the four operators $O(^pxy_1)$, $O(^py_ax)$, $O(^pxz_1)$, and $O(^pz_bx)$, which meet at the common vertex x. We may successively sum over the spin and isospin of particles $y_1, y_2, \ldots, y_{a-1}$ and reduce the $O(^pxy_1)\Pi_{j=1,a-1}O(^py_j\,y_{j+1})$ to a second operator $O(^pxy_a)$ at the position of the operator $O(^pxy_1)$, with a coefficient $C_y/A(^pxy_a)$. [We write A^q as $A(q)$ when q has subscripts.] Doing the reduction for Z also gives

$$C(\text{unseparated}) = [C_yC_z/A(^pxy_a)A(^pxz_b)] \times C[:O(^pxy_a)O(^py_ax)O(^pxz_b)O(^pz_bx):] \tag{5.21}$$

where the four operators between the :: are to be taken in the order in which $O(^pxy_1)$, $O(^py_ax)$, $O(^pxz_1)$, and $O(^pz_bx)$ occur in the unseparated diagram.

The $C[:O(^pxy_a)O(^py_ax)O(^pxz_b)O(^pz_bx):]$ has only two distinct values. The first equals $A(^pxy_a)A(^pxz_b)$ and is obtained in the case of four possible "successive" orders in which two $O(^pxy_a)$ and/or $O(^pxz_b)$ occur successively and thus can be squared. In the remaining two "alternating" orders of type $O(^pxy_a)O(^pxz_b)O(^py_ax)O(^pz_bx)$ the $C(::)$ may be expressed simply as a function of the symmetric matrix D_{ij},

$$\sum_{\sigma_c,\tau_c} O^i_{ac}O^j_{ab}O^k_{ac} = \delta_{ik}A^i(1+D_{ij})O^j_{ab}. \tag{5.22}$$

In the case of tensor operators the above equation as-

sumes an integration over the angle between $\mathbf{r}_{ac}$ and $\mathbf{r}_{ab}$. The value of D_{ij} depends only on the types of operators involved:

$$D_{\sigma\tau}=0\,,\quad D_{\nu\nu}=-8/9\,,$$
$$D_{\sigma\sigma}=D_{\tau\tau}=D_{\sigma\nu}=D_{\tau\nu}=-4/3\,. \tag{5.23}$$

Thus the $C(::)$ for alternating order equals $(1+D_{yz})A(^{p}xy_a)A(^{p}xz_b)$ where y and z are the types of operators in the SOR Y and Z.

The operators in $C(::)$ can occur in various orders in the connected diagram. Let m be the probability of their occurring in the alternating order. The C part of the separable diagram is then given by $\mathrm{m}\,D_{yz}C_yC_z$. For evaluating the expectation value (4.1) with the diagrammatic expansion (4.16), such separable diagrams may be treated as vertex corrections of magnitude

$$\mathrm{m}\,D_{yz}\times\text{contribution of ring } Z\,, \tag{5.24}$$

to the SOR diagram Y at its vertex x.

As an example, we illustrate the calculation of m for the diagram 9.3 in the case where $O(^{t}mn)=O(^{k}mn)=1$. The operators p_{12} and q_{12} associated with the $f_{12}^{p>1}f_{12}^{q>1}$ must be identical or the C part will be zero. One $O(^{p}12)$ comes from Ψ^* and the other from Ψ, while $O(^{p}n1)$ may come from either Ψ^* or Ψ. The $O(^{p}m1)$ associated with the exchange occurs at the far left where the Ψ^* is antisymmetrized, while the interaction operator for particles m and n, $O(^{p}mn)$, must come in the middle. The possible operator orders are then obtained from:

$$\tfrac{1}{2}O(^{p}m1)[\tfrac{1}{2}\{O(^{p}12),O(^{p}n1)\}\,O(^{p}mn)O(^{p}12)$$
$$+\tfrac{1}{2}O(^{p}12)O(^{p}mn)\{O(^{p}12),O(^{p}n1)\}]\,, \tag{5.25}$$

where the outside factor $\frac{1}{2}$ compensates for the factor 2 in the definition of $F(^{p}n1)$, and the other factors of $\frac{1}{2}$ account for the normalization of SΠF. By inspection of Eq. (5.25) the probability of alternating order m is $\frac{1}{2}$ in this case.

In general m depends upon the source of the four operators that meet at the vertex x. The possible sources are the v, F, and the exchange. The operator from v defines the center. An operator associated with a single wavy line $F^{p>1}$ can be on either side of the center with equal probability. The two operators associated with a double wavy line $f^{p>1}f^{q>1}$ must be on opposite sides of the center. An operator from the exchange must always appear on the extreme left, where Ψ^* is antisymmetrized.

The possible types of the common vertex x can be described by four variables, x_t, x_y, x_z, and x_q. The variable x_t specifies the operator elements of the interacting SOR at the common vertex: $x_t=I$ if a v^{i} is connected at the vertex, $x_t=f^2$ if a double wavy line $f^{p>1}f^{q>1}$ connects at the vertex, and $x_t=P$ otherwise. The variable x_q specifies the operator elements coming from the passive SOR, and it may be f^2 or P. The $\mathrm{m}(x_t,x_y,x_z,x_q)$ is symmetric under interchange of x_t and x_q, except for the $x_t=I$ case.

The x_y,x_z indicate whether exchange operators connected to the common vertex are present in either the Y or Z SOR. The possible cases are $x_y,x_z=d,d$ for no exchange, d,e for an exchange in Z connected to the vertex, and e,d for an exchange in Y. The case $x_y,x_z=e,e$ cannot be treated as a vertex correction because the spatial parts do not factorize. There may also be cases where x is exchanged with some particle that is in neither SOR, for example the exchange between n and 1 in diagram 9.5 of Fig. 9. This "passive" exchange does not affect the operator order, but it prohibits other exchanges at the common point. For the case where the "passive" exchange is in a hypernet of the Y SOR, we add the category $x_y,x_z=e_p,d$. We can take care of "passive" exchanges in hypernets of the Z SOR without considering an $x_y,x_z=d,e_p$ category explicitly.

The $\mathrm{m}(x_t,x_y,x_z,x_q)$ are given in Table III. There is no $x_t,x_y=f^2,e$ because Y would not be an SOR, nor is the combination $x_z,x_q=e,f^2$ allowed. The $x_y=e_p$ values are the same as those for $x_y=d$, except that no $x_z=e$ are present, since the "passive" exchanges do not affect the operator order.

For diagrams of the type $[\overbrace{A\;a\;b}]$, as in OD 9.5, we may define the C part to be that of the appropriate expression in curly brackets in Eq. (4.16):

$$\{[\overbrace{A\;a\;b}]-[\overbrace{A\;a}][b]-[A][\overbrace{a\;b}]+[A][a][b]\}. \tag{5.26}$$

All the terms in Eq. (5.26) have identical spatial integrals, but again the C parts vary. Let C_A, C_a, and C_b be the C parts of the separated SOR in Eq. (5.26), where we again assume there is only one operator present in the interaction line in A. Let $\mathrm{m}_{Aa},\mathrm{m}_{ab}$ be the appropriate probabilities for alternating order at vertices Aa and ab. Then it can be shown that

$$C([\overbrace{A}][a][b])=C_AC_aC_b\,, \tag{5.27}$$
$$C([\overbrace{A\;a}][b])=C_AC_aC_b(1+\mathrm{m}_{Aa}D_{Aa})\,, \tag{5.28}$$
$$C([A][\overbrace{a\;b}])=C_AC_aC_b(1+\mathrm{m}_{ab}D_{ab})\,, \tag{5.29}$$
$$C([\overbrace{A\;a\;b}])=C_AC_aC_b(1+\mathrm{m}_{Aa}D_{Aa})(1+\mathrm{m}_{ab}D_{ab})\,, \tag{5.30}$$

and thus

$$C(5.26)=C_AC_aC_b\mathrm{m}_{Aa}\mathrm{m}_{ab}D_{Aa}D_{ab}\,. \tag{5.31}$$

Similarly, the C part of the diagrams of type $[\overbrace{Aab}]$ can be factorized to $C_AC_aC_b\mathrm{m}_{Aa}\mathrm{m}_{Ab}D_{Aa}D_{Ab}$. These results are valid for SOR in general, irrespective of the nature of the vertex, interacting or passive, and they allow contributions of separable diagrams in which there are only four operators at the articulation point to be treated as vertex corrections. When the articulation point has more than four operator lines present,

TABLE III. The $\mathrm{m}(x_t,x_y,x_z,x_q)$.

$x_z,x_q=$	d,f^2	d,P	e,P
$\mathrm{m}(I,d,x_z,x_q)$	1/2	1/3	1/4
$\mathrm{m}(I,e,x_z,x_q)$	1	1/2	
$\mathrm{m}(I,e_p,x_z,x_q)$	1/2	1/3	
$\mathrm{m}(P,d,x_z,x_q)$	5/12	1/3	1/3
$\mathrm{m}(P,e,x_z,x_q)$	1/2	1/3	
$\mathrm{m}(P,e_p,x_z,x_q)$	5/12	1/3	
$\mathrm{m}(f^2,d,x_z,x_q)$	1/2	5/12	1/2
$\mathrm{m}(f^2,e_p,x_z,x_q)$	1/2	5/12	

these relations are no longer exact. Nevertheless the vertex corrections may still be a useful approximation.

VI. FHNC/SOC EQUATIONS

A. Single and hypernetted chains in Bose systems

A set of coupled integral equations that sums single chains of operator links and hypernetted chains of central links has been derived by Wiringa and Pandharipande(1978). These equations are a generalization of the FHNC equations of Fantoni and Rosati (1975), which in turn are themselves a generalization of the HNC equation for Bose systems of van Leeuwen *et al.*(1959).

Historically, equations to sum single chains of simple central links were developed first. Consider the diagrams having only F^c links shown in Fig. 12.1. The contribution of all single chains of F^c links to the expectation value $\langle X\rangle$ of Eq. (4.1) can be expressed as

$$\langle X\rangle_{\text{single } F^c \text{ chains}} = \frac{A\rho}{2}\int F_{mn}X_{mn}F_{mn}G_{mn}d^3r_{mn}, \tag{6.1}$$

$$G_{mn} = \Theta(F^c_{m1}; F^c_{1n}) + \Theta[F^c_{m1}; \Theta(F^c_{12}; F^c_{2n})] + \Theta\{F^c_{m1}; \Theta[F^c_{12}; \Theta(F^c_{23}; F^c_{3n})]\} + \cdots, \tag{6.2}$$

$$\Theta(x_{ij}; y_{jk}) = \rho\int x_{ij}y_{jk}d^3r_j. \tag{6.3}$$

G_{mn} is called a chain function, and Θ is an integral operator that connects elements to form chains. Chain functions satisfy the integral equation

$$G_{ik} = \Theta([\text{link}]_{ij}; [\text{link} + G]_{jk}), \tag{6.4}$$

and we can generalize the kind of chain by generalizing the link and the Θ operator. For the simple chain approximation in Eq. (6.2), the link is obviously F^c.

For systems like liquid helium the single-chain (SC) approximation is not adequate, because G^c is large, being of order unity at least to the radius of the core. In nuclear matter, however, the SC approximation may be good for the noncentral $G^{p>1}$ because they tend to be quite small (<0.1 in v_6 model throughout their range). For the large central links a better approximation is that of hypernetted chains.

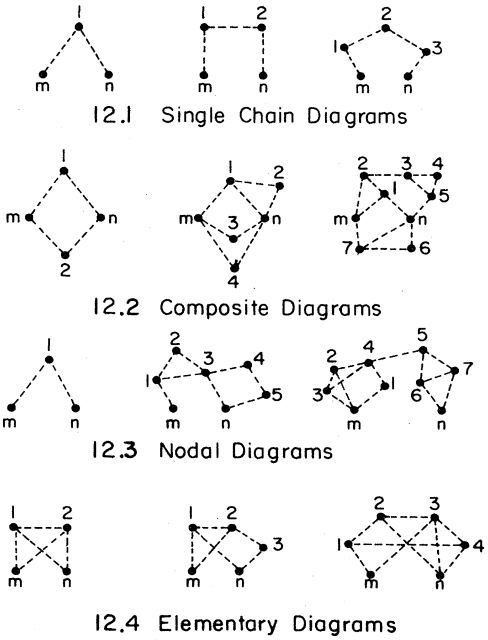

FIG. 12. An illustration of the classification of diagrams with a Bose liquid having Jastrow correlations.

Consider the two-particle distribution function $g(r)$ defined by

$$g(r) = (1/A\rho)\langle\delta(r - r_{mn})\rangle; \tag{6.5}$$

$\rho g(r)$ gives the probability of finding a particle at a distance r from a chosen particle. The diagrams for g_{mn} can be classified as composite, nodal, and elementary; examples of these are shown in diagrams 12.2, 12.3, and 12.4, respectively, of Fig. 12. Composite diagrams have more than one unconnected path between m and n. Nodal diagrams have one or more points through which all paths between m and n must pass. By definition all nodal diagrams are chains, and the section between any two nodal points are links, so links cannot contain nodal points. Diagrams that are neither composite nor nodal are elementary, and both composite and elementary diagrams can be links. If we let E_{mn} denote the sum of all elementary diagrams in the same sense that G_{mn} is a sum of nodal diagrams, then the exact distribution function $g(r)$ in Bose fluids with simple central correlations is given by

$$g_{mn} = (f^c)^2_{mn}\exp(G_{mn} + E_{mn}). \tag{6.6}$$

Expanding the exponential, we have

$$g_{mn}^{-1} = F^c_{mn} + G_{mn} + E_{mn} + F^c_{mn}(G_{mn} + E_{mn}) + \tfrac{1}{2}(G_{mn} + E_{mn})^2 + \cdots = \sum_{\text{all}}(\text{links} + \text{chains})_{mn}. \tag{6.7}$$

Then the sum of all links is obviously just $g_{mn} - 1 - G_{mn}$, and substituting into Eq. (6.4) we have the exact relation

$$G_{mn} = \Theta([g - 1 - G]_{m1};\ [g - 1]_{1n}), \tag{6.8}$$

in which E_{mn} is contained indirectly through Eq. (6.6). The G of Eq. (6.8) is a hypernetted chain, so called because of the many "nets" of correlations generated.

The E_{mn} in Eq. (6.6) is hard to calculate, and in general must be approximated. The simplest choice is to let $E_{mn} = 0$; this is the HNC or hypernetted chain approximation. All composite and nodal diagrams that do not contain elementary diagrams are summed by HNC. It is thus the zeroth order of an expansion in elementary diagrams. (The HNC/4 approximation mentioned earlier includes the simplest elementary diagram, the four-point diagram in Fig. 12.4.)

B. Modifications for Fermi systems

The generalization to Fermi systems (FHNC) requires the subdivision of G_{ik} into parts $G_{xy,ik}$ in order to keep track of the exchange patterns. The xy labels indicate the nature of exchanges at the end points i and k of the chain: xy may be dd, de, ed, ee, or cc. The subscript d stands for a "direct" end, e for an "exchange" end, and c for a "circular" exchange end. $G_{dd,ik}$ thus denotes

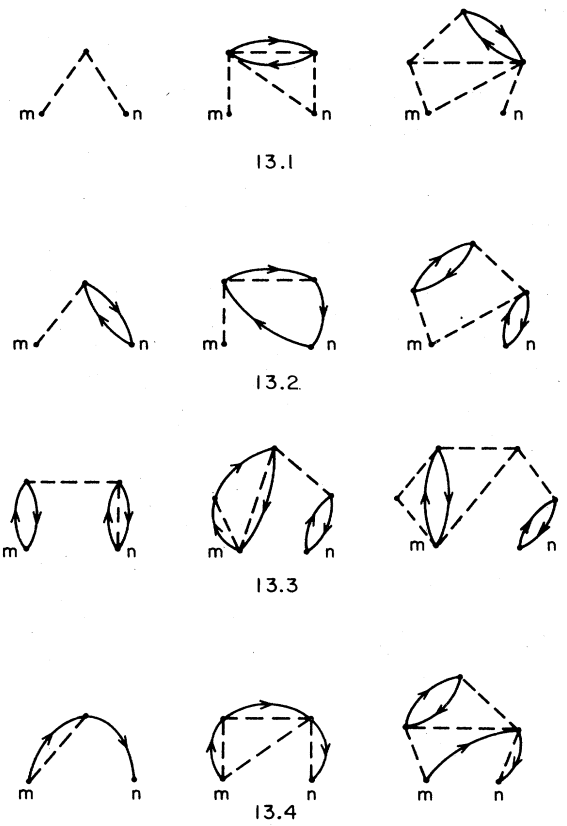

FIG. 13. Examples of diagrams contributing to the $G^c_{xx'}$.

the sum of all chains in which neither i nor k is exchanged. $G_{de,ik}$ is the sum of chains in which k is exchanged with particles in the chain, and i is not. $G_{ed,ik}$ just reverses the roles of i and k and is numerically equal to $G_{de,ik}$. Chains that contribute to $G_{ee,ik}$ have both i and k exchanged in independent exchange loops contained in the chains, while chains with an incomplete exchange loop passing through both i and k are included in $G_{cc,ik}$. Examples of dd, de, ee, and cc chains are given in Fig. 13, diagrams 13.1–13.4. The generalized links that enter Eq. (6.4) are designated $X_{xy,ik}$, and have the same exchange classification. However, since a link can be composite, the $X_{ee,ik}$ can have both i and k exchanged in the same loop, or in two independent loops within the link.

The end points labeled d, c, and e in chains have zero, one, and two exchange lines, respectively. Since any point in a diagram must have either zero or two exchange lines, we can join $X_{xx',ij}$ with $X_{y'y,jk}$ or $G_{y'y,jk}$ at j only in the combinations $x'y' = dd, de, ed, cc$. For $xy = dd, de, ee$, the Fermi chain equations become

$$G_{xy,ik} = \sum_{x',y}{}' \Theta(X_{xx',ij}; [X+G]_{y'y,jk}), \tag{6.9}$$

where the sum is over $x'y' = dd, de, ed$. The links X_{xy} are given by

$$X_{dd} = f^{c^2}\exp(G_{dd}) - 1 - G_{dd}, \tag{6.10}$$

$$X_{de} = f^{c^2}G_{de}\exp(G_{dd}) - G_{de}, \tag{6.11}$$

$$X_{ee} = f^{c^2}(G^2_{de} + G_{ee} - \mathsf{L}^2/s)\exp(G_{dd}) - G_{ee}, \tag{6.12}$$

where

$$\mathsf{L} = -l + sG_{cc}, \tag{6.13}$$

is a generalized Slater function that includes the G_{cc} chain, and s is the degeneracy factor ($s = 4$ for nuclear matter). The G_{cc} chain equation is

$$G_{cc,ik} = \Theta(X_{cc,ij}; [X_{cc} + \mathsf{L}/s]_{jk}), \tag{6.14}$$

$$X_{cc} = f^{c^2}\mathsf{L}\exp(G_{dd})/s - \mathsf{L}/s. \tag{6.15}$$

The X_{xy} can be constructed by considering the possible elements F^c and l and how they may be joined with the G_{xy} to form composite diagrams that have the proper exchange character.

The chain equations (6.9) are different, but hopefully more transparent than those given by Fantoni and Rosati. Schmidt (1978) has demonstrated that the two versions are exactly equivalent.

C. Operator chains

In nuclear matter the chain functions become $G^p_{xy,ik}$ where p denotes the operator dependence associated with the chain. The $G^{p>1}_{xy,ik}$ can be easily calculated in the single-operator chain (SOC) approximation, where each link can contain only one operator element or chain, but may have additional central dressings. (For the remainder of this section, $p = 2, 6$ unless explicitly stated otherwise.)

Examples of G^p_{dd}, G^p_{de}, and G^p_{ee} are shown in Fig. 14, diagrams 14.1–14.3. Because all exchange links but one in an exchange loop carry operator dependence, we cannot have any correlation operator links in a closed exchange loop contained within the SOC. For an incomplete circular exchange chain, there is one "gap" in the operator diagram which may be filled with either an F^p or G^p_{dd} to obtain an SOC. It is convenient to separate G^p_{cc} into two parts, G^p_{ca} and G^p_{cb} (diagrams 14.4 and 14.5), which have the F^p or G^p_{dd} in the first and last links, respectively. A G^p_{cc} chain with an F^p or G^p_{dd} somewhere in the middle is more easily treated as a G^c_{cc} with an independent SOR in the middle (diagram 16.4).

The contribution of separable diagrams, whose articulation points are at the nodes of the SOC, can be included in the G^p_{xy} as vertex corrections $\mathsf{M}(t_p, x_t, x_y)$. The t_p denotes the chain type, x_t is P or f^2 within a chain, and x_y can be d, e, or e_p, depending upon the exchange nature of the vertex. The $\mathsf{M}(t_p, x_t, x_y)$ are related to the $\mathsf{m}(x_t, x_y, x_z, x_q)$ of Table III (exact relations are given below), and we find in practice that $\mathsf{M}(t_p, P, e) \simeq \mathsf{M}(t_p, P, e_p) \simeq \mathsf{M}(t_p, f^2, e_p)$ generally within 1%. The $\mathsf{M}(t_p, P, d)$ and $\mathsf{M}(t_p, f^2, d)$ differ somewhat more, perhaps 5% from each other and 15% from the e, e_p cases. It is possible to write chain equations that treat the $\mathsf{M}(t_p, x_t, x_y)$ exactly, but they are far more complicated than necessary. In the equations below we shall simply denote the (P, e), (P, e_p), and (f^2, e_p) vertex corrections by M^p_e and the (P, d) and (f^2, d) by M^p_d.

Defining the direct functions,

$$h^p = F^p + f^{c^2}G^p_{dd}, \tag{6.16}$$

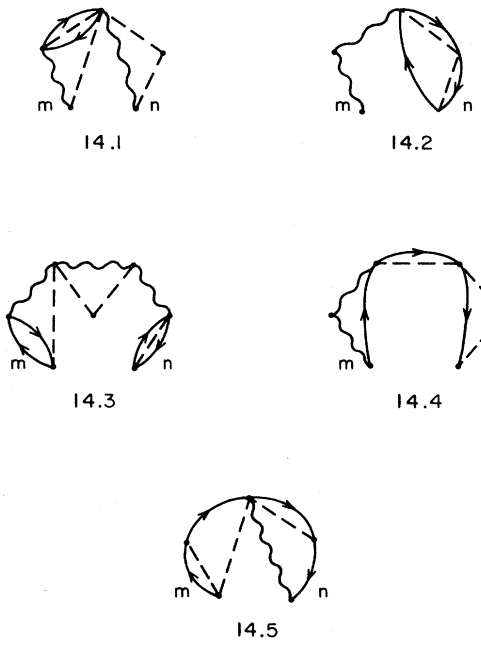

FIG. 14. Examples of diagrams contributing to the $G^{p\geq 2}_{xx'}$.

$$h^c = \exp(G^c_{dd}) , \tag{6.17}$$

the dd, de, and ee links are given by

$$X^p_{dd} = h^p h^c - G^p_{dd} , \tag{6.18}$$

$$X^p_{de} = (h^p G^c_{de} + f^{c^2} G^p_{de}) h^c - G^p_{de} , \tag{6.19}$$

$$X^p_{ee} = (h^p [G^{c^2}_{de} + G^c_{ee}] + f^{c^2} [-(L^2/4)\Delta^p + G^p_{ee} + 2G^p_{de} G^c_{de}]) h^c - G^p_{ee} , \tag{6.20}$$

where $\Delta^p = 1$ for $p = 1, 4$ and zero otherwise. The ξ^{pqr}_{ijk} needed to join operator links can be included in the Θ function:

$$\Theta^{pqr}_{ijk}(x^p_{ij}; y^q_{jk}) = \rho \int \xi^{pqr}_{ijk} x^p_{ij} y^q_{jk} d^3r_j . \tag{6.21}$$

The SOC equations for $xy = dd$, de, and ee are then

$$G^r_{xy,ik} = \sum_{x',y}{}' \sum_{p,q} \Theta^{pqr}_{ijk}(X^p_{xx',ij}; [X+G]^q_{y'y,jk}) M^r_z , \tag{6.22}$$

where the vertex correction subscript $z = d$ for $x'y' = dd$, and $z = e$ for $x'y' = de$ or ed. For the circular exchange chains we need the links

$$X^p_{cx=a,b} = (h^p M^p_e L/4 + f^{c^2} G^p_{cx}) h^c - G^p_{cx} , \tag{6.23}$$

$$X^c_{cc} = (f^{c^2} h^c - 1) L/4 . \tag{6.24}$$

The X^p_{cx} can come only at an end specified by $x = a, b$ in the integral equation, while other links in G^p_{cx} are given by the X^c_{cc}. Since there is only one F^p or G^p_{dd} link, there is only one point at which the vertex correction should be applied, which is done in Eq. (6.23). We find

$$G^r_{ca,ik} = \sum_{p,q} \Theta^{pqr}_{ijk}(X^p_{ca,ij}; \Delta^q [X^c_{cc} + L/4]_{jk}) , \tag{6.25}$$

$$G^r_{cb,ik} = \sum_{p,q} \Theta^{pqr}_{ijk}(\Delta^p X^c_{cc,ij}; [X+G]^q_{cb,jk}) , \tag{6.26}$$

$$G^r_{cc,ik} = G^r_{ca,ik} + G^r_{cb,ik} . \tag{6.27}$$

Every nodal point in G^p_{xy} is vertex corrected, but not the end points. Terms linear in $[M(t_p, x_t, x_y) - 1]$ sum once-separable diagrams like 9.3, while quadratic and higher-order terms sum diagrams like 9.6. Diagrams which have three or more SOR touching at the same point, as in 9.7, are neglected. The exact expression for M is

$$M(t_p, x_t, x_y) = 1 + \sum_{r=2,6} D_{t_p t_r} \times \sum_{x_z, x_q} m(x_t, x_y, x_z, x_q) J^r(x_y, x_z, x_q) . \tag{6.28}$$

The $J^r(x_y, x_z, x_q)$ represent contributions of the passive SOR. If $x_y = d$, these SOR can have an exchange at the articulation point, but if $x_y = e$, they cannot. Thus we have the classification:

$$J^r(d, d, f^2) = \rho A^r \int d^3r f^{r^2} h^c \times [(1 + G^c_{de}) M^r_d + (G^c_{de} + G^{c^2}_{de} + G^c_{ee}) M^r_e] , \tag{6.29}$$

$$J^r(e, d, f^2) = \rho A^r \int d^3r f^{r^2} h^c (M^r_d + G^c_{de} M^r_e) , \tag{6.30}$$

$$J^r(d, d, P) = \tfrac{1}{2} \rho A^r \int d^3r F^r h^c \{G^r_{dd} [(1 + G^c_{de}) M^r_d + (G^c_{de} + G^{c^2}_{de} + G^c_{ee}) M^r_e] + G^r_{de} (1 + G^c_{de}) M^r_e\} , \tag{6.31}$$

$$J^r(e, d, P) = \tfrac{1}{2} \rho A^r \int d^3r F^r h^c \{G^r_{dd} [M^r_d + G^c_{de} M^r_e] + G^r_{de} M^r_e\} , \tag{6.32}$$

$$J^r(d, e, P) = -\tfrac{1}{4} \rho A^r \int d^3r h^r h^c L^2 M^r_e . \tag{6.33}$$

Examples of the $J^r(x_y, x_z, x_q)$ are shown in Fig. 15, diagrams 15.1, 15.6 with $(x_y, x_z, x_q) = ddf^2$, edf^2, ddP, edP, and two examples of deP, respectively. The articulation point is denoted by n. The J^r themselves contain vertex corrections (but not at the articulation point) both explicitly and self-consistently through the chain functions in their definitions. Thus diagrams like 9.5 are also summed. Typical values for $M(t_p, x_t, x_y)$ are given in Table IV.

The $G^c_{xy,ik}$ continue to be calculated in the FHNC approximation, but the links may now contain closed SOR. The dd, de, and ee links become

$$X^c_{dd} = \left\{ f^{c^2} + \sum_p A^p M^{p^2}_e (f^{p^2} + h^p G^p_{dd}) \right\} h^c - 1 - G^c_{dd} , \tag{6.34}$$

$$X^c_{de} = \left\{ f^{c^2} G^c_{de} + \sum_p A^p M^{p^2}_e [(f^{p^2} + h^p G^p_{dd}) G^c_{de} + h^p G^p_{de}] \right\} h^c - G^c_{de} , \tag{6.35}$$

$$X^c_{ee} = \left\{ f^{c^2} (G^{c^2}_{de} + G^c_{ee} - L^2/4) + \sum_p A^p M^{p^2}_e [(f^{p^2} + h^p G^p_{dd})(G^{c^2}_{de} + G^c_{ee}) + h^p (G^p_{ee} + 2G^p_{de} G^c_{de} - L^2 \Delta^p/4) + f^{c^2} (G^{p^2}_{de} - 2G^p_{cc} L \Delta^p / M^p_e)] \right\} h^c - G^c_{ee} , \tag{6.36}$$

and Eq. (6.9) is still used to calculate these chains. Examples of the new diagrams containing SOR that are

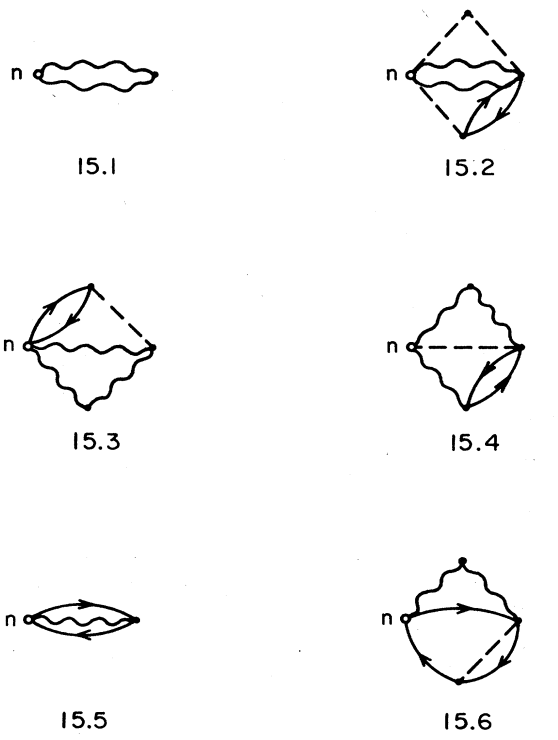

FIG. 15. Examples of diagrams contributing to $J^r(x_y, x_z, x_q)$.

summed are shown in Fig. 16, diagrams 16.1–16.3. The circular exchange chains are also modified to include diagrams like 16.4. The G^c_{cc} equation becomes

$$G^c_{cc,ik} = \Theta\left(X^c_{cc,ij}; \left[X^c_{cc} + 1/4 + \sum_p A^p \Delta^p M^p_e f^{c2} h^c G^p_{ca}\right]_{jk}\right) + \Theta\left(\left[\sum_p A^p \Delta^p M^p_e (f^{c2} h^c - 1) G^p_{cb}\right]_{ij}; [X^c_{cc} + 1/4]_{jk}\right). \quad (6.37)$$

Each closed SOR in the links needs two vertex corrections for where the ends of the f^p, F^p, and G^p_{xy} are joined. They could be either direct or exchange, depending upon how the link is connected to other links. For simplicity, we use M^p_e throughout, since in practice the chains with exchange links give the largest contribution.

The above G^c_{xy} equations will generally count diagrams like 16.5, having touching SOR's, with a wrong C factor because the commutators are neglected. The biggest SOR elements, however, turn out to be the exchange ones, such as on the right side of diagram 16.5, and since exchanges are prohibited from touching anyway, the miscounting is probably not serious. The effect of modifying the G^c_{xy} to include SOR is relatively small (<1 MeV).

TABLE IV. The $M(t_p, x_t, x_y)$ for the Reid v_6 model at $k_F = 1.6$ fm^{-1}, $d = 2.25 r_0$, $\beta_{\sigma\tau} = 0.4\beta_{t\tau} = 1$.

t_p	σ	τ	ν
$M(t_p, I, d)$	0.881	0.881	0.909
$M(t_p, I, e)$	0.890	0.893	0.924
$M(t_p, I, e_p)$	0.945	0.947	0.963
$M(t_p, P, d)$	0.870	0.869	0.898
$M(t_p, P, e)$	0.945	0.947	0.963
$M(t_p, P, e_p)$	0.955	0.956	0.969
$M(t_p, f^2, d)$	0.818	0.817	0.856
$M(t_p, f^2, e_p)$	0.946	0.948	0.963

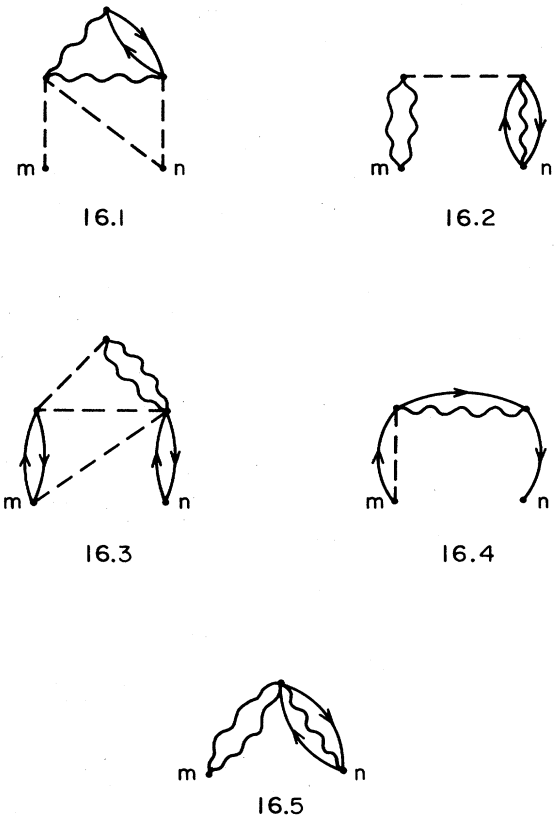

FIG. 16. Examples of G^c_{xx}, diagrams containing closed SOR's.

The most important chains in nuclear matter are the ν-type chains, $G^{\sigma\tau}_{xy}$ and $G^{t\tau}_{xy}$. The largest of these are the $xy = dd$ and de chains shown in Fig. 17. They appear to be small, but their effect is not because (i) they are often multiplied by A^p, which is 9 for $\sigma\tau$ and 18 for $t\tau$; (ii) they are long ranged ($r^2 G^\nu_{xy}$ peaks $\simeq 2\, r_0$), so their integrals are significant; (iii) the $v^{\sigma\tau}$ and $v^{t\tau}$ dominate the long-range part of the NN interaction. The chains should therefore be calculated carefully, and truncation of the chain summation at three- or four-body level is not justified because some of the G^p are of the order of F^p. However, the small magnitude of the F^p and G^p suggest that the SOC approximation is valid. Every multiple-operator chain diagram containing a given number of nodal points is smaller by at least a factor of G^p or F^p than a similar SOC diagram.

The central G^c_{xy} chains are shown in Fig. 18. The necessity of the central correlation hypernets is evident from the large magnitude of G^c_{dd}, particularly at short distances. The G^c_{dd} is always exponentiated, and it gives about a 15% boost to two-body functions at $r \simeq r_0$. It is added to every diagram, since it is purely direct. The G^c_{de} is also important, being fairly long ranged due to

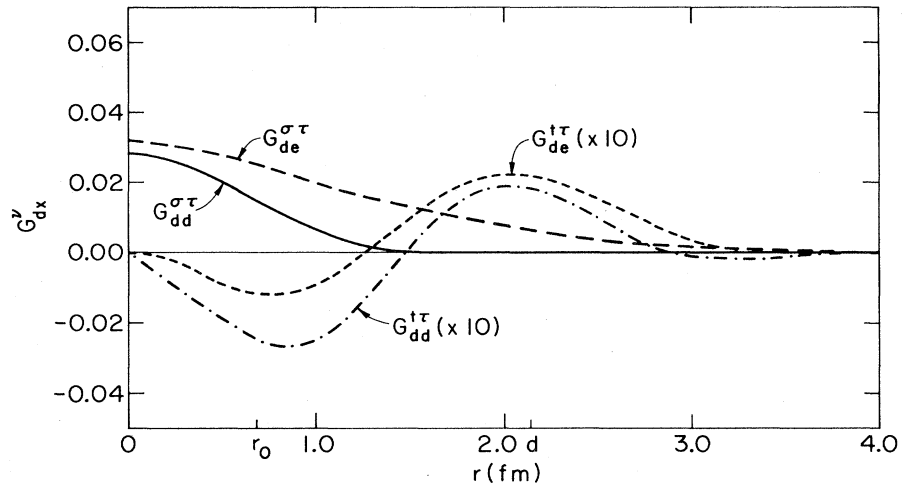

FIG. 17. The functions $G^{p\tau}_{dx}(r)$ at $k_F = 1.6$ fm^{-1}, $d = 2.25 r_0$, $\beta_i = 1$, in the Reid v_6 model.

the exchange leg. It frequently has an accompanying factor of 2 when it is used (to count both *de* and *ed* cases) and can make >5% contributions out to $r = d$. The G^c_{cc} is also important, despite its apparent small size, because it appears with a factor of 4 in the generalized Slater function L of Eq. (6.13), and can make a modification of $\simeq 10\%$ to l out to large distances. Only the G^c_{ee} is relatively unimportant, which is understandable in view of the fact its leading term is a four-body one, as opposed to three-body terms in the other G^c_{xy}.

VII. CALCULATION OF ENERGY

The energy expectation value is expressed as a sum of five terms,

$$E/A = T_F + W + W_F + U + U_F, \tag{7.1}$$

according to the different parts of Ψ that the Hamiltonian (1.9) acts upon. When ∇^2_m operates only on ϕ_m we get the Fermi gas energy $T_F = 0.3\hbar^2 k_F^2/m$. The other terms must be evaluated through the diagrammatic cluster expansion. The W includes the potential energy and kinetic energy terms having $\nabla^2_m F_{mn}$. It is given by the sum of all diagrams having the interaction line, as in diagram 7.5, containing the operator H_{mn},

$$H^c_{mn} = -(\hbar^2/m)\nabla^2_{mn} + v^c_{mn}, \quad H^{p>1}_{mn} = v^p_{mn}, \tag{7.2}$$

plus two F_{mn}, with the ∇^2_{mn} in H_{mn} operating only on the F_{mn}. The U represents the sum of kinetic energy terms $\nabla_m F_{mn} \cdot \nabla_m F_{no}$ $(o \neq n)$. Its diagrams have two derivative lines of type 7.6–7.8. Kinetic energy terms $\nabla_m F_{mn} \cdot \nabla_m \phi_m$ are counted in the W_F and U_F. As mentioned in Sec. IV, they contribute only when particle m is exchanged, and thus U_F or W_F diagrams have a derivative exchange line and a $\nabla_m F_{mn}$ line. If the exchange pattern of the diagram is such that a $\nabla_m l_{mn}$ element appears, the diagram is included in W_F, whereas those having a $\nabla_m l_{mo}$ element contribute to U_F.

A. Calculation of W

The interaction energy W is the sum of all diagrams with the interaction line $f^i_{mn} H^j_{mn} f^k_{mn}$. In the FHNC/SOC approximation it may be subdivided into four parts (Wiringa and Pandharipande, 1979),

$$W = W_0 + W_s + W_c + W_{cs}. \tag{7.3}$$

W_0 is the sum of all diagrams that do not have an operator chain connecting points m and n. Central correlation chains do not affect the operator algebra, and

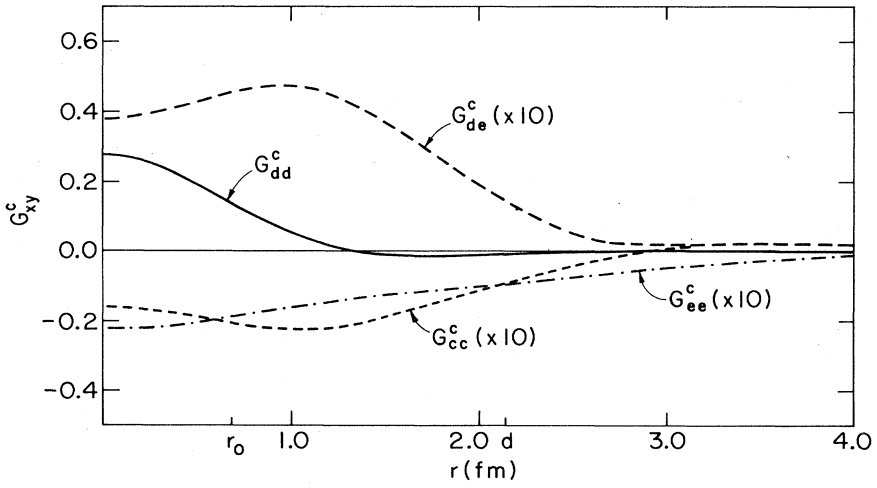

FIG. 18. The functions $G^c_{xx'}(r)$ at $k_F = 1.6$ fm^{-1}, $d = 2.25 r_0$, $\beta_i = 1$, in the Reid v_6 model.

there may be any number of them in a W diagram of any class. W_c diagrams have one SOC connecting m and n in addition to the interaction line, while W_s has a reducible SOR at either vertex m or n. The W_{cs} diagrams have both an SOC between m and n, and an SOR at m or n. This classification is illustrasted in Fig. 19, diagrams 19.1–19.4. Diagrams such as 19.5 (19.6) are included in W_c (W_s) through the vertex corrections to the chain functions $G^{l>1}_{xx'}$, as discussed in Sec. VI. Diagrams like 19.7 are also included approximately in the equations for W_s and W_{cs}, but diagrams like 19.8 have so far been neglected, along with diagrams with two or more SOC connecting m and n.

The expressions for W_0, W_c, and W_s can be derived easily with the use of the various matrices defined in Sec. V. W_{cs} is more difficult to calculate, but it is small, and a relatively simple approximation, which is physically reasonable and numerically accurate, may be used to estimate it.

The W_0 is given by

$$W_0=\frac{\rho}{2}\int d^3r f^i H^j f^k h^c[(1+G^c_{de})^2+G^c_{ee}]K^{ijk}A^k - \frac{\rho}{8}\int d^3r f^i H^j f^k h^c \mathsf{L}^2\Delta^n K^{nim}K^{jkm}A^m. \tag{7.4}$$

We assume a summation over all indices $i,j,k,m,n\ldots$

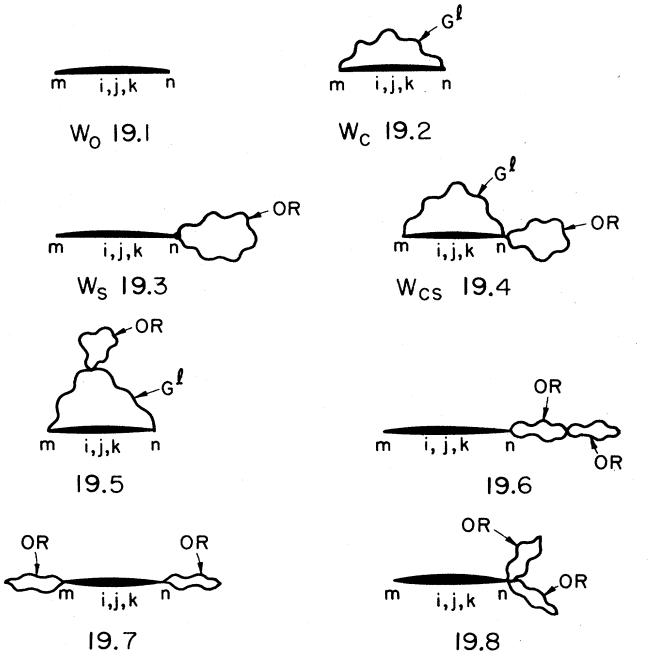

FIG. 19. Classification of W diagrams. The diagrams may contain any number of hypernetted central correlation chains that are not shown; neither are the exchanges shown explicitly. Only the positions of operator chains, G^l, and operator rings, OR, are shown.

from 1 to 6 unless otherwise indicated. The first term of Eq. (7.4) includes the interaction line plus all possible central dressings in which the interacting particles are not in a common exchange loop. The second term counts those diagrams in which m and n are in the same exchange loop. In the first term there are three operators between the same two points, giving a C part of $K^{ijk}A^k$. In the second term there is an additional operator $O^{n\leq 4}_{mn}$ from the exchange, and an intermediate summation variable m is required.

In the calculation of W_c we have to keep track of the order of operators O^i_{mn}, O^j_{mn}, and O^k_{mn} from the $(fHf)_{mn}$, and $O^{l'}_{ma}$ and $O^{l''}_{nb}$ from the SOC $G^{l>1}_{xx',mn}$, and possibly an exchange operator $O^{n\leq 4}_{mn}$. The positions of $O^{l'}_{ma}$ and $O^{l''}_{nb}$ depend upon whether these operators come from the correlations F_{ma}, F_{nb}, or exchanges e_{ma}, e_{nb}. It is thus necessary to divide W_c into parts $W_c(xx')$ which give the contribution of $G^{l>1}_{xx'}$ to W_c.

Let us consider $W_c(dd)$ and abbreviate the operators $O^i_{mn}, O^j_{mn},\ldots$ by $i,j,\ldots$. The $W_c(dd)$ diagrams represent terms in W_c that include $F^{l'}_{ma}F^{l''}_{nb}f^i_{mn}H^j_{mn}f^k_{mn}$, and the operators occur in order:

$$\tfrac{1}{4}[\tfrac{1}{4}\{i,l'\}j\{k,l''\}+\tfrac{1}{4}\{i,l''\}j\{k,l'\} + \tfrac{1}{6}(\{\{l',l''\},i\}+l'il''+l''il')jk + \tfrac{1}{6}ij(\{k,\{l',l''\}\}+l'kl''+l''kl')]. \tag{7.5}$$

There is an overall 1/4 which compensates for the factor two in the definition of $F^{l'}_{ma}$ ($=2f^{l'}_{ma}f^c_{ma}$) and $F^{l''}_{nb}$ ($=2f^{l''}_{nb}f^c_{nb}$). The first (second) term in (7.5) has $f^{l'}_{ma}$ in Ψ^* (Ψ) and $f^{l''}_{nb}$ in $\Psi(\Psi^*)$; the 1/4 in these terms comes from the normalization of symmetrized products $\mathsf{S}(\mathsf{F}_{ma}\mathsf{F}_{mn})$ and $\mathsf{S}(\mathsf{F}_{nb}\mathsf{F}_{mn})$. The third (fourth) term of (7.5) has both $f^{l'}_{ma}$ and $f^{l''}_{nb}$ in Ψ^* (Ψ) and the 1/6 is the normalization of $\mathsf{S}(\mathsf{F}_{ma}\mathsf{F}_{nb}\mathsf{F}_{mn})$. All other correlation and exchange operators that occur in the SOC between points a and b are omitted from (7.5) because their order is immaterial.

The possible orders of the operators i,j,k,l',l'' in $W_c(dd)$ diagrams, and the probability of their occurrence are obtained from (7.5) and shown in Table V. It is not necessary to differentiate between orders such as $il'jkl''$ and $il''jkl'$ because interchanging the positions of l' and l'' leaves the C part invariant. If the interacting particles are exchanged with each other, the $W_c(dd)$ diagram has an additional $O^{n\leq 4}_{mn}$ that appears at the extreme left, and is not explicitly shown in the table.

The C part for any W_c diagram can be written as a product of the ξ functions, which are built into the definition of $G^{l>1}_{xx'}$ and are independent of the operator order, and a coefficient depending on the order of i,j,k,l',l'' which can be constructed from the A, K, and L matrices. This coefficient is also exhibited in Table V for each operator order in both direct and exchange cases. The result for $W_c(dd)$ is

$$W_c(dd)=\frac{\rho}{2}\int d^3r f^i H^j f^k G^{l>1}_{dd} h^c[(1+G^c_{de})^2+G^c_{ee}]\,\tfrac{1}{24}(11K^{ijm}K^{klm}A^m+5K^{ijm}L^{klm}+5K^{jkm}L^{ilm}+3K^{ikm}L^{jlm}) - \frac{\rho}{8}\int d^3r f^i H^j f^k G^{l>1}_{dd} h^c \mathsf{L}^2[\tfrac{1}{8}(K^{jkm}K^{nim'}L^{m'lm}+K^{ijm}K^{mkm'}L^{nlm'}+K^{knm}K^{mim'}L^{jlm'}+K^{ijm}K^{knm'}L^{m'lm}) + \tfrac{1}{12}(4K^{nlm}K^{ijm'}K^{mm'k}A^k+K^{jkm}K^{mnm'}L^{ilm'}+K^{nim}K^{mjm'}L^{klm'})]. \tag{7.6}$$

TABLE V. Operator orders in $W_c(dd)$ diagrams.

No.	Operator order	Probability	Direct	Exchange
1	$il'jkl''$	1/8	$K^{jkm}L^{ilm}$	$K^{jkm}K^{nim'}L^{m'lm}$
2	$l'ijkl''$	1/8	$A^mK^{ijm}K^{klm}$	$K^{ijm}K^{mkm'}L^{nlm'}$
3	$il'jl''k$	1/8	$K^{kim}L^{jlm}$	$K^{knm}K^{mim'}L^{jlm'}$
4	$l'ijl''k$	1/8	$K^{ijm}L^{klm}$	$K^{ijm}K^{knm'}L^{m'lm}$
5	$l'l''ijk$	1/12	$A^mK^{ijm}K^{klm}$	$A^kK^{nlm}K^{ijm'}K^{mm'k}$
6	$il'l''jk$	1/12	$A^mK^{ijm}K^{klm}$	$A^kK^{nlm}K^{ijm'}K^{mm'k}$
7	$l'il''jk$	1/12	$K^{jkm}L^{ilm}$	$K^{jkm}K^{mnm'}L^{ilm'}$
8	$ijkl'l''$	1/12	$A^mK^{ijm}K^{klm}$	$A^kK^{nlm}K^{ijm'}K^{mm'k}$
9	$ijl'l''k$	1/12	$A^mK^{ijm}K^{klm}$	$A^kK^{nlm}K^{ijm'}K^{mm'k}$
10	$ijl'kl''$	1/12	$K^{ijm}L^{klm}$	$K^{nim}K^{mjm'}K^{klm'}$

The $W_c(de)$ and $W_c(ee)$ may be calculated analogously:

$$W_c(de)=\rho\int d^3r f^i H^j f^k G_{de}^{l>1} h^c(1+G_{de}) \times\tfrac{1}{4}(2K^{ijm}K^{klm}A^m+K^{ijm}L^{klm}+K^{jkm}L^{ilm}), \quad (7.7)$$

$$W_c(ee)=\frac{\rho}{2}\int d^3r f^i H^j f^k G_{ee}^{l>1} h^c K^{ijm}K^{klm}A^m. \quad (7.8)$$

The contribution due to cc chains is slightly more complicated because there is a subset of diagrams that are reducible [see Pandharipande and Bethe (1973)]. For example, diagrams 20.1–20.3 of Fig. 20 are all irreducible, 20.1 and 20.2 being taken care of by G_{ca}^l, and 20.3 by G_{cb}^l. However, diagram 20.4 has a reducible counterpart in 20.5, which must be subtracted out according to the cluster expansion. (This is the case x_y, $x_z=e,e$ mentioned in Sec. V that cannot be treated as a vertex correction.) The magnitudes of G_{cx}^l do not depend on the direction of exchange, so in practice we sum diagrams of type 20.1–20.4 by using G_{ca}^l and summing over both exchange directions. The contribution of diagrams of type 20.5 is proportional to $G_{ca}^l - G_{cb}^l$, which is subtracted from the sum to obtain $W_c(cc)$:

$$W_c(cc)=-\frac{\rho}{4}\int d^3r f^i H^j f^k G_{ca}^{l>1} h^c \llcorner\Delta^n[2K^{ijm}K^{kmm'}(L^{nlm'}+K^{nlm'}A^{m'})+L^{lmm'}(K^{ijm}K^{nkm'}+K^{jkm}K^{nim'})+K^{jnm}(K^{imm'}L^{klm'}+K^{kmm'}L^{ilm'})] + \rho\int d^3r f^i H^j f^k (G_{ca}^{l>1}-G_{cb}^{l>1}) h^c \llcorner K^{jkm}K^{nim}A^mA^l\Delta^n\Delta^l. \quad (7.9)$$

The diagrams contributing to W_s are conveniently divided into "direct" and "exchange" categories. Direct W_s diagrams have no exchange between the interacting particles, while in exchange W_s diagrams they are in a common exchange loop. Direct diagrams are constructed using the interaction line, with possible central chains as dressings, and the SOR function J^l given in Eqs. (6.29)–(6.33) attached at the end points. The appropriate $J^l(x_y,x_z,x_q)$ is selected so that the common vertex does not participate in more than one exchange. The C part is easily calculated by keeping track of the possible operator orders as in the W_c case.

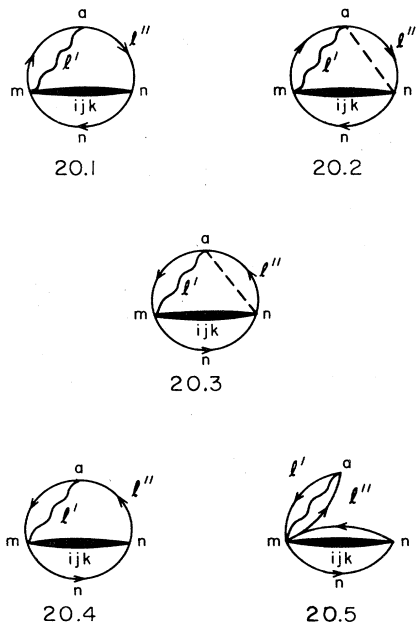

FIG. 20. The simplest diagrams that contribute to $W_c(cc)$.

Consider the case where $J^l(d,d,f^2)$ is the separable SOR, an example of which is shown in diagram 15.1. The C part of the separable diagram is given by

$$\tfrac{1}{4}C(\{i,l\}j\{l,k\})-C(ijk)C(ll)) = \tfrac{1}{4}K^{ijk}A^kA^l(D_{il}+D_{jl}+D_{kl}), \quad (7.10)$$

where the D_{pq} are given by Eq. (5.23). The C parts of all W_s diagrams can be similarly calculated using the matrices A, K, and D. The total W_s can be written compactly as

$$W_s=\frac{\rho}{2}\int d^3r f^i H^j f^k h^c K^{ijk}A^k \times[M_{dd}^2-1+2G_{de}^c(M_{dd}M_{de}-1)+(G_{de}^{c2}+G_{ee}^c)(M_{de}^2-1)] -\frac{\rho}{16}\int d^3r f^i H^j f^k h^c \llcorner^2\Delta^n(K^{nim}K^{jkm}+K^{nkm}K^{ijm})A^m(M_{ee}^2-1). \quad (7.11)$$

The first (second) term is the direct (exchange) part. Terms linear in $(M_{xx'}-1)$ sum diagrams having only one separable SOR, like 19.3, while those quadratic in

$(M_{xx'}-1)$ give a fair approximation to diagrams like 19.7 having two separable SOR. The $M_{xx'}$ are analogous to the vertex corrections M discussed in Sec. VI, but depend on all three variables i, j, and k, as opposed to only one in, for example, $\mathrm{M}(t_j, I, x)$. The direct M_{dx} are given by

$$M_{dx}=1+\sum_l \{\tfrac{1}{4}(D_{il}+D_{jl}+D_{kl})\mathrm{J}^l(x,d,f^2) + \tfrac{1}{24}(3D_{jl}+5D_{il}+5D_{kl})\mathrm{J}^l(x,d,P) + \delta_{xd}\tfrac{1}{4}(D_{il}+D_{kl})\mathrm{J}^l(d,e,P)\}. \quad (7.12)$$

The exchange correction M_{ee} depends in addition on the intermediate summation variable m:

$$M_{ee}=1+\sum_l \{\tfrac{1}{4}(2D_{ml}+D_{jl}+D_{nl})\mathrm{J}^l(e,d,f^2) + \tfrac{1}{24}(6D_{ml}+3D_{jl}+3D_{nl}+2D_{il}+2D_{kl})\mathrm{J}^l(e,d,P)\}. \quad (7.13)$$

The W_{cs} is very messy, since we need to keep track of the orders of seven to eight operators to calculate it exactly. However, it is small, and of order $W_c(M^2-1)$, where M is an appropriate vertex correction. To the extent the $f^cH^jf^c$ term in W_c dominates, we can use the interacting vertex corrections $\mathrm{M}(t_j, I, x)$ of Eq. (6.28) to calculate the contribution of H^j to W_{cs}. In practice we find that terms containing H^ν, f^ν, and G^ν dominate the W_c, and it is probably adequate to calculate the W_{cs} with $\mathrm{M}(\nu, I, x)$. Keeping track of exchanges, we have

$$W_{cs}\simeq W_c(dd)_{\mathrm{dir}}[\mathrm{M}(\nu,I,d)^2-1] + W_c(de)[\mathrm{M}(\nu,I,d)\mathrm{M}(\nu,I,e)-1] + [W_c(dd)_{\mathrm{ex}}+W_c(ee)+W_c(cc)][\mathrm{M}(\nu,I,e)^2-1], \quad (7.14)$$

where $W_c(dd)_{\mathrm{dir}}$ and $W_c(dd)_{\mathrm{ex}}$ are the two terms of Eq. (7.6). The exact vertex corrections for $W_c(dd)_{\mathrm{dir}}$, $W_c(de)$ (which is the dominant term in W_c) and $W_c(ee)$ have been calculated, and we find numerically that the approximation in Eq. (7.14) is quite good, typically within $\simeq 0.1$ MeV up to $k_F=2.0$ fm^{-1}. The exact calculation requires the introduction of new matrices, and has not been done yet for the $W_c(dd)_{\mathrm{ex}}$ and $W_c(cc)$, so it is probably not worthwhile to discuss it here. We believe the above approximation for W_{cs} is valid to within $\simeq 0.2$ MeV.

B. Calculation of U

The U diagrams are evaluated up to the SOC level with vertex corrections. They are conveniently divided into four parts

$$U=U_1+U_2+U_3+U_4, \quad (7.15)$$

where U_1 has no operator links and U_2, U_3, and U_4 have one SOR passing through the points *no*, *mn* or *mo*, and *mno*, respectively. Samples of diagrams contributing to U_1-U_4 are shown in Fig. 21, diagrams 21.1–21.4.

The U_i can always be expressed as

$$U_i=-\frac{\hbar^2}{8m}\rho^2\int d^3r_{mn}d^3r_{mo}\cos\theta_m u_i(r_{mn},r_{mo},r_{no}), \quad (7.16)$$

and in the FHNC/SOC approximation the u_i contain products of functions of r_{mn}, r_{mo}, r_{no}, and ξ^{pql}_{nmo}. The functions of r_{no} denoted by $R_{xx'}$, $Y_{xx'}$, and $Z^{p>1}_{xx'}$, respectively, depict central correlations, closed SOR, and operator links in the U diagrams.

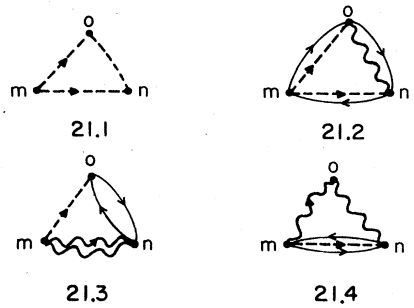

FIG. 21. Examples of U diagrams.

$$R_{dd}=f^{c2}h^c,$$
$$R_{de}=R_{dd}G^c_{de},$$
$$R_{ee}=R_{dd}(G^{c2}_{de}+G^c_{ee}-\mathrm{L}^2/4),$$
$$R_{cc}=R_{dd}\mathrm{L}/4. \quad (7.17)$$

The $Y_{xx'}$ and $Z^{p>1}_{xx'}$ are multiplied by the vertex corrections M^p_x discussed in Sec. VI to correct for separable U diagrams:

$$Y_{dd}=\sum_{p>1}A^p[f^{p2}+h^pG^p_{dd}]M^{p2}_d h^c,$$
$$Y_{ee}=\sum_{p>1}A^p\{f^{p2}(G^{c2}_{de}+G^c_{ee})+f^{c2}(G^{p2}_{de}-2G^p_{cc}\mathrm{L}\Delta^p/M^p_e) + h^p[G^p_{dd}(G^{c2}_{de}+G^c_{ee})+2G^p_{de}G^c_{de}+G^P_{ee}-\mathrm{L}^2\Delta^p/4]\}M^{p2}_e h^c,$$
$$Y_{de}=\sum_{p>1}A^p[f^{p2}G^c_{de}+h^p(G^p_{dd}G^c_{de}+G^p_{de})]M^p_d M^p_e h^c,$$
$$Y_{cc}=\sum_{p>1}A^p\Delta^p[\tfrac{1}{4}h^p\mathrm{L}M^p_e+f^{c2}G^p_{cc}]M^p_e h^c; \quad (7.18)$$

$$Z^{p>1}_{dd}=h^ph^cM^{p2}_d,$$
$$Z^{p>1}_{de}=(h^pG^c_{de}+f^{c2}G^p_{de})h^cM^p_dM^p_e,$$
$$Z^{p>1}_{ee}=[h^p(G^{c2}_{de}+G^c_{ee})+f^{c2}(G^p_{ee}+2G^p_{de}G^c_{de}-\Delta^p\mathrm{L}^2/4)]h^cM^{p2}_e. \quad (7.19)$$

There are no $Z^{p>1}_{cc}$ links in the SOC approximation. The corresponding functions of r_{mn} and r_{mo} containing the gradients are denoted by $\bar{R}_{xx'}$, $\bar{Y}_{xx'}$, and $\bar{Z}^{p>1}_{xx'}$. They are obtained by making the following substitutions in Eqs. (7.17–7.19):

$$f^{c2}\to(f^{c2})',$$
$$f^{p2}\to(f^{p2})',$$
$$h^p\to(F^p)'+(f^{c2})'G^p_{dd}, \quad (7.20)$$

where the primes represent derivatives with respect to r. The $\bar{Z}^{t(t\tau)}_{xx'}$ generated by these substitutions contain $(f^cf^{t(t\tau)})'$ terms. Two new $\bar{Z}$ links, $\bar{Z}^{t',(t'\tau)}_{xx'}$, are needed to take into account the gradients of the tensor operator. They are obtained from $Z^{t(t\tau)}$ with the replacements

$$h^{t(t\tau)}\to F^{t(t\tau)}/r,$$
$$f^{c2}\to 0. \quad (7.21)$$

The $u_i(r_{mn},r_{mo},r_{no})$ containing all the twenty-nine possible exchange patterns are given by

$$u_1 = \bar{R}_{dd,mn}(\bar{R}_{dd} + 4\bar{R}_{de} + 2\bar{R}_{ee})_{mo}(R_{dd} + R_{de})_{no} + \bar{R}_{dd,mn}(\bar{R}_{dd} + 2\bar{R}_{de})_{mo}(R_{de} + R_{ee})_{no}$$
$$+ \bar{R}_{de,mn}(3\bar{R}_{de} + 2\bar{R}_{ee})_{mo}R_{dd,no} + 2\bar{R}_{de,mn}\bar{R}_{de,mo}R_{de,no} - 8\bar{R}_{cc,mn}\bar{R}_{cc,mo}R_{cc,no}. \quad (7.22)$$

The u_2 may be obtained by replacing the $R_{xx',no}$ in u_1 by $Y_{xx',no}$ while u_3 is the sum of the two terms obtained by replacing the $\bar{R}_{xx',mn}$ and $\bar{R}_{xx',mo}$ by $\bar{Y}_{xx',mn}$ and $\bar{Y}_{xx',mo}$, respectively. The u_4 contains a $\xi^{pql}_{nmo}A^l$ for the C part and an $(M_d^p)^{-3}$ because each Z or $\bar{Z}$ link has two vertex corrections.

$$u_4 = \sum_{p,q=2-6,t',t'\tau} \sum_{l=2-6} \xi^{pql}_{nmo} A^l / M_d^{p3} \{\bar{Z}^p_{dd,mn}(\bar{Z}^q_{dd} + 4\bar{Z}^q_{de} + 2\bar{Z}^q_{ee})_{mo}(Z^l_{dd} + Z^l_{de})_{no}$$
$$+ \bar{Z}^p_{dd,mn}(\bar{Z}^q_{dd} + 2\bar{Z}^q_{de})_{mo}(Z^l_{de} + Z^l_{ee})_{no} + \bar{Z}^p_{de,mn}(3\bar{Z}^q_{de} + 2\bar{Z}^q_{ee})_{mo}Z^l_{dd,no} + 2\bar{Z}^p_{de,mn}\bar{Z}^q_{de,mo}Z^l_{de,no}\}. \quad (7.23)$$

The ξ^{pql}_{nmo} having p or $q = t'(t'\tau)$ give the C parts of SOR containing gradients of tensor operators. Those with nonzero values are found to be

$$\xi^{t'\sigma t}_{nmo} = \xi^{t'\tau\sigma\tau t\tau}_{nmo} = -3\left(\frac{\cos\theta_n\cos\theta_o}{\cos\theta_m} + \cos^2\theta_n\right), \quad (7.24)$$

$$\xi^{t'tk}_{nmo} = \xi^{t'\tau t\tau k\tau}_{nmo} = 6(1 - \cos^2\theta_m)\delta_{k\sigma} + \left[9\cos\theta_m\cos\theta_n\cos\theta_o + \tfrac{9}{2}\cos^2\theta_o + 3(\cos^2\theta_m + \cos^2\theta_n) - \tfrac{3}{2}\frac{\cos\theta_n\cos\theta_o}{\cos\theta_m} - 3\right]\delta_{kt}, \quad (7.25)$$

$$\xi^{t't'k}_{nmo} = \xi^{t'\tau t'\tau k\tau}_{nmo} = 12\cos^2\theta_m\delta_{k\sigma} + \left[-18\cos\theta_m\cos\theta_n\cos\theta_o - 6\cos^2\theta_m - 9(\cos^2\theta_n + \cos^2\theta_o) - \frac{9}{2}\frac{\cos\theta_n\cos\theta_o}{\cos\theta_m} + \frac{9}{2}\right]\delta_{kt}. \quad (7.26)$$

C. Calculation of W_F and U_F

The W_F diagrams can conveniently be broken down like W into parts, W_{F0}, W_{Fc}, W_{Fs}, and W_{Fcs}. The W_{F0} and W_{Fs} are given by

$$W_{F0} + W_{Fs} = -\frac{\hbar^2}{8m}\rho\int d^3r(f^if^k)'l'\,Lh^c\Delta^j K^{ijk}A^kM^2_{de}. \quad (7.27)$$

In the operator algebra the exchange operator j in W_{Fs} diagrams plays the role of the j operator associated with H^j in direct W_s diagrams, so the vertex correction in Eq. (7.27) is identical to the M_{de} of Eq. (7.12). At present the W_{Fc} and W_{Fcs} are calculated in strictly the single-operator ring approximation:

$$W_{Fc} + W_{Fcs} \simeq -\frac{\hbar^2}{4m}\rho\int d^3r f^cf^{c'}l'h^c\Delta^n A^n(G^n_{dd}M^{n2}_e L + 4G^n_{cc}M^n_e). \quad (7.28)$$

The U_F is treated like U, its diagrams being grouped into five classes which, respectively, have no SOR connecting m, n, and one, SOR passing through either n and o, m and n, m and o, or m, n, and o. The mn and mo links are symmetric in U, but not in U_F, hence the extra class. The U_F may be written as

$$U_{Fi} = -\frac{\hbar^2}{2m}\rho^2\int d^3r_{mn}d^3r_{mo}\cos\theta_m u_{Fi}(r_{mn}, r_{mo}, r_{ro}). \quad (7.29)$$

The u_{Fi} contain $(R, Y, \text{or } Z)_{no}$, $(\bar{R}, \bar{Y}, \text{or } \bar{Z})_{mn}$, and new functions $(\tilde{R}, \tilde{Y}, \text{or } \tilde{Z})_{mo}$ containing the l'_{mo}:

$$\tilde{R}_{ee} = f^{c2}h^cl'L/4,$$
$$\tilde{R}_{cc} = (f^{c2}h^c - 1)l',$$
$$\tilde{Y}_{ee} = \sum_{p>1} A^p[h^ch^pM^{p2}_e L/4 + (f^{c2}h^c - 1)G^p_{cc}M^p_e]l'\Delta^p,$$
$$\tilde{Y}_{cc} = \sum_{p>1} A^p\Delta^ph^ch^pM^{p2}_e l',$$
$$\tilde{Z}^{p>1}_{ee} = \Delta^p\tilde{R}_{ee}M^{p2}_e. \quad (7.30)$$

The u_{F1} is given by

$$u_{F1} = \bar{R}_{dd,mn}\tilde{R}_{ee,mo}(R_{dd} + R_{de})_{no} + \bar{R}_{de,mn}\tilde{R}_{ee,mo}R_{dd,no} + \bar{R}_{cc,mn}\tilde{R}_{cc,mo}R_{cc,no}, \quad (7.31)$$

while the u_{F2}, u_{F3}, and u_{F4} are obtained by, respectively, substituting the $R_{xx'}$ by $Y_{xx'}$, the $\bar{R}_{xx'}$ by $\bar{Y}_{xx'}$, and the $\tilde{R}_{xx'}$ by $\tilde{Y}_{xx'}$ in u_{F1}. The u_{F5} is given by

$$u_{F5} = \sum_{p=2-6,t',t'\tau} \sum_{q,l=2-6} \xi^{pql}_{nmo}A^l/M^{p3}_d \times [\bar{Z}^p_{dd,mn}\tilde{Z}^q_{ee,mo}(Z^l_{dd} + Z^l_{de})_{no} + \bar{Z}^p_{de,mn}\tilde{Z}^q_{ee,mo}Z^l_{dd,no}]. \quad (7.32)$$

VIII. FURTHER VARIATIONS OF THE THEME

A. Hypernetted operator chain equations

Fantoni and Rosati (1978) have developed a set of integral equations that approximately sums hypernetted operator chains (HOC) by neglecting a number of commutators. Consider the HOC diagram 22.1 of Fig. 22, and assume for simplicity that all the operator links are τ type. The seven $\tau_a \cdot \tau_b$ operators in the diagram occur in various orders labeled i with weights w^i; however, we could rearrange them and express

$$\sum_i w^i \prod{}^i O^\tau_{ab} = \tau_m\cdot\tau_1(\tau_1\cdot\tau_4\tau_4\cdot\tau_2)(\tau_1\cdot\tau_3\tau_3\cdot\tau_2)\tau_1\cdot\tau_2\tau_2\cdot\tau_n + \text{terms having commutators}. \quad (8.1)$$

On summing over τ_3 and τ_4 we get

$$\sum_{\tau_3,\tau_4,i} w^i \prod{}^i O_{ab} = \tau_m\cdot\tau_1(\tau_1\cdot\tau_2)^3\tau_2\cdot\tau_n + \text{commutator terms}. \quad (8.2)$$

Since

$$(\tau_1\cdot\tau_2)^3 = -6 + 7\tau_1\cdot\tau_2, \quad (8.3)$$

the 1–2 link in the first term of Eq. (8.2) is effectively a single-operator link and may simply be included in

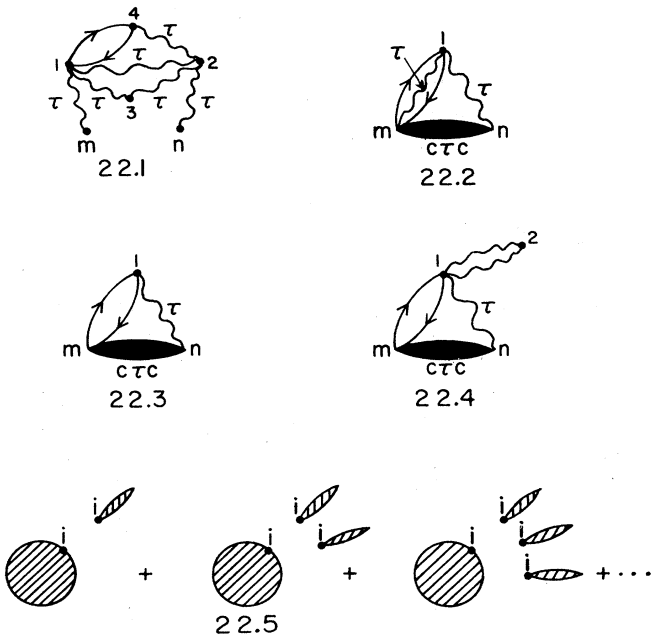

FIG. 22. Diagrams 22.1 and 22.2 are typical of chain diagrams having multiple-operator links, while 22.3 is the SOC diagram corresponding to 22.2, and 22.4 is a correction to 22.3. Diagrams 22.5 illustrate the simple structure of typical diagrams that are summed analytically to obtain vertex corrections in Owen's method.

the links $X^p O^p$ of the chain equation (6.22). The commutator terms in (8.2) are much more difficult to sum.

The HOC equations neglect all commutator terms, and have the same form as Eq. (6.22) with the vertex corrections M_z^r set to unity. The links $X_{xx'}^p$, however, include all operator hypernets, such as the one in diagram 22.1, treated approximately in the manner illustrated above. The X_{dd}^p, for example, is given by the operator equation

$$\sum_{p=1,6} X_{dd}^p O^p = \left(\sum_{p'} f^{p'} O^{p'}\right)^2 \exp\left(\sum_{p'} G_{dd}^{p'} O^{p'}\right) - 1 - \sum_{p} G_{dd}^p O^p , \tag{8.4}$$

which is a direct generalization of the link equation (6.10) of FHNC. Fantoni and Rosati have introduced a very useful set of projection operators P^i to calculate the exponential in Eq. (8.4). The P^i are linear combinations of O^i,

$$\mathrm{P}^{i=1,6} = P^1\pi^1, Q\pi^1, (1-Q)P^3\pi^1, P^1\pi^3, Q\pi^3, (1-Q)P^3\pi^3 , \tag{8.5}$$

where P and π are standard spin, isospin projection operators:

$$P^1 = \tfrac{1}{4}(1-\sigma_1\cdot\sigma_2), \quad P^3 = \tfrac{1}{4}(3+\sigma_1\cdot\sigma_2),$$
$$\pi^1 = \tfrac{1}{4}(1-\tau_1\cdot\tau_2), \quad \pi^3 = \tfrac{1}{4}(3+\tau_1\cdot\tau_2), \tag{8.6}$$

and

$$Q = \tfrac{1}{6}(3+\sigma_1\cdot\sigma_2+S_{12}). \tag{8.7}$$

The P^p satisfies equations of projection operators,

$$\mathrm{P}^p \mathrm{P}^q = \delta_{pq} \mathrm{P}^p , \tag{8.8}$$

and the exponentiation is carried out by defining new chain functions $\hat{G}^p$ such that

$$\sum_{p=1,6} \hat{G}_{dd}^p \mathrm{P}^p = \sum_{p=1,6} G_{dd}^p O^p , \tag{8.9}$$

$$\exp\left(\sum_{p=1,6} \hat{G}_{dd}^p \mathrm{P}^p\right) = 1 + \sum_{p=1,6} [\exp(\hat{G}_{dd}^p) - 1]\,\mathrm{P}^p . \tag{8.10}$$

If the commutator terms were indeed small, the HOC equations would constitute a substantial improvement over the FHNC/SOC equations. However, there is no reason for the commutator terms in Eq. (8.2) to be small. Consider the multiple-operator diagram 22.2. Its contribution in the HOC approximation is easily calculated by taking the O_{ml}^τ next to the exchange operator e_{ml} and neglecting the commutators. It is found to be

$$+\frac{3}{4}\rho^2 \int d^3r_{mn} d^3r_{ml}\, l_{ml}^2 f_{mn}^c v_{mn}^\tau f_{mn}^c F_{ml}^\tau F_{ml}^\tau . \tag{8.11}$$

The contribution of this rather simple diagram may be calculated exactly by treating all the operator orders. It is found to be zero; the commutator terms of Eq. (8.2) just cancel the first term in this case.

In the FHNC/SOC summation the multiple-operator diagram 22.2 is viewed as a correction to the SOC diagram 22.3. It will be a small correction when the $F^{p>1}$ and $G^{p>1}$ are $\ll 1$, as is the case in nuclear matter. Further, the SOC diagram 22.3 has other commutator corrections, such as 22.4, which the present HOC equations neglect. These vertex corrections can be significant when the $f^{p>1}$ have a long range.

B. Calculations with independent-pair wave function

Owen (1979a) has developed a very promising variational theory based on the wave function Ψ_{IP} given by Eqs. (2.25) and (2.26). He has recently (1979b) applied it to the v_6 model of nuclear matter. The $f^p(r_{ij}, d, \beta_p)$ of Sec. III are used to calculate the u_{ij}, and so his method also has the same variational parameters d and β_p. In the low-density limit the Ψ_{IP} and the "symmetrized product" Ψ_{SP} [Eq. (2.19)] become identical.

The diagrammatic cluster expansion of expectation values with Ψ_{IP} has been carried out by Owen (1979a) by a generalization of the method of Gaudin, Gillespie, and Ripka (1971). However, the application of the method described in Sec. IV gives the same results, and we shall continue to use the diagrammatic notation of Sec. IV, which is only superficially different from Owen's, to describe his method.

The diagrams depicting expectation values with Ψ_{IP} are formed with the elements 1–9 of Fig. 7; however, the wavy lines must be labeled either L or R to specify whether they come from the expansion of the left-hand Ψ_{IP}^* or the right-hand Ψ_{IP}. The Ψ_{IP} has no terms of type $u_{ij}u_{jk}$ in which two or more u's have a common particle. This restriction of Ψ_{IP} is simply incorporated by an additional diagram rule stating that no two wavy L lines or R lines touch. A consequence of this rule is that we cannot have diagrams in which three or more wavy lines touch at a point.

The wavy lines must also carry the operator label p. In the previous theory a wavy line labeled p represented $2f^c f^p O^p$, and the operator O^p could be on the left or right side of the Hamiltonian H with a probability of 1/2. The wavy lines $pL(pR)$ represent $f^c f^p O^p$ with the operator on the left (right) of H. The double wavy line (element 3 of Fig. 7) must now be labeled pL, qR, and it represents $f^p f^q O^p O^q$, the operators O^p and O^q being on the left and right side of H, respectively.

In building chains with the Ψ_{IP} we have to be careful to avoid connecting links $X^p_{xx',ij}$ to $X^q_{y'y,jk}$ or $G^q_{y'y,jk}$ [Eq. (6.22)] when both contain wavy L lines or R lines ending in the nodal point j. This requires a more elaborate classification of chains $G^p_{xx',kj}$ and links $X^p_{xx',ij}$. The subscript x referring to the end i must now specify both the exchange pattern and the occurrence of wavy L and R lines at i. Thus the number of chains is much larger. For example, the four parts $G^p_{dLdR,ij}$, $G^p_{dLdL,ij}$, $G^p_{dRdL,ij}$, and $G^p_{dRdR,ij}$ of the single operator $G^p_{dd,ij}$ have to be considered explicitly. Symmetry under the exchange of L with R can, however, be used to reduce the number of required chain functions. Owen writes the chain equation (6.22) in a matrix form

$$G^r_{xy,ij} = \Theta \; {}^{pqr}_{ijk}(X^p_{xx',ij} M^{pq}_{x'y'}; [X+G]^q_{y'y,jk}) , \tag{8.12}$$

and puts all the restrictions and vertex corrections in his coupling matrix $M^{pq}_{x'y'}$. The elements such as M^p_{dLdL} or M^{pq}_{eLeR} would obviously need to be zero because such couplings build wrong diagrams. The elements such as M^{pq}_{dLdR} which build allowed chains equal the vertex correction at the vertex j in the chain built.

The somewhat larger number of chain functions does not seem to pose a significant problem. The main advantage of the method is that it is much simpler to go beyond the SOC approximation. Complicated operator hypernets such as that in diagram 22.1 do not exist in this method. The maximum number of operators at a nodal point in a chain can be four, two from wavy lines and two from exchange. These generate very few multiple-operator links, such as diagram 22.2, which can be easily calculated.

Separable diagrams such as 9.3, 9.5–9.7 do not exist. In the typical case, for example when i is a dL vertex in both the irreducible and the separated parts, only the separated diagrams illustrated in diagram 22.5 exist. These form a simple geometric series which can be summed analytically. In the previous method the calculation of separable diagrams having many operator rings with a common articulation point becomes very tedious. Thus Owen's method, though a little more complicated at the SOC level of computation, has enormous advantages in computing multiple-operator diagrams.

It is interesting to ask whether Ψ_{IP} or Ψ_{SP} is a better variational wave function. Such a question can always be settled by computing numerically the energy expectation value with both Ψ_{IP} and Ψ_{SP}, but simpler arguments could be more illuminating. The central correlations in Ψ_{IP} [Eq. (2.26)] are treated in the Jastrow (or equivalently SP) approximation, but in principle we could also treat them in the independent-pair approximation. Let

$$f^c = 1 + u^c . \tag{8.13}$$

Then the IP analogue of the Ψ_J will become

$$\Psi^c_{IP} = \left(1 + \sum_{i<j} u^c_{ij} + \sum_{\substack{i<j,\,k \\ k<l}} u^c_{ij} u^c_{kl} + \cdots\right)\Phi . \tag{8.14}$$

This Ψ^c_{IP} is not a very good wave function; for example, it gives only half of the correlation energy of Bose liquids interacting with nuclear-type Yukawa potentials (Owen, 1978). One understands the deficiency of Ψ^c_{IP} by noting that when the potential has a strong repulsive core $f^c(r \to 0) \to 0$, and $\Psi_J \to 0$ as any $r_{ij} \to 0$; but the Ψ_{IP} does not vanish when $r_{ij} \to 0$. However, such a simple criterion for deciding between Owen's Ψ_{IP} and Ψ_{SP} is not yet available.

The Ψ_{SP} has additional terms of the type $f^p_{ij} f^q_{jk} \{O^p_{ij}, O^q_{jk}\}$, absent in the Ψ_{IP}. They contribute to many different separable and chain diagrams, and *a priori* it is difficult to estimate their net contribution. As a matter of fact, the current results in nuclear matter indicate that Ψ_{SP} and Ψ_{IP} give very comparable energies. The Ψ_{SP} has a formal advantage which can be easily seen by considering a spin-one-half fermion fluid having central v^c and spin–spin v^σ parts in its two-body potential. If we completely spin-polarize the liquid, its variational wave function may be expected to go over to a Jastrow wave function for fermions interacting with an effective central potential $v^c + v^\sigma$. The Ψ_{SP} has this property while the Ψ_{IP} does not.

IX. RESULTS

In this section we summarize the results obtained by the variational methods using correlation operators, as discussed in the preceding sections, and compare them with results obtained by other methods.

A. Neutron matter model v_3

The v_3 model interaction is of the form $v^c_{ij} + v^\sigma_{ij}(\sigma_i \cdot \sigma_j)$; the v^c_{ij} and v^σ_{ij} are given by Owen (1979a) and are based on the potentials of Bethe and Johnson (BJ) (1974). The F operator has the form $f^c_{ij} + \beta_\sigma f^\sigma_{ij}(\sigma_i \cdot \sigma_j)$, and has been used in both the Ψ_{SP} [Eq. (2.19)] and Ψ_{IP} [Eq. (2.26)] wave functions. The calculation with Ψ_{SP} (Lagaris *et al.*, 1978) uses the FHNC/SOC approximation, while that with the Ψ_{IP} (Owen, 1979) sums all hypernetted operator chains. The results of both calculations are summarized in Table VI. Owen gives results for both the PB and JF kinetic energy prescriptions (Zabolitzky, 1977), while the Ψ_{SP} calculation uses the PB form only. Also listed are energies obtained with the Jastrow wave function without any f^σ correlation; both Ψ_{IP} and Ψ_{SP} reduce to the same Ψ_J in the limit $\beta_\sigma \to 0$.

The f^σ has a very small effect on the $E(\rho)$ of the v_3

TABLE VI. The $E(\rho)$ in MeV of the v_3-model of neutron matter.

ρ	$E(\Psi_{IP}, JF)$	$E(\Psi_{IP}, PB)$	$E(\Psi_V, PB)$	$E(\Psi_J, PB)$
0.17	17.2	17.0	17.4	17.8
0.3	29.1	28.2	28.8	29.2
0.4	41.1	38.8	39.9	40.3

model due to very large cancellations. The W_0 and W_F decrease, while W_c increases, as β_σ is increased keeping the total energy almost constant. For example, at $d=2.3r_0$, the $E(\Psi_{SP},\mathrm{PB})$ and W_c are, respectively, 29.2 and 0.0 MeV for $\beta_\sigma=0$, and 28.8 and 7.4 MeV for $\beta_\sigma=0.5$. Thus it is very difficult to calculate the energy gain due to the f^σ correlation in this model. However, it is encouraging to note that the SOC approximation used to calculate the large W_c contributions seems to be reasonably accurate in this case. Owen also does a calculation which he calls "SOC" using the Ψ_{IP}. He fails to obtain a minimum in $E(d)$ in this calculation, but his "SOC" calculation is significantly different from the single-operator chain approximation which is presented here, and used in the Ψ_{SP} calculations.

B. Nuclear matter v_6 models

The Reid $v_{6,8}$ and BJ-II $v_{6,8}$ models are obtained by expressing the $^1S_0$, $^3S_1-{}^3D_1$, $^1P_1$, and $^3P_2-{}^3F_2$ potentials in the Reid (1968) and Bethe–Johnson-II (1974) interaction models as $\sum_i v^i(r)O^{i=1,8}$. The $v_{i=7,8}$ potentials are neglected in the v_6 models. The HJ v_6 model is obtained by neglecting the $(L\cdot S)$ and quadratic spin–orbit terms in the Hamada–Johnston (1962) potential, while the GT-5200 potential of Gammel and Thaler (1960) is itself of a v_6 form.

The $\sigma\tau$ and $t\tau$ correlations and chains are most important in nuclear matter, and the energy is more sensitive to $\beta_{t\tau}$ and d than to $\beta_{\sigma\tau}$. It is very insensitive to β_σ, β_τ, and β_t. In the calculations based on the FHNC/SOC equations the equilibrium value of $\beta_{t\tau}$ is generally close to unity, but that of $\beta_{\sigma\tau}$ is generally <1. The contributions to $E(k_F,d,\beta_i)$ for the Reid (BJ-II) v_6 model at its minimum are given in Table VII(VIII). The f^σ, f^τ, and $f^{\sigma\tau}$ lower the energy by 2(5) MeV. As in the v_3 model of neutron matter, there is a very large cancellation between the two-body and the W_c contributions due to f^σ, f^τ, and $f^{\sigma\tau}$. The largest contribution of f^t and $f^{t\tau}$ from many-body clusters is via the W_s term. The contributions to $E(k_F=1.3\ \mathrm{fm}^{-1})$ of the Reid, BJ-II, HJ, and GT-5200 v_6 models in FHNC/SOC calculations are compared in Table IX.

The $E(k_F)$ of the v_6 and v_8 models, as obtained in various calculations, is shown in Figs. 23–26. A brief description of the various calculations along with their references is given in Table X. An estimate of the errors in SOC calculations is discussed in the next section. The error in the energy expectation value of the Reid and BJ-II v_6 models is ~±1 MeV at $k_F=1.6\ \mathrm{fm}^{-1}$. However, the variational wave function neglects the explicit k-dependent terms in the correlation operator F. From Fig. 4 we may expect these to lower the energy in the $k_F=1.6\ \mathrm{fm}^{-1}$ region by ~1 MeV. Thus the estimated error in the SOC energies in the equilibrium region is +0 to −2 MeV. The errors in SOC calculations of the HJ and GT-5200 models have not been analyzed in such detail, but we may expect them to be similar.

The energies with Ψ_{IP} (Figs. 23 and 24) have been calculated with the Jackson–Feenberg (JF) kinetic energy expression, and at all $\beta_i=1$. The JF energies were found to be higher by an MeV in the v_3 model, and we may also expect some lowering of the Ψ_{IP} energies by varying the β_i. So the error in the preliminary IP curves is probably −1 to −4 MeV in the range $k_F=1.4$–$1.8\ \mathrm{fm}^{-1}$. The IP energies may be very reliable upper bounds. Owen's method is capable of giving more accurate energies and error estimates, which we hope will soon be available. From the present results it appears that Ψ_{IP} and Ψ_{SP} may give similar $E(\rho)$ in Reid v_6 and GT-5200 models, the Ψ_{IP} being a little better at low densities, and Ψ_{SP} a little better at high densities.

TABLE VII. Reid v_6 $E(k_F=1.6\ \mathrm{fm}^{-1}, d=2.5r_0)$ in MeV.

$\beta_i\geq 2$	$\beta_i=1$	$\beta_{i=5,6}=1$ $\beta_{i=2,4}=0.4$	$\beta_{i=5,6}=1$ $\beta_{i=2,4}=0$	$\beta_i=0$
T_F	31.85	31.85	31.85	31.85
2-body	−65.76	−59.16	−52.75	−10.75
W_0(MB)	−6.91	−6.30	−5.28	1.97
W_c	13.02	6.46	0.77	0.0
W_s	18.30	12.21	10.35	0.0
W_{cs}	−2.97	−1.01	0.05	0.0
W_F(MB) + U_F	−1.07	−0.20	0.48	0.18
U	−0.91	−0.80	−0.60	1.93
E	−14.45	−16.95	−15.13	25.18

Typically the LOBT approximation gives too high energies; however, the three- and four-body cluster contributions lower the BBG energy of the Reid v_6 model below the variational SOC and IP energies. The estimated error in BBG energies in the Reid v_6 model is ~±0.5 to ±3 MeV over $k_F=1.4$ to $1.8\ \mathrm{fm}^{-1}$. The BHF equilibrium density for the HJ and GT-5200 v_6 models is ~30% lower than that given by SOC calculations, while the RBHF calculations, if carried to higher densities, might give equilibrium densities closer to the variational results. The RBHF $E(\rho)$ is probably too low in the HJ v_6 model.

At low densities the CBPT energies are in excellent agreement with the SOC energies, but at large densities they are much lower. The cluster expansion is truncated rather severely at the three-body level, and only the second-order correlated basis perturbation term is included in the present CBPT calculations. A higher-order calculation in the CBPT approach will probably give higher energies at high ρ. The failure of the present CBPT calculations to obtain a minimum in the $E(\rho)$ of the GT-5200 model also indicates that they overestimate the binding at high ρ.

The present HOC results should be taken with some

TABLE VIII. BJ-II v_6 $E(k_F=1.2\ \mathrm{fm}^{-1}, d=2.25r_0)$ in MeV.

$\beta_{i\geq 2}$	$\beta_i=1$	$\beta_{i=5,6}=1.1$ $\beta_{i=2,4}=0.6$	$\beta_{i=5,6}=1.1$ $\beta_{i=2,4}=0$	$\beta_i=0$
T_F	17.92	17.92	17.92	17.92
2-body	−39.70	−35.48	−24.17	−8.40
W_0(MB)	−0.82	−0.98	−0.80	−0.12
W_c	3.43	1.85	0.58	0.0
W_s	14.68	10.73	6.79	0.0
W_{cs}	−1.03	−0.56	0.25	0.0
W_F(MB) + U_F	0.62	0.42	0.12	−0.01
U	−0.19	−0.54	−0.78	0.45
E	−5.09	−6.64	−1.25	9.83

TABLE IX. $E_{\min}$ (k_F=1.3 fm^{-1}) for various potentials in MeV.

Model	Reid v_6	BJ-II v_6	HJ v_6	GT-5200
d/r_0	2.25	2.25	2.35	2.42
$\beta_{i=2,4}$	0.4	0.6	0.5	0.75
$\beta_{i=5,6}$	1.0	1.1	1.0	1.0
T_F	21.03	21.03	21.03	21.03
2-body	−42.28	−37.55	−37.04	−50.28
W_0(MB)	−0.21	−3.96	−0.15	1.77
W_c	2.79	4.01	2.31	3.43
W_s	6.44	11.71	5.19	6.83
W_{cs}	−0.42	−0.87	−0.35	−0.66
W_F(MB) + U_F	0.26	−0.17	0.23	0.69
U	−0.59	−0.76	−0.23	−0.32
E	−12.98	−6.56	−9.01	−17.51

caution because the calculated energies do not exhibit a minimum with respect to variations in the correlation range d. The CBPT calculations also have this problem to some extent at high ρ. The HOC energies are quite sensitive to d (Fig. 25) and thus very uncertain. The present HOC calculations neglect all commutator terms, including those of the separable type. The W_s is quite large, and hopefully the HOC calculations will exhibit minima when the separable and other commutator terms are included. It was noted by Wiringa and Pandharipande (1978) that the variational energies in the FHNC/SOC scheme decrease rapidly with d, without exhibiting a minimum when the commutator terms are neglected.

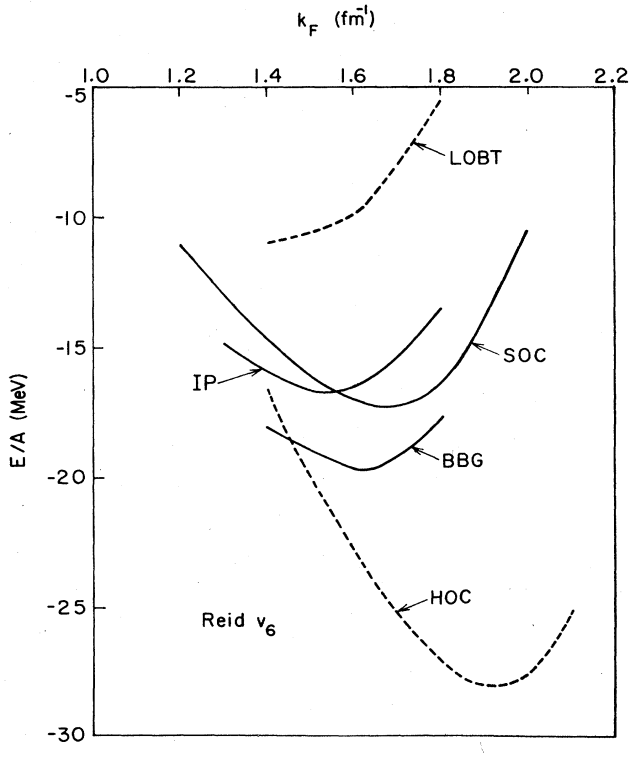

FIG. 23. The $E(k_F)$ for nuclear matter in the Reid v_6 model in various calculations, as described in Table X.

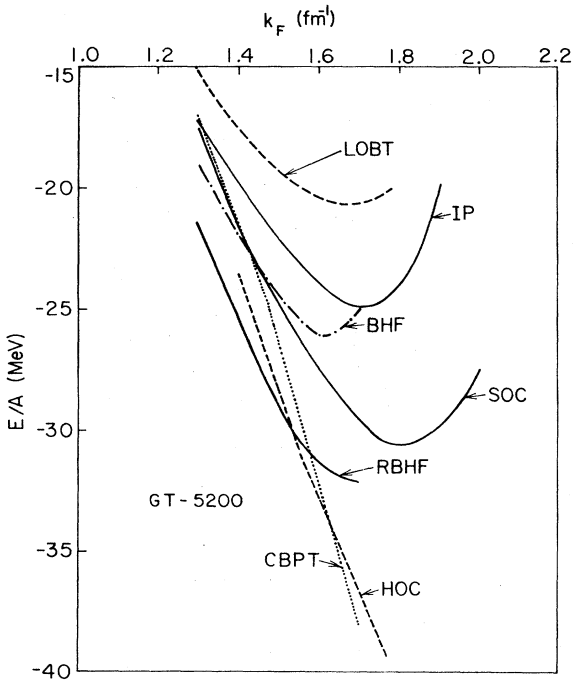

FIG. 24. The $E(k_F)$ for nuclear matter with the Gammel–Thaler 5200 potential in various calculations, as described in Table X.

C. Convergence of FHNC/SOC calculations

There are two major approximations involved in the FHNC/SOC summations. First is the assumption that the major contribution of passive noncentral correla-

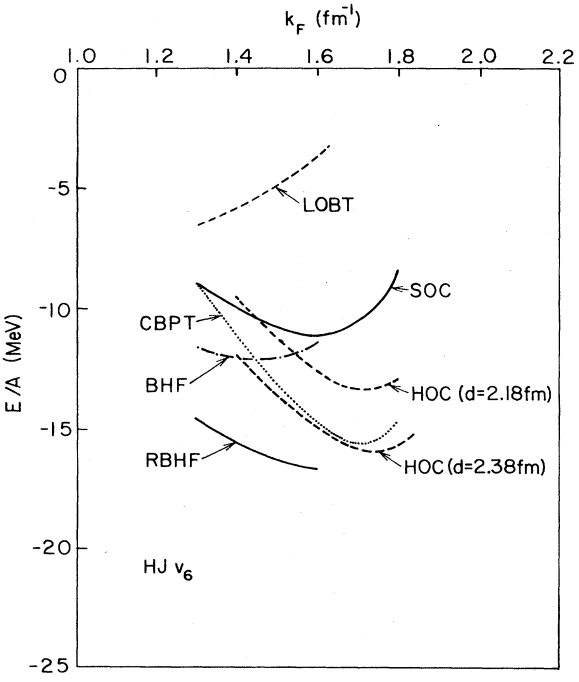

FIG. 25. The $E(k_F)$ for nuclear matter in the Hamada–Johnston v_6 model in various calculations, as described in Table X.

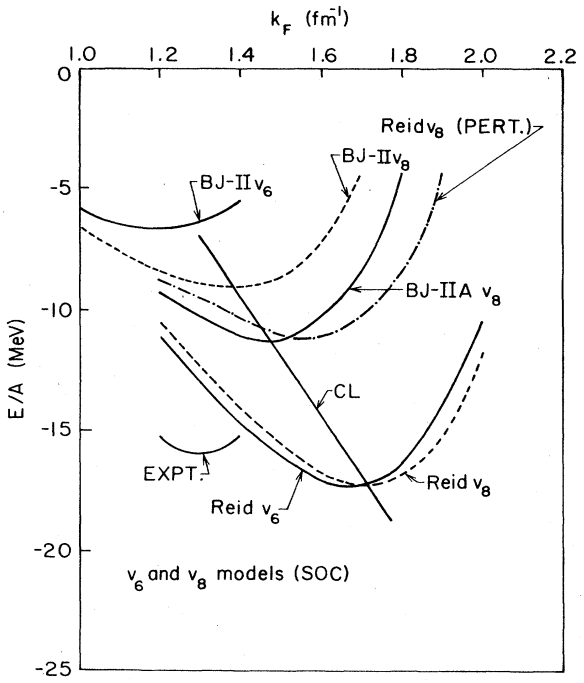

FIG. 26. The $E(k_F)$ for nuclear matter in Reid models v_6 and v_8, Bethe–Johnson II (BJ-II) models v_6 and v_8, and BJ-IIA model v_8, calculated in the SOC approach, and Reid model v_8 calculated with a simple perturbation method (PERT). The solid line CL denotes the "Coester line" passing through the equilibrium points of the phase-equivalent v_8 models. The curve labeled EXPT has a compressibility of 250 MeV and the empirical equilibrium point.

tions can be taken into account with single-operator chains. Second is that separable diagrams having many operator rings at a common articulation point are smaller than those having only two. These two approximations have been recently studied by Wiringa (1979) by calculating the leading corrections. The corrections are found to be quite small (~1/10) compared to the leading terms. Moreover they tend to cancel out, and the net change in the energy-density curve of the Reid and BJ-II v_6 models is negligible.

The SOC approximation may be tested by looking at corrections to W_c (diagram 19.2), which gives the contribution of diagrams with one SOC. The bulk of W_c comes from the G^p_{de} chain, whose leading contributor is the three-body diagram 27.1 of Fig. 27 we have discussed so often. The importance of this diagram was also stressed by Brueckner (1976), who finds that it represents the bulk of Pauli exclusion effects in variational theory. At $k_F = 1.6$ fm^{-1} it gives a total contribution of ~9.5 MeV, where the total W_c is ~6.5 MeV. The leading multiple-operator correction to diagram 27.1 is 27.2, which is found to be $\sim -1/7$ of 27.1 over a wide density range. The other possible corrections, such as diagram 27.3, should be even smaller. For example, in going from 27.1 to 27.2 an f^c_{m1} is replaced by $2f^{q>1}_{m1}$, while the $2f^c_{n1}$ in diagram 27.1 goes to $f^{q>1}_{n1}$ in 27.3.

Terms with more than one SOC have also been examined. The diagram 27.4 with two G_{de} chains is typically much less than 1/20th of the W_c, which is understandable since the G^p's are <0.1 (Fig. 17).

All once-separable diagrams having passive SOR, plus some twice- and more-separable diagrams like 19.6, are included in the basic FHNC/SOC calculation, in an exact self-consistent manner. Diagrams like 19.7 are approximated and those like 19.8 are neglected. The diagrams 19.7 and 19.8 are now calculated; the results are given in Table XI. The total W_0 is −64.4 MeV at the parameters in Table XI. But the part of the W_0 (diagram 19.1) having $(f^c H^c f^c)_{mn}$ does not contribute to separable diagrams. The first line of Table XI gives the operator ring parts of W_0 which can form separable diagrams. It is clear that the addition of a separable ring reduces the diagram by ~0.1. The consistent solution of SOC equations sums many important diagrams,

TABLE X. Index to calculations shown in Figs. 23–26.

LOBT:	Lowest-order Brueckner theory; two-body cluster calculation with standard choice $[U(k>k_F)=0]$ of spectrum; Day (1978b); Lejeune and Mahaux (1979).
BBG:	Brueckner–Bethe–Goldstone; two-, three-, and estimates of four-body cluster contributions with standard choice of spectrum; Day (1978b).
BHF:	Brueckner–Hartree–Fock; two-body cluster contribution with continuous choice $[U(k>k_F)\neq 0]$ of spectrum; Lejeune and Mahaux (1979).
RBHF:	Renormalized Brueckner–Hartree–Fock; two- and parts of four-body clusters with continuous choice of spectrum; Lejeune and Mahaux (1979).
CBPT:	Correlated basis perturbation theory; two- and three-body contributions to variational energy expectation value plus two-body second-order perturbation correction; Kürten, Ristig, and Clark (1979).
SOC:	Single-operator chain (with commutators): Variational energy for symmetrized product wave function calculated with FHNC/SOC method; Lagaris, Pandharipande, and Wiringa (1978).
HOC:	Hypernetted operator chain (without commutators): Variational energy for symmetrized product wave function with a fixed correlation range calculated with HOC method; Benhar, Ciofi degli Atti, Fantoni, and Rosati (1978).
IP:	Independent pair; variational energy calculation with independent-pair wave function; includes hypernetted operator chain and commutator contributions; Owen (1979).

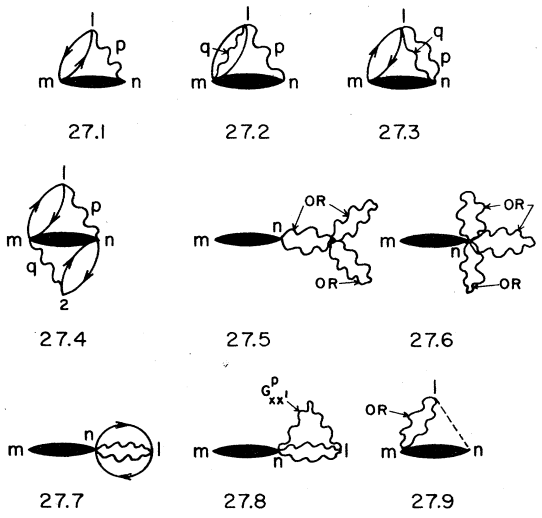

FIG. 27. Diagrams illustrating the leading corrections to the basic FHNC/SOC calculation.

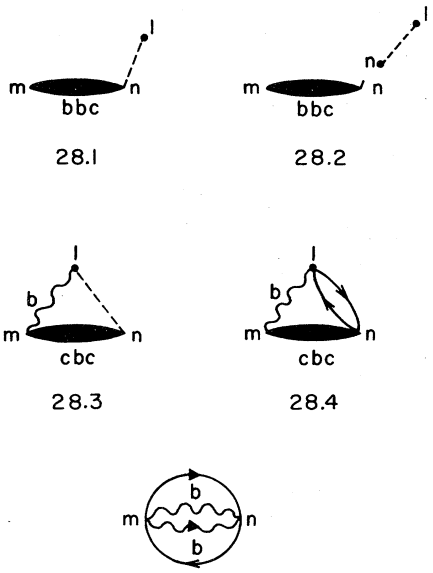

FIG. 28. Diagrams 28.1–28.3 occur only in the v_8 models; they give zero contribution in v_6 models. The leading $G_{de}^{b(b\tau)}$ and BW_F terms are shown by diagrams 28.4 and 28.5.

such as 19.6 and 19.7. The remaining diagram 19.8 is $\sim -1/10$ of 19.3. The vertex correction in 19.8 must be iterated self-consistently to sum diagrams of type 27.5 The net correction from these diagrams is 10% (~ -1.5 MeV at $k_f = 1.65$ fm^{-1}) to the total W_s. These solutions still do not sum diagrams like 27.6, which would give ~1% of W_s.

The basic equations also neglect separable diagrams of the type 27.7, 27.8, which have passive multiple operator rings. Of these, 27.7 could be significant, while the rest should be much smaller than 27.7. The vertex correction in diagram 27.7 is the largest correction to the basic FHNC/SOC calculation. It increases the W_s by ~15% ($\sim +2.5$ MeV at $k_f = 1.65$ fm^{-1}). Curiously enough this repulsive correction just about cancels the attractive contributions of diagrams 27.2 and 19.7.

Diagrams of type 27.9 superficially appear to be corrections to the large separable diagrams in W_s, but in fact they are much smaller. The W_s is large because of the long range of $f^{p>1}$; however, at large r_{n1} the $n1$ link in diagram 27.9 is practically zero. These diagrams are incorrectly treated in the basic scheme as SOR in the central chains $G^c_{xx'}$ [Eqs. (6.34)–(6.37)]. A modification of the FHNC equations by Wiringa (1979) allows one to sum all central chains with nontouching SOR in the middle, and no SOR at either end. Diagrams like 27.9 can then be added explicitly and exactly. They give a contribution of ~ -1 MeV, which largely compensates the change in W_0 from cleaning up the touching SOR's in the $G^c_{xx'}$.

TABLE XI. Contribution of separable diagrams W_s in MeV in Reid v_6 model at $k_F = 1.65$ fm^{-1}, $d = 2.6r_0$, $\beta_\sigma = \beta_\tau = \beta_{\sigma\tau} = 0.5$ and $\beta_t = \beta_{t\tau} = 0.95$.

Description	Diagram No.	Contribution
Irreducible OR		−92.0
Once-separable	19.3	+18.1
Twice-separable	19.6	−1.8
Twice-separable	19.7	−1.2
Twice-separable	19.8	−1.9

In view of the cancellations among all these higher-order corrections, the energy minima for the Reid and BJ-II v_6 models calculated by the FHNC/SOC prescription are probably accurate within ±1 MeV. This cancellation may not persist in other systems or at very high densities. Hence it is advisable to supplement the FHNC/SOC calculation with diagrams of type 19.8, 27.2, 27.7, and 27.9 and the corrected $G^c_{xx'}$ equation.

D. The v_8 problem

There are two striking differences between the v_6 and the v_8 problems. First, the C parts of a product of v_6 operators is a number or a function of $\mathbf{r}_i$, the particle coordinates, but that of a product of v_8 operators is in general an operator because of the ∇ in the angular momentum operator $\mathbf{L}$. So we have a number of new terms; for example the separable diagram 28.1 of Fig. 28 now contributes because the ∇'s in b_{mn} operators (the $\mathbf{L}\cdot\mathbf{S}$ is denoted by b) can operate on the f_{m1} in the connected diagram 28.1, but not in the separated diagram 28.2. Second, the eight v_8 operators do not form a closed set. Lagaris and Pandharipande (1979) find that the set of operators needed to treat the v_8 problem includes twenty-two operators: 1, σ, τ, $\sigma\tau$, $\alpha(\mathrm{A},\mathrm{B})$, $\alpha(\mathrm{A},\mathrm{B})\tau$, $\beta(\mathrm{A})$, and $\beta(\mathrm{A})\tau$. Here A and B are the vector operators $\mathbf{r}$, ∇, and $\mathbf{L}$; $\alpha(\mathrm{A},\mathrm{B})$ are generalizations of the tensor operator:

$$\alpha(\mathrm{A},\mathrm{B}) = \tfrac{3}{2}(\sigma_1\cdot\mathrm{A}\sigma_2\cdot\mathrm{B} + \sigma_2\cdot\mathrm{A}\sigma_1\cdot\mathrm{B}) - \sigma_1\cdot\sigma_2\,\mathrm{A}\cdot\mathrm{B}\,; \qquad (9.1)$$

and $\beta(\mathrm{A})$ that of the spin–orbit operator:

$$\beta(\mathrm{A}) = \tfrac{1}{2}(\sigma_1 + \sigma_2)\cdot\mathrm{A}\,. \qquad (9.2)$$

The vector operators A do not commute, but it may be verified that

$$\alpha(\mathrm{A},\mathrm{B}) = \alpha(\mathrm{B},\mathrm{A})\,. \qquad (9.3)$$

The α and β operators retain the useful property

$$\sigma_1 \cdot \sigma_2 \alpha(\mathrm{A},\mathrm{B}) = \alpha(\mathrm{A},\mathrm{B})\sigma_1 \cdot \sigma_2 = \alpha(\mathrm{A},\mathrm{B}) , \tag{9.4}$$

$$\sigma_1 \cdot \sigma_2 \beta(\mathrm{A}) = \beta(\mathrm{A})\sigma_1 \cdot \sigma_2 = \beta(\mathrm{A}) , \tag{9.5}$$

of the tensor and spin–orbit operators.

The spin–orbit interaction cannot be treated as a weak perturbation. The first-order shift

$$\Delta E = \langle \Psi_6 | \Delta H | \Psi_6 \rangle / \langle \Psi_6 | \Psi_6 \rangle , \tag{9.6}$$

where

$$\Delta H = \sum_{i<j} v^b(r_{ij}) O^b_{ij} + v^{b\tau}(r_{ij}) O^{b\tau}_{ij} \tag{9.7}$$

and Ψ_6 is the variational wave function for the ground state of the v_6 model is quite large and positive. The Reid v_8 energies obtained by a first-order perturbation treatment of the spin–orbit interaction are shown in Fig. 26. The W diagrams containing $f^{t(t\tau)}_{mn} v^{b(b\tau)}_{mn} f^{t(t\tau)}_{mn}$ give the dominant contribution to ΔE.

As shown in Figs. 5 and 6, the spin–orbit forces generate significant spin–orbit correlations and also have an effect on the $f^{p\leq 6}$. An interesting quantity is the expectation value of the v_6 Hamiltonian with the $f^{p\leq 6}$ of the v_8 correlation operator. This quantity, called "$E6$" in Table XII, can be calculated easily with the FHNC/SOC method. It corresponds to the sum of all energy diagrams of the v_8 model that do not contain the $v^{b(b\tau)}$ or $f^{b(b\tau)}$. The E6 is generally 2–3 MeV higher than the ground-state energy of the v_6 model shown in Fig. 26.

Lagaris and Pandharipande (1979) calculate the v_8 model energies by adding the contribution of selected diagrams having $v^{b(b\tau)}$ and $f^{b(b\tau)}$ to $E6$. These extra contributions are prefixed by a letter B in Table XII. For example the $B2$-body gives the contribution of two-body diagrams having spin–orbit potential and/or correlations. It is negative, since the contribution from terms having $f^c v^{b(b\tau)} f^{b(b\tau)}$ overcomes the positive contribution of the $f^{t(t\tau)} v^{b(b\tau)} f^{t(t\tau)}$ terms. It is also much smaller than the two-body contribution contained in $E6$. The order of magnitudes of the contributions in $E6$ can be obtained from Tables VII and VIII.

The many-body contributions to BW_0 are calculated with the $G^c_{xx'}$, and found to be rather small, while BW_c containing $G^{p=2,6}_{xx'}$ is estimated to be <0.5 MeV and neglected. Separable diagrams having b operators in the interacting ring only (BIW_s) and the passive ring only (BPW_s) are large but tend to cancel. It is necessary to calculate these separable diagrams correctly to obtain a reasonable minimum with respect to variation in $\beta_{b(b\tau)}$. The BIW_s has large negative contributions that are linear in $\beta_{b(b\tau)}$. These come from the L operators in v^b_{mn} and f^b_{mn} operating on the F_{m1}. The BPW_s is totally quadratic in $\beta_{b(b\tau)}$ and repulsive.

Unlike the $O^{p=1,6}_{ij}$, which are either linear in both σ_i and σ_j or independent of σ_i and σ_j, the $O^{b(b\tau)}_{ij}$ have two terms, one linear in σ_i, the other in σ_j. Hence operator rings having single $b(b\tau)$ links do not contribute. The simplest many-body rings containing two $b(b\tau)$ links are shown in Fig. 28, diagrams 28.3 and 28.4. These give rather small contributions, labeled BIC in Table XII, indicating that the effect of $f^{b(b\tau)}$ in chains may not be very important. The diagrams containing derivative $b(b\tau)$ lines also appear to be small. The two-body W_F diagram 28.5, which is generally the largest, is itself quite small. In Reid v_8 it is -0.23 MeV at $k_F = 1.7$ fm^{-1}, while in BJ-II v_8 it is -0.17 MeV at $k_F = 1.4$ fm^{-1}; it is included in the $B2$-body of Table XII. The many-body BW_F, BU_F, and BU are neglected. The $BTOT$ of Table XII gives the estimated contribution of all diagrams containing $v^{b(b\tau)}$ and/or $f^{b(b\tau)}$, and $E(v_8)$ gives the total energy.

The $E(k_F)$ of Reid v_6 and v_8 models is quite similar; however, this is due to chance cancellations. The intrinsic effect of the L·S correlations is better described by the difference between Reid v_8 (perturbation method) and v_8 (SOC method) curves. The L·S potentials are much stronger in the BJ-II model (~three times those in the Reid model), and they have a more visible effect on the BJ-II $E(k_F)$.

Earlier estimates (Wiringa and Pandharipande, 1979) of the effect of L·S potentials on the $E(k_F)$ were much too large, mostly because the repulsive BPW_s diagrams were not calculated in these calculations. We note that in the present density range ($k_F < 2.5$ fm^{-1}) the v_8 variational calculations do not exhibit instability towards collapse as predicted by Calogero and Simonov (1970) at very high densities.

We have also shown in Fig. 26 the $E(k_F)$ of a BJ-IIA v_8 model calculated similarly. The interaction in the $TS = 10$, 11, and 00 states of this model is the same as that in BJ-II, but it has the $^3S_1 - {}^3D_1$ potential "5.595" in the $TS = 01$ states, where BJ-II uses the potential "6.55." The BJ $^3S_1 - {}^3D_1$ potentials are labeled by the percentage of D state in the deuteron. Thus the BJ-IIA has a slightly weaker tensor potential and it gives a little more binding.

TABLE XII. Contributions to the energy of Reid and BJ-II v_8 models.

	Reid	BJ-II
k_F(fm^{-1})	1.7	1.4
$\beta_\sigma = \beta_\tau = \beta_{\sigma\tau}$	0.83	0.9
$\beta_t = \beta_{t\tau}$	1.1	1.1
$\beta_b = \beta_{b\tau}$	0.65	0.7
$E6$ (MeV)	−14.09	−3.79
$B2$-Body	−3.11	−4.82
BW_0 (MB)	0.23	−0.03
BIW_s	−2.98	−3.51
BPW_s	+2.44	+3.05
BIC	+0.32	+0.14
$BTOT$	−3.09	−5.17
$E(v_8)$	−17.18	−8.95

X. OUTLOOK

The three v_8 models (Reid, BJ-II, and BJ-IIA) are phase equivalent; they all fit the $^1S_0$, $^3S_1 - {}^3D_1$, $^1P_1$, and $^3P_2 - {}^3F_2$ phase shifts. The equilibrium points predicted by these models form a "Coester line" shown in Fig. 26. It misses the empirical point by a significant margin. This clearly indicates deficiencies in the considered model Hamiltonians for nuclear matter and/or the many-body calculation. We first discuss possible improvements in the many-body theory; much of the

work reviewed here is meant to eliminate the uncertainties in the many-body calculation. The discussion of errors in the preceding section suggests that we can currently calculate the equilibrium energy of Reid type models with a ~2 MeV accuracy, and the equilibrium k_F within ~.2 fm^{-1}.

A. Variational method

In the past few years significant advances were made in the variational theory of helium liquids to remove inherent restrictions in the variational wave function Ψ_v. Euler–Langrange equations were developed, by minimizing the energy expectation value, to find the optimized f_J without any external constraints such as the range d (Lantto and Siemens, 1977). Much of this work has been reviewed recently by Ripka (1979), and it could be possible to extend it and obtain Euler–Lagrange equations for the f^p of the correlation operator. These would eliminate the need for external parameters such as d and β_p. The leading part of the momentum dependence of the F operator, and a three-body correlation, were included in the variational wave function by Schmidt and Pandharipande (1979a), thus eliminating other restrictions in the traditional Ψ_J. It would be quite possible to calculate nuclear matter energy with momentum-dependent correlations, which are in fact no more difficult than the spin–orbit correlations. It would also be possible to include a simple $f_3(\mathbf{r}_i, \mathbf{r}_j, \mathbf{r}_k)$ in the Ψ_v. However, comparison of the energies obtained for the v_6 models with the IP and SP wave functions suggests that we examine the effects of three-body spin-dependent correlations in nuclear matter. This comparison could be premature at present, for other differences such as those in β_p and the kinetic energy prescriptions also contribute to the difference between the available SP and IP energies. Nevertheless, the Ψ_{SP} contains three-particle correlations of the type $f^p(r_{ij})f^q(r_{ik})\{O^p_{ij}, O^q_{ik}\}$ absent in Ψ_{IP}. This extra correlation appears to increase the energy at small ρ. The results displayed in Fig. 23 definitely indicate that the Ψ_{SP} energies are too high by ~2 MeV in the Reid v_6 model at $k_F = 1.4$ fm^{-1}. If the Ψ_{IP} energies continue to remain above the Ψ_{SP} energies at high ρ, even after varying β_p and kinetic energy prescriptions, then we have a more complex problem.

In studies of helium liquids it was necessary to improve upon the calculation of the energy expectation value when more general Ψ_v were introduced. The PB kinetic energy prescription, which works quite well with the short-ranged $f_J(d, r)$, $d \sim 2r_0$, can give arbitrarily low energies when more general f_J allowed. So most calculations use the JF kinetic energy prescription when optimum f_J are used. However, the JF energy is too high in the HNC approximation, and it converges rather slowly. Smith *et al.* (1978) had to calculate diagrams up to HNC/6 to obtain reasonable energies for liquid ^{4}He with the optimum f_J. Schmidt and Pandharipande (1979b) find it convenient to generalize the HNC scheme to three point functions which represent contributions of hypernetted cloth (rather than chain) with three ends. Such generalizations were considered in statistical mechanics by Wertheim (1967), and may be used to calculate leading HNC/5, 6... diagrams by integral equations.

The energy of nuclear matter is much more difficult to calculate because of the spin operators. The FHNC/SOC method may be useful only when $f^{p>1}$ and $G^{p>1}$ are $\ll 1$. The Ψ_{IP} offers many advantages in this respect. It will probably be necessary to incorporate the commutator terms in Fantoni and Rosati's HOC equations if it becomes necessary to calculate the energies with Ψ_{SP}'s containing stronger $f^{p>1}$. The most accurate energy evaluations are done with the Monte Carlo method. Development of techniques to perform Monte Carlo simulations of spin-isospin correlated nuclear matter on computers will significantly reduce the uncertainties in the many-body calculation. Further, it should be much simpler to treat finite nuclei with the Monte Carlo method. The chain summation techniques become much more complex in a finite system (Fantoni and Rosati, 1979).

B. Brueckner-Bethe-Goldstone expansion

The results of BBG calculations stress the need to go beyond two-body cluster contributions to obtain a reasonable $E(\rho)$ in the region of equilibrium density. Rajaraman and Bethe's (1967) work indicated that the three-hole line graphs that correspond to bubble insertions in particle line, three-body rings, and three-body ladders have contributions of order κW_2, and Day's (1978a) results for Reid v_6 models, summarized in Table XIII, confirm this. We note that in all v_6 models $\kappa > 0.25$ at equilibrium density (Lejeune and Mahaux, 1978), and κW_2 is of the order of 10 MeV.

All lowest-order calculations, LOBT, BHF, or RBHF, can have errors of order κW. Their inadequacy can be most clearly seen in the results obtained for the v_1 model of nuclear matter and summarized in Table XIV. The v_1 model has only a central interaction, and has been studied by Zabolitzky (1976) with a Jastrow wave function, and by Lagaris (1979) with a symmetrized product wave function. The backflow has little effect, and the Jastrow wave function is a very good approximation in this model.

Grange and Lejeune (1979) have studied the v_1 model with the standard $[U(k > k_F) = 0]$ and continuous $[U(k > k_F) \neq 0]$ choices of particle spectrum. In this simple model it is seen that the LOBT energies are too high, BHF energies are low, and RBHF much too low. At the (two + three)-body level the $U(k > k_F) = 0$ and $U(k > k_F) \neq 0$ energies become rather similar and are only ~5% above the variational results.

Detailed calculations of the four-body cluster contri-

TABLE XIII. The details of three-hole line contributions in BBG theory with Reid v_6 potential.

k_F	Bubble in particle line	Three-body ring	Three-body ladder	Hole–hole
1.4	+3.3	−5.7	−4.0	−0.4
1.6	+9.5	−10.9	−8.5	−0.6
1.8	+22.2	−18.6	−17.1	−0.9

TABLE XIV. Nuclear matter model v_1.

Method	$U(k>k_F)$	$k_F=1.6$ fm^{-1}	$k_F=1.8$ fm^{-1}
		Brueckner theory $E(k_F)$ in MeV.	
LOBT (2-body)	0	−83.6	−120.3
BHF (2-body)	$\neq 0$	−108.4	−164.1
RBHF (2+parts of 4)-body	$\neq 0$	−115.2	−180.1
(2+3)-body	0	−88.6	−127.4
(2+3)-body	$\neq 0$	−89.3	−133.5
(2+3+estimate of 4)-body	0	−89.1	−128.7
(2+3+estimate of 4)−body	$\neq 0$	−96.9	−137.0
		Brueckner theory κ_2	
LOBT	0	0.06	0.07
BHF	$\neq 0$	0.22	0.28
		Variational $E(k_F)$	
Jastrow FHNC		−95.1	−141.2
(Symmetrized product FHNC/SOC)		−96.9	−143.1

bution are not yet available. Their estimates, however, seem to be rather different for the two choices. The present results indicate that the $U(k>k_F)=0$ energies converge rather rapidly to a value higher than the variational result, while $U(k>k_F)\neq 0$ energies have a poorer convergence, but they may converge to the variational result. The general trend of cluster contributions with the $U(k>k_F)\neq 0$ choice is quite similar to that in variational calculations; the two-body is too low, the (two+three)-body too high, and the four-body substantially attractive.

The two-body contribution κ_2 to the κ is quite different with the two choices, indicating that many-body cluster contributions to κ are significant in either or both choices of $U(k>k_F)$. The possibility of the energy calculated with Brueckner–Bethe–Goldstone theory being dependent on choice of $U(k>k_F)$ was discussed earlier by Baker and co-workers (see Baker, 1978, and references therein). Arguments in favor of a continuous choice for the $U(k)$ have been recently discussed by Lejeune and Mahaux (1978). The $U(k)$ in the v_1 model can be very large (>100 MeV), and thus it is suitable for such studies. Accurate calculations of the four-body cluster contributions of the v_1 model would be very interesting.

C. The nuclear Hamiltonian

Of the three v_8 models, BJ-II is probably the most promising. In the FHNC/SOC approximation it gives equilibrium $k_F=1.4$ fm^{-1} against the empirical 1.3 fm^{-1}. However, from Fig. 23 it appears that the FHNC/SOC calculation may overestimate the equilibrium k_F; thus it is possible that BJ-II v_8 gives the experimental density. It, however, underestimates the binding by more than 5 MeV. The BJ-IIA has a weaker tensor force, giving a 5.5% D state in the deuteron, while BJ-II gives 6.5%. The BJ-IIA gives more binding, but the ρ_0 is already too high. The Reid v_8 and BJ-II v_8 have similar tensor forces, but the L·S potential and the core in the $T,S=1,1$ state in Reid are both weaker than in BJ-II. The Reid v_8 gives more than enough binding but too high density.

It is well known that the interaction in the $^1D_2$ state is not as attractive as that in the $^1S_0$ state. This difference indicates the presence of quadratic spin–orbit or just plain repulsive $\mathbf{L}^2$ terms in the nuclear Hamiltonian. The v_8 models are not very realistic, and a study of v_{10} models which include $\mathbf{L}^2$ terms is necessary.

A signficant part of the attraction between nucleons comes from the coupling of the N–N channel to N–Δ and Δ–Δ channels in two-pion exchange processes, much as the r^{-6} attraction in the interatomic Lennard-Jones potentials comes from the coupling to 1^- dipole states in two-photon exchange processes. However, the N–Δ mass difference (~300 MeV) is not enormous compared to typical energies (~50 MeV) involved in nuclear matter, and it has been suggested that the N–Δ and Δ–Δ channels must be treated explicitly in nuclear matter. The coupling is produced by the four operators $(\sigma_1\cdot\mathbf{S}_{t,2})(\tau_1\cdot\mathbf{T}_{t,2})$, $S_{12}^{II}(\tau_1\cdot\mathbf{T}_{t,2})$, $(\mathbf{S}_{t,1}\cdot\mathbf{S}_{t,2})(\mathbf{T}_{t,1}\cdot\mathbf{T}_{t,2})$, and $S_{12}^{III}(\mathbf{T}_{t,1}\cdot\mathbf{T}_{t,2})$ in the nuclear Hamiltonian. The $\mathbf{S}_t,\mathbf{T}_t$ are transition spins and isospins that convert nucleons into Δ's, and S_{12}^{II} and S_{12}^{III} are tensor operators that contain transition spins $\mathbf{S}_t$ (see the review by Green 1976). Nucleon–nucleon phase shifts in the S and P states can be fitted by static potentials containing twelve operators, eight of the v_8 model and the above four (Smith and Pandharipande, 1976). Probably two more quadratic $\mathbf{L}^2$ terms are needed to obtain reasonable phases in the D waves.

The N–Δ and Δ–Δ components in the nuclear matter wave function can be produced via correlation operators containing transition spin and isospin. An explicit treatment of these channels is expected to reduce both the equilibrium density and binding energy of nuclear matter. In LOBT the equilibrium ρ_0 and E_0 with the Reid potential are found to be $\simeq 0.2$ fm^{-3} and -11.6 MeV, and these reduce to $\simeq 0.14$ fm^{-3} and -7.9 MeV if the N–Δ channel in the $^1S_0$ interaction is treated in the LOBT approximation (Day and Coester, 1976). This effect has also been studied by lowest-order constrained-variational (LOCV) methods (Howes *et al.*, 1978; Moddares and Irvine, 1979). In this approximation the equilibrium with Reid potential occurs at $\simeq 0.29$ fm^{-3} and -23 MeV, and it shifts to $\simeq 0.25$ fm^{-3} and -16 MeV when the N–Δ channel in the $^1S_0$ interaction is treated explicitly. So it appears that to be reasonably realistic

we may have to consider a v_{14} problem in which the interaction is a sum of 14 operators.

A complete variational calculation with the transition spin operators $\mathbf{S}_t$ and $\mathbf{T}_t$ in the Hamiltonian and the correlation operator will include a variety of chain and separable diagrams formed with "transition" correlations. The algebra of transition spin operators is quite similar to that of Pauli spins. We have the basic relations:

$$\mathbf{T}_t^\dagger \cdot \mathbf{T}_t = 2 \tag{10.1}$$

$$\mathbf{T}_t^\dagger \times \mathbf{T}_t = -\tfrac{2}{3} i\boldsymbol{\tau} \tag{10.2}$$

$$(\mathbf{T}_t^\dagger \cdot \mathbf{A})(\mathbf{T}_t \cdot \mathbf{B}) = \tfrac{2}{3}\mathbf{A}\cdot\mathbf{B} - \tfrac{1}{3} i\boldsymbol{\tau}\cdot(\mathbf{A}\times\mathbf{B}) \tag{10.3}$$

which are also valid for $\mathbf{S}_t$. The C parts of products of transition spin operators can be calculated easily.

The three-body force illustrated by the Feynman diagram 29.1 of Fig. 29 is often included in nuclear matter. Contributions of this force will form a part of the SOR diagrams of type 29.2, and they are attractive. However, the presently available results suggest that the repulsive contributions from diagrams such as 29.3 and 29.4 may be dominant. For example, the contribution of the three-body force, in units of MeV and fm, is estimated to be $\sim -0.34\, k_F^{3.6}$, while that of the dispersion and Pauli correction due to transition potentials is estimated from the LOBT (and LOCV) calculations to be $\sim +0.7\, k_F^{5.9}$ (Niskanen, 1977).

The N–N interaction in high partial waves is relatively unknown, but it seems to have a significant influence on the equilibrium density. In Day's calculations the leading contribution of the interaction in $l \geq 3$ states is via the three-hole line cluster energy. It is -5.3 MeV at $k_F = 1.8$ fm^{-1} in the Reid v_6 model, and can influence the ρ_0 by 20–30%. These states are relatively unimportant in determining the two-body cluster energy because of the small momenta of hole states. Thus a reasonable treatment of the interaction in $l \geq 3$ states seems necessary to calculate the many-body cluster contributions. The N–N scattering data are very inadequate for determining the potential in high partial waves. There have been substantial improvements in our understanding of the N–N interaction from the meson exchange point of view (Brown and Jackson, 1976) which may be useful in choosing the potential in $l \geq 3$ states. The recent meson-theoretic potentials are strongly momentum dependent, and Maxwell and Smith (1979) have attempted to extend the variational method to treat them.

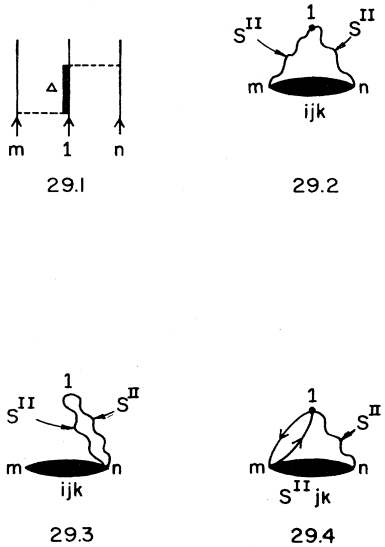

FIG. 29. The Feynman diagram 29.1 generates a "three-body" force between nucleons. The cluster expansion diagrams 29.2–29.4 illustrate various new terms generated by the transition potentials and correlations.

In the search for a better nuclear Hamiltonian we may also take into account some of the failures of the Reid and HJ models in very light nuclei. For example, the $d(\gamma, p)$ measurements of Hughes *et al.* (1976) and calculations of Arenhovel and Fabian (1977) indicate that the D-state percentage P_D in the deuteron should be ~4% instead of the 5.5%–7% in the Reid and BJ models.

Recent measurements of the charge form factors of ^{3}He and ^{4}He nuclei (Arnold *et al.*, 1978) suggest that the point proton densities ρ_p in these nuclei have a substantial hole. In ^{3}He, for example, the estimated ρ_p is ~0.08 fm^{-3} at the center, and it rises to a maximum of ~0.13 fm^{-3} at 0.7 fm away from center (Sick, 1978). The ρ_p obtained for ^{3}He by Faddeev calculations with the Reid model, however, peaks at ~0.13 fm^{-3} at the center and falls off monotonically.

Thus we must conclude that a suitable nuclear Hamiltonian has not yet been found. The many-body theory for nuclear matter (as well as other strongly interacting quantum systems) has made considerable progress in recent years, and we hope that it will prove to be useful in the search for the nuclear Hamiltonian.

ACKNOWLEDGMENTS

The authors wish to thank O. Benhar, H. A. Bethe, J. W. Clark, B. D. Day, S. Fantoni, I. E. Lagaris, L. J. Lantto, C. Mahaux, J. C. Owen, G. Ripka, K. E. Schmidt, P. J. Siemens, and R. Smith for clarifying discussions. A number of new results included in this this review were communicated to the authors at the Trieste (October 1978) meeting, and special thanks are due to the organizers: C. Ciofi degli Atti, A. Kallio, and S. Rosati. Parts of this review were prepared for the Nordic workshop in Copenhagen (May 1978), and it is a pleasure to thank its organizer, G. E. Brown. We also wish to thank D. Hunter for suggesting the title, and the medium energy physics division of the Los Almos Scientific Laboratory for partial support.

REFERENCES

Arenhovel, H., and W. Fabian, 1977, Nucl. Phys. A **282**, 397.
Arnold, R. G., B. T. Chertok, S. Rock, W. Schutz, Z. M. Szalata, D. Day, J. S. McCarthy, F. Martin, B. A. Mecking, I. Sick, and G. Tamas, 1978, Phys. Rev. Lett. **40**, 1429.
Baker, G., 1978, Phys. Rev. C **17**, 1253.
Bäckman, S.-O., J. W. Clark, W. J. Ter Louw, D. A. Chakkalakal, and M. L. Ristig, 1972, Phys. Lett. B **41**, 247.
Bäckman, S.-O., O. Sjöberg, and A. D. Jackson, 1979, preprint.
Benhar, O., C. Ciofi degli Atti, S. Fantoni, and S. Rosati, 1977, Phys. Lett. B **70**, 1.
Benhar, O., C. Ciofi degli Atti, S. Fantoni, and S. Rosati, 1978, to be published in Nucl. Phys.

Bethe, H. A., 1956, Phys. Rev. **103**, 1353.
Bethe, H. A., 1971, Annu. Rev. Nucl. Sci. **21**, 93.
Bethe, H. A., 1977, invited talk at Workshop on Nuclear and Dense Matter, Urbana, unpublished.
Bethe, H. A., and R. F. Bacher, 1936, Rev. Mod. Phys. **8**, 82.
Bethe, H. A., and M. B. Johnson, 1974, Nucl. Phys. A **230**, 1.
Blaizot, J. P., D. Cogny, and B. Grammaticos, 1976, Nucl. Phys. A **265**, 315.
Brandow, B. H., 1966, Phys. Rev. **152**, 863.
Brown, G. E., 1971, Rev. Mod. Phys. **43**, 1.
Brown, G. E., and A. D. Jackson, 1976, *The Nucleon-Nucleon Interaction* (North-Holland, Amsterdam).
Brueckner, K. A., 1954, Phys. Rev. **96**, 908.
Brueckner, K. A., 1976, Phys. Rev. C **14**, 1999.
Brueckner, K. A., and C. A. Levinson, 1955, Phys. Rev. **97**, 1344.
Calogero, F., and Yu. A. Simonov, 1970, Phys. Rev. Lett. **25**, 881.
Ceperley, D. M., G. V. Chester, and M. H. Kalos, 1977, Phys. Rev. B **16**, 3081.
Ceperley, D. M., and M. H. Kalos, 1978, in *Monte Carlo Methods in Statistical Physics*, edited by K. Binder (Springer, Berlin).
Chang, C. C., and C. E. Campbell, 1977, Phys. Rev. B **15**, 4238.
Clark, J. W., 1978, *Progress in Particle and Nuclear Physics*, in press.
Day, B. D., 1967, Rev. Mod. Phys. **39**, 719.
Day, B. D., 1978a, Rev. Mod. Phys. **50**, 495.
Day, B. D., 1978b, invited talk at Conference on Recent Progress in Many-Body Theories, Trieste, to be published in Nucl. Phys.
Day, B. D., and F. Coester, 1976, Phys. Rev. C **13**, 1720.
de Boer, J., and A. Michaels, 1938, Physica (Utrecht) **5**, 945.
Euler, H., 1937, Z. Phys. **105**, 553.
Fantoni, S., and S. Rosati, 1975, Nuovo Cimento A **25**, 593.
Fantoni, S., and S. Rosati, 1978, Nuovo Cimento A **43**, 413.
Fantoni, S., and S. Rosati, 1979, to be published in Nucl. Phys.
Feenberg, E., 1969, *Theory of Quantum Fluids* (Academic, New York).
Feynman, R. P., and M. Cohen, 1956, Phys. Rev. **102**, 1189.
Friman, B. L., and E. M. Nyman, 1978, Nucl. Phys. A **302**, 365.
Gammel, J. L., and R. M. Thaler, 1960, in *Progress in Elementary Particle and Cosmic Ray Physics*, edited by J. G. Wilson and S. A. Wouthuysen (North-Holland, Amsterdam), Vol. V.
Gaudin, M., J. Gillespie, and G. Ripka, 1971, Nucl. Phys. A **176**, 237.
Goldstone, J., 1957, Proc. R. Soc. London, Ser. A **239**, 267.
Grangé, P., and A. Lejeune, 1979, to be published in Nucl. Phys.
Green, A. M., 1976, Rep. Prog. Phys. **39**, 1109.
Hamada, T., and I. D. Johnston, 1962, Nucl. Phys. **34**, 382.
Howes, C., R. F. Bishop, and J. M. Irvine, 1978, J. Phys. G; Nucl. Phys. **4**, L123.
Hughes, R. J., A. Zieger, H. Waffler, and B. Ziegler, 1976, Nucl. Phys. A **267**, 329.
Iwanato, F., and M. Yamada, 1957, Prog. Theor. Phys. **18**, 543.
Jastrow, R., 1955, Phys. Rev. **98**, 1479.
Jeukenne, J.-P., A. Lejeune, and C. Mahaux, 1975, Nucl. Phys. A **245**, 411.
Kalos, M. H., 1970, Phys. Rev. A **2**, 250.
Kalos, M. H., 1977, invited talk at Workshop on Nuclear and Dense Matter, Urbana, unpublished.
Kalos, M. H., D. Levesque, and L. Verlet, 1974, Phys. Rev. A **9**, 2178.
Kurten, K. E., M. L. Ristig, and J. W. Clark, 1978, Phys. Lett. B **74**, 153.
Kurten, K. E., M. L. Ristig, and J. W. Clark, 1979, Nucl. Phys. A **317**, 87.
Lagaris, I. E., 1979, private communication.
Lagaris, I. E., V. R. Pandharipande, and R. B. Wiringa, 1978, to be published in Nucl. Phys.
Lagaris, I. E., and V. R. Pandharipande, 1979, to be published.
Lantto, L. J., and P. J. Siemens, 1977, Phys. Lett. B **68**, 308.
Lantto, L. J., and P. J. Siemens, 1979, Nucl. Phys. A **317**, 55.
Lejeune, A., and C. Mahaux, 1978, Nucl. Phys. A **295**, 189.
Lejeune, A., and C. Mahaux, 1979, Nucl. Phys. A **317**, 37.
Maxwell, O., and R. A. Smith, 1979, preprint.
Moddares, M., and J. M. Irvine, 1979, J. Phys. G; Nucl. Phys. **5**, 511.
Niskanen, J. A., 1977, Ph.D. Thesis, University of Helsinki, ISBN 951-99140-1-3.
Owen, J. C., 1978, Phys. Lett. B **77**, 9.
Owen, J. C., 1979a, Ann. Phys. (New York) **118**, 373.
Owen, J. C., 1979b, private communication.
Pandharipande, V. R., 1971, Nucl. Phys. A **174**, 641.
Pandharipande, V. R., 1972, Nucl. Phys. A **181**, 33.
Pandharipande, V. R., 1978, Phys. Rev. B **18**, 218.
Pandharipande, V. R., and H. A. Bethe, 1973, Phys. Rev. C **7**, 1312.
Pandharipande, V. R., and Naoki Itoh, 1973, Phys. Rev. A **8**, 2564.
Pandharipande, V. R., and K. E. Schmidt, 1977, Phys. Rev. A **15**, 2488.
Pandharipande, V. R., and R. B. Wiringa, 1976, Nucl. Phys. A **266**, 269.
Pandharipande, V. R., R. B. Wiringa, and B. D. Day, 1975, Phys. Lett. B **59**, 205.
Rajaraman, R., H. A. Bethe, 1967, Rev. Mod. Phys. **39**, 745.
Reid, R. V., 1968, Ann. Phys. (N.Y.) **50**, 411.
Ripka, G., 1979, preprint.
Schmidt, K. E., 1978, private communication.
Schmidt, K. E., and V. R. Pandharipande, 1978, Nucl. Phys., in press.
Schmidt, K. E., and V. R. Pandharipande, 1979a, Phys. Rev. B, **19**, 2504.
Schmidt, K. E., and V. R. Pandharipande, 1979b, private communication.
Sick, I., 1978, Invited talk, International Conference on Few Body Problems and Nuclear Forces, Graz, unpublished.
Smith, R. A., and V. R. Pandharipande, 1976, Nucl. Phys. A **256**, 327.
Smith, R. A., A. Kallio, M. Puoskari, and P. Toropainen, 1978, preprint.
Speth, J., E. Werner, and W. Wild, 1977, Phys. Rep. **33C**, 129.
van Kampen, N. G., 1961, Physica (Utrecht) **27**, 783.
van Leeuwen, J. M. J., J. Groeneveld, and J. de Boer, 1959, Physica (Utrecht) **25**, 792.
von Weizsacker, C. F., 1935, Z. Phys. **96**, 431.
Wertheim, M. S., 1967, J. Math. Phys. **8**, 927.
Wiringa, R. B., 1979, to be published.
Wiringa, R. B., and V. R. Pandharipande, 1978, Nucl. Phys. A **299**, 1.
Wiringa, R. B., and V. R. Pandharipande, 1979, Nucl. Phys. A **317**, 1.
Youngblood, D. H., 1978, Bull. Am. Phys. Soc. **23**, 42.
Youngblood, D. H., C. M. Rozsa, J. M. Moss, D. R. Brown, and J. D. Bronson, 1977, Phys. Rev. Lett. **39**, 1188.
Zabolitzky, J. G., 1976, Phys. Lett. B **64**, 233.
Zabolitzky, J. G., 1977, Phys. Rev. A **16**, 1258.

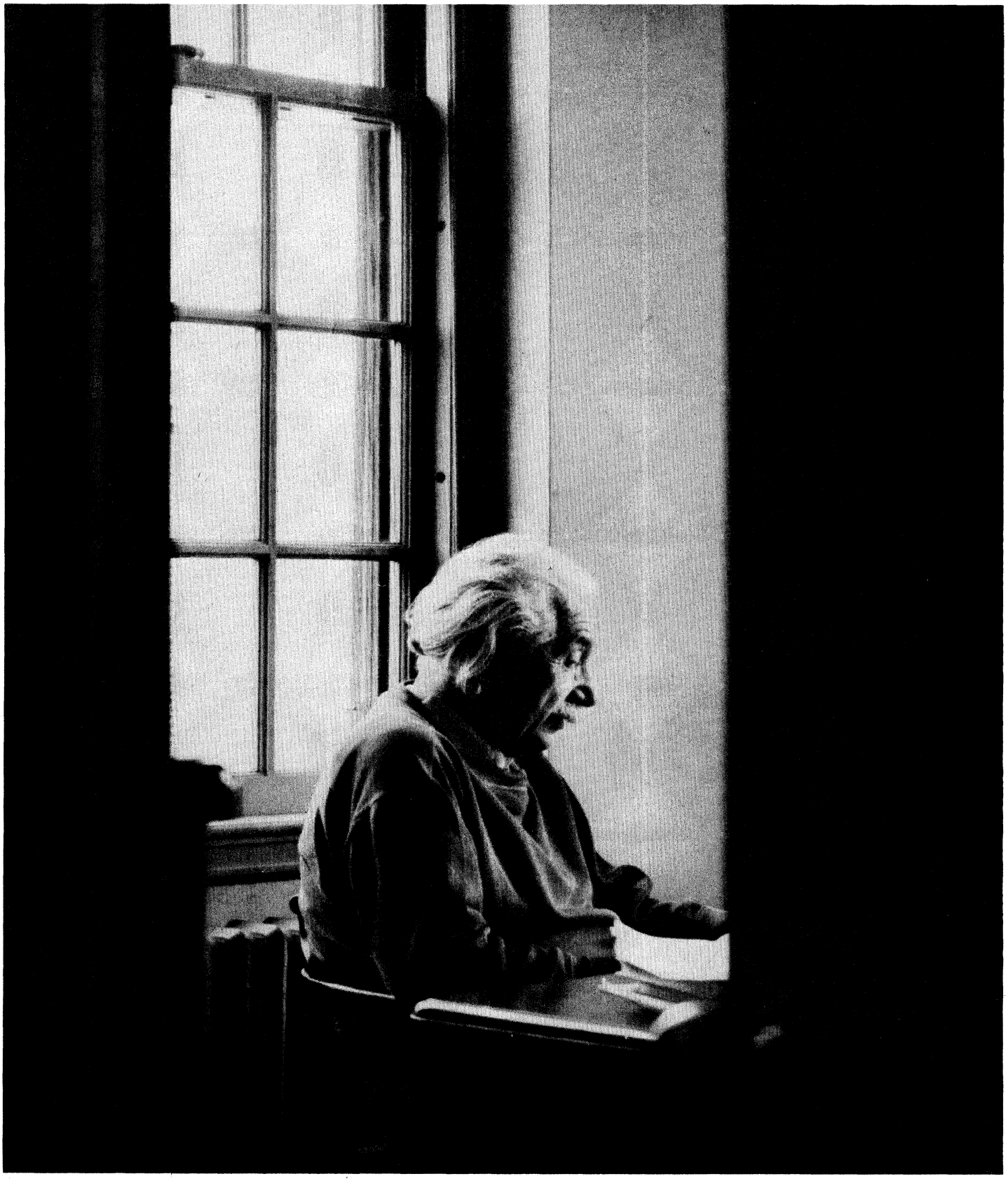

Photographed by Alfred Eisenstaedt, Life Magazine, Copyright © 1947, Time Inc.

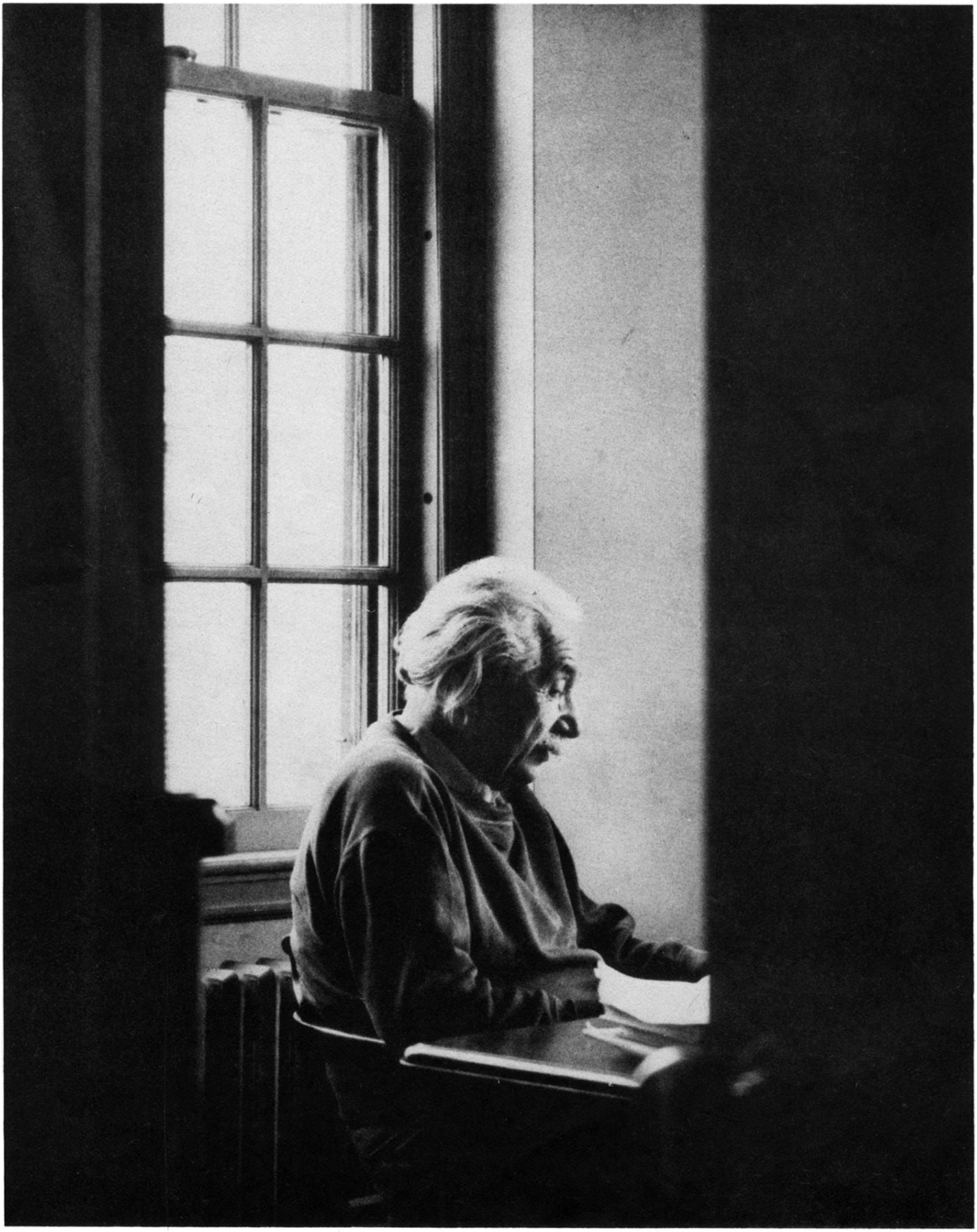

Photographed by Alfred Eisenstaedt, Life Magazine, Copyright © 1947, Time Inc.